Rheology of Polymers with Nanofillers

Utracki, Leszek A; Sepehr, Maryam M; Carreau, Pierre J.

Publisher's version / Version de l'éditeur:
https://doi.org/10.1002/9780470600160.ch16
Polymer Physic: From Suspensions to Nanocomposites and Beyond, pp. 639-707, 2010-08-02

16

RHEOLOGY OF POLYMERS WITH NANOFILLERS

LESZEK A. UTRACKI AND MARYAM M. SEPEHR

National Research Council Canada, Industrial Materials Institute, Boucherville, Quebec, Canada

PIERRE J. CARREAU

Chemical Engineering Department, École Polytechnique, Montreal, Quebec, Canada

Polymer Physics: From Suspensions to Nanocomposites and Beyond, Edited by Leszek A. Utracki and Alexander M. Jamieson

16.1 INTRODUCTION

As a part of continuum mechanics, rheology has been developed assuming continuity, homogeneity, and isotropy. In multiphase systems such as nanocomposites, these assumptions are rarely valid. Thus, the rheology of multiphase systems (MPSs) determines volume-average properties or bulk quantities [Hashin, 1965]. The volume-averaged rate of strain tensor, $\langle \dot{\gamma}_{ij} \rangle$, and the corresponding stress tensor are expressed, respectively, as

$$\langle \dot{\gamma}_{ij} \rangle = \left\langle \frac{\partial \upsilon_i}{\partial x_j} \right\rangle + \left\langle \frac{\partial \upsilon_j}{\partial x_i} \right\rangle \quad \text{where} \quad \left\langle \frac{\partial \upsilon_i}{\partial x_j} \right\rangle = \frac{1}{\Delta V} \int_{\Delta V} \frac{\partial \upsilon_i}{\partial x_j} dV \tag{16.1}$$

$$\langle \sigma_{ij} \rangle = -P\delta_{ij} + \eta_0 \langle \dot{\gamma} \rangle + \frac{1}{\Delta V} \sum_{\Delta V} (S_{ij} - x_i F_j) \tag{16.2}$$

where υ_i is the local velocity, x_i a local coordinate, ΔV an elementary volume, P the pressure, δ_{ij} the components of the unit tensor, η_0 the viscosity of the continuous phase, and S_{ij} and F_i represent the hydrodynamic and nonhydrodynamic forces acting on a dispersed-phase particle. Since the thermodynamic interactions affect the hydrodynamic forces and vice versa, the latter forces are coupled. The first two terms of Eq. (16.2) represent the contribution to the stress tensor of the matrix and are identical to those of a homogeneous fluid, and the third term describes the perturbing influences of the dispersed phase [Batchelor, 1970, 1971, 1974, 1977].

Consequently, the rheological measurements of MPSs should be carried out such that the dimension of the flow channel is significantly larger than the size of the flow element. For example, the relative viscosity, η_r, of diluted spherical suspensions measured in a capillary instrument depends on the $(d/D)^2$ factor, where D is the sphere diameter and d that of the capillary—for $d (\geq 10D$, the error is around 1% [Happel and Brenner, 1983]. Thus, if 1% error is acceptable, the size of the dispersion should be at least 10 times smaller than the characteristic dimension of the measuring device (e.g., diameter of a capillary in capillary viscometers, distance between stationary and rotating cylinders or plates). Following this recommendation is not always possible, which lead to "the decline and fall of continuum mechanics" [Tanner, 2009].

The major distinction between the rheometry of the single-phase material and MPSs is the effect of flow on morphology and on the resulting rheological response. Depending on the type and intensity, the morphology of MPSs may be modified significantly by flow. Since the stress and strain affect the dispersion and the distribution of the dispersed phase, different structures are expected from dissimilar flow fields (e.g., irrotational flow in uniaxial experiments and shear flow), even under steady-state conditions. Because of the morphology sensitivity to the test conditions, there are disagreements between predictions of continuum theories and experiments [see Utracki and Kamal, 2002, Table 7.10]. Since in most MPSs the morphology of a given material controls its performance, testing the same MPSs under different flow conditions is equivalent to testing different materials. In consequence, the test method selected

should reflect the final use of the data (e.g., when simulation of the flow through dies is important, capillary data are useful, but in general, for MPS characterization, low strain dynamic tests are preferred [Utracki, 1988, 1989, 1995]). Recognizing the flow effects on the structure and physical properties, simultaneous methods of the structure characterization in flow have been developed. For example, Ho et al. [2001] used small-angle neutron scattering (SANS) for characterizing clay dispersion in aqueous media. Bousmina [2006] studied the kinetics of clay intercalation during flow by x-ray diffraction (XRD). The nanoscale rheology became possible after the invention by Israelachvili [1985] of the surface force apparatus (SFA). In the device, the steady-state and dynamic shear behavior of liquid films, 0.3 nm to 1 μm thick, might be studied [Luengo et al., 1997; Mukhopadhyay and Granick, 2001]. These measurements revealed strong effects of the crystalline solid substrate on the molecular or segmental mobility at a distance of $\leq$ 120 nm. Evidently, the ultimate reduction of scale for the rheological measurements is the study of single macromolecules [Sakai et al., 2002; Wang et al., 2005; Nakajima et al., 2006; Watabe et al., 2006], discussed authoritatively by Nakajima and Nishi in Chapter 3.

Before discussing the flow behavior of polymeric nanocomposites (PNCs), the nature of these materials should be outlined. As the name indicates, PNCs must contain at least two components, a polymeric matrix with dispersed nanoparticles [Utracki, 2004]. PNCs with thermoplastics, thermosets, and elastomers have been produced. The nanoparticles, by IUPAC's definition, must have at least one dimension that is not larger than 2 nm. They can be of any shape, but the most common for structural PNCs are sheets about 1 nm thick with the aspect ratio $p = D/t = 20$ to 6000, where D is the inscribed (or equivalent) diameter and t is the thickness of the sheet. These inorganic lamellar solids might be either natural or synthetic [Utracki et al., 2007].

Molecular modeling of SFA experiments show that the incorporation of crystalline solids with high surface energy to an organic phase creates a gradient structure in the orthogonal direction to the clay surface, z. The first few layers at $z \leq 6$ nm are solidlike, with slow segmental mobility and low free-volume content. At increasing distance from the solid surface, $6 < z$ (nm) < 120, the segmental mobility exponentially increases, accompanied by a reduction of the shear viscosity from $\eta \approx 10^{12}$ Pa·s to the value characteristic for the molten polymer [Simha et al., 2001; Utracki and Simha, 2004; Utracki, 2007]. This type of structure is also present in PNCs comprising intercalants and compatibilizers.

The degree of clay dispersion depends on the interactions between the components, the intercalation kinetics, imposed stress/orientation, and concentration (i.e., "crowding"). In perfectly dispersed PNCs six types of morphologies have been observed: isotropic, nematic, smectic, columnar, house of cards, and crystalline [Balazs et al., 1999; Ginzburg et al., 2000]. As the concentration increases, the degree of clay dispersion decreases. When the volume fraction exceeds $\phi = 0.008$, the crowding causes formation of local stacks with diminishing interlayer spacing, d_{001}. Evidently, poor dispersion may also result from thermodynamic immiscibility or insufficient mixing. Thus, as the degree of dispersion increases, the system changes from a composite type with micrometer-sized particles, to an intercalated mesosystem ($d_{001} = 1.6$ to 8.8 nm), and finally, to a fully exfoliated PNC ($d_{001} > 8.8$ nm).

Depending on the type of PNC and the method of preparation, the system might be either end-tethered or nontethered [i.e., with matrix ionically or covalently bonded to the nanofiller surface, or only adsorbed on it (directly, or through a compatibilizer)]. The former resembles highly branched *hairy clay platelet* with tens of thousands of macromolecules attached to a single clay platelet through the initially reactive intercalant molecules [Okada et al., 1988; Utracki and Lyngaae-Jørgensen, 2002]. The latter systems resemble a composite: polymer reinforced with platelike solids for which the inorganic phase dimensions are enlarged by the intercalation and adsorption of organic molecules.

Work with PNCs is seriously complicated by the thermal decomposition of the quaternary intercalant at $T \geq 150°C$, which in the presence of oxygen may lead to formation of peroxyradicals and degradation of the matrix [Hofmann, 1851]. Thus, the PNC behavior and performance greatly vary from one system to another, depending on the method of preparation, composition, dispersion, orientation, and so on. In this chapter the focus will be on common elements (*e.g.*, the unprecedented strong interparticle interactions at low deformation rates).

16.1.1 Flow of Suspensions at Vanishing Deformation Rates

The relative viscosity, η_r, of suspensions in a Newtonian medium as a function of the volume fraction of the suspended particles, ϕ, might be expressed as

$$\eta_r = 1 + [\eta]\phi + k_1([\eta]\phi)^2 + \cdots + k_{n-1}([\eta]\phi)^n \tag{16.3}$$

where the intrinsic viscosity, $[\eta]$, depends on the rigidity and shape of the suspended particles. In a shear field the particles rotate with a period dependent on the rate of shearing, $\dot{\gamma}$, and the aspect ratio, p:

$$t = \frac{2\pi}{\dot{\gamma}}\left(p + \frac{1}{p}\right) \tag{16.4}$$

For ellipsoids of rotation, the aspect ratio is frequently defined as a ratio of the major to minor axes; $p' = a_1/a_2$ (i.e., for prolate ellipsoids, $p' > 1$, and for oblate ellipsoids, $p' < 1$). Equation (16.4) is symmetrical, predicting the same period of rotation for prolate and oblate ellipsoids provided that their aspect ratio is, respectively, p' and $1/p'$ [Goldsmith and Mason, 1967]. Such symmetry is not observed for $[\eta]$, as the flow is affected differently by rods than by platelets. Thus, a customary definition of the aspect ratio is used in this chapter, p being defined as the ratio of the largest to the smallest dimension; that is, for rods, $p =$ length/diameter, and for disks, $p =$ diameter/thickness, so for both geometries, $p > 1$.

In 1940, Simha derived dependencies for $[\eta]$ of the freely rotating monodispersed ellipsoids. The derivation considered the viscosity increase due to the disorienting influence of the thermal motion. At the limit of the shear rate to the rotational diffusion coefficient ratio, $\dot{\gamma}/D_r \to 0$, $[\eta]$ of the prolate and oblate ellipsoid suspension with high aspect ratio, $p \gg 1$, was derived as, respectively [Simha, 1940;

Frisch and Simha, 1956],

$$[\eta] \approx \frac{14}{15} + \frac{p^2}{15\,(\ln 2p - 3/2)} + \frac{p^2}{5\,(\ln 2p - 1/2)}; \quad p = \frac{a_1}{a_2} \tag{16.5}$$

$$[\eta] \approx \frac{16}{15} + \frac{p}{(\arctan p)}; \quad p = \frac{a_2}{a_1} \tag{16.6}$$

The experimental data of $[\eta]$ versus p for disks polydispersed in size and shape with $p \leq 300$ followed the empirical dependence [Utracki, 1989]

$$[\eta] = 2.5 + a(p^b - 1) \tag{16.7}$$

where $a = 0.025 \pm 0.004$, $b = 1.47 \pm 0.03$, the correlation coefficient squared, $r^2 = 0.9998$, and the standard deviation, $\sigma = 0.622$. Figure 16.1 displays the $[\eta]$ versus p dependence for differently shaped particles; the strongest enhancement is for the prolate ellipsoids, an intermediate for oblate ellipsoids and the smallest for spheres. The Eq. (16.6) prediction for disks is systematically higher than that of Eq. (16.7), with the difference decreasing with p. Extensive discussions on the suspension behavior in diluted region have been presented by Goldsmith and Mason [1967] and van de Ven [1989].

When the concentration increases, terms higher than linear have to be included in Eq. (16.3). For suspensions of spherical particles a monotonic increase was observed and predicted in the full range of $0 \leq \phi \leq \phi_{max}$, where ϕ_{max} is the maximum packing volume fraction; experimentally, $\phi_{max} = 0.62$ for monodispersed hard spheres and

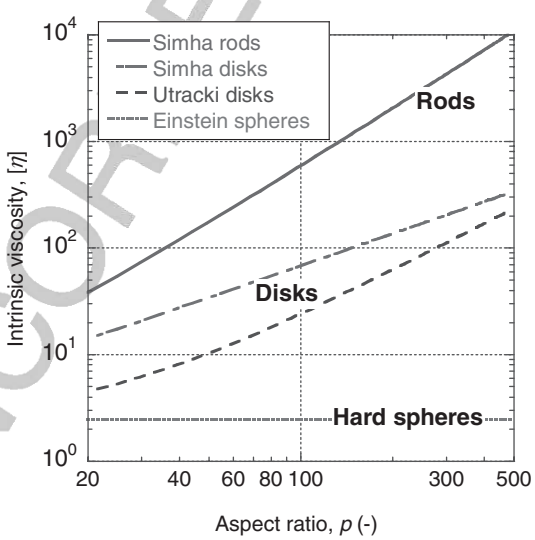

FIGURE 16.1 Intrinsic viscosity for monodispersed rods, disks, and hard spheres. The empirical dependence for polydispersed disks is also shown.

$\phi_{max} = 0.78$ to 0.87 for polydispersed spheres [Utracki, 1989]. Within this concentration range the disks show two regions of behavior, the first stretching from zero up to the limit of free rotation (encompassed volume), corresponding to ϕ_{max}, and the second above it. Within the first, the disks are free to assume a random orientation, thus in molten polymer they represent exfoliated PNC. Within the second, $\phi > \phi_{max}$, free rotation is impossible, thus the platelets align, forming local stacks with decreasing interlayer spacing. The limiting concentration, corresponding to ϕ_{max}, can be calculated: for example, assuming that the disks are monodispersed, circular, and that the volume they require for free rotation is that of the encompassed spheres. Geometrical consideration shows that $\phi_{max} = a_0/p$, where the constant $a_0 = 0.93$ and 1.24 ± 0.07 for monodispersed and polydispersed oblate ellipsoids, respectively [Jogun and Zukoski, 1999; Utracki, 2004]. Empirically, for $p < 100$ the following dependence was found:

$$\frac{1}{\phi_{max}} = 1.55 + 0.0598\,p \tag{16.8}$$

Recent analysis of old experimental data [Utracki and Fisa, 1982] suggested another relation:

$$\frac{1}{\phi_{max}} = 0.136 + 1.401\,p^{1/3} \tag{16.9}$$

Figure 16.2 displays the experimental data and the three dependencies. The results originating from geometrical consideration of fully exfoliated plates predict faster reduction of ϕ_{max} than observed experimentally, especially for particles with a large

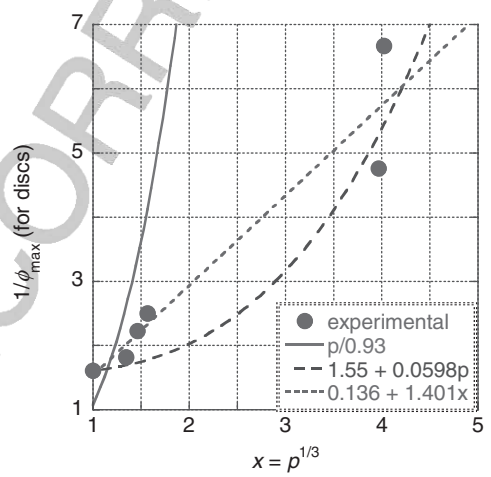

FIGURE 16.2 Maximum packing volume fraction for disks versus the aspect ratio. Lines are calculated, while the points are experimental. (See the text.)

aspect ratio. Of the two empirical relations, Eq. (16.8) or (16.9), the latter describes observed data better. However, since for low p the geometrical dependence offers a reasonable ϕ_{max} prediction, it is possible that the high-aspect-ratio suspensions contained stacks of locally aligned platelets, or in PNC terminology they are intercalated. These dependencies are valid for suspensions of disks without strong interactions. Since clays have anions on the flat surfaces and cations on the edges, they may form a three-dimensional structure known as a *house of cards* [Jogun and Zukoski, 1996]. Okamoto et al. [2001b] observed these structures of montmorillonite (MMT) preintercalated with octadecyl ammonium (MMT-ODA) dispersed in a mixture of polypropylene (PP) and maleated-PP (PP-MA).

16.1.2 Nanoparticles and Their Surface Modification

Nanoparticles used in PNCs are one-dimensional (e.g., fibers, tubes, whiskers), two-dimensional (platelets), or three-dimensional (spheres or nearly so, e.g., see Chapter 15). The latter ones are rather meso- than nano-sized and are used mainly in functionalized PNCs. Currently, structural PNCs of industrial interest contain platy inorganic substances that can be exfoliated into dispersions of individual platelets about $t \simeq 1$ nm (or less) thick; examples are given in Table 16.1.

Natural clays have been formed from alkaline volcanic ashes, structurally modified during about 100 million years in seas or lakes [Keller, 1979; Giese and van Oss, 2002]. Evidently, neither the original ash nor the sea or lake composition has been identical around the globe; thus, the clay compositions vary with geographical location and deposit strata. Natural clays also contain organic and inorganic contaminants (e.g., algae, nonhumic and humic substances, carbonates, silica, feldspar, gypsum, albite, anorthite, orthoclase, apatite, halite, calcite, dolomite, siderite, biotite, muscovite, chlorite, stilbite, pyrite, kaolinite, hematite) and must be laboriously purified [Norrish, 1954; Cohn, 1966].

Clays of interest to PNCs are crystalline, composed of plate-shaped crystals about 1 nm thick with $p = 50$ to 6000 ($p \approx 250$ of most commercial organoclays). They have large specific surface area, $A_{sp} \approx 750$ to 800 m^2/g, and cation-exchange capacity, $CEC = 0.5$ to 2 (meq/g). Bulk clays absorb a large volume of water, and under suitable conditions fully exfoliate in it. Two natural clays with $CEC \approx 1$ meq/g are of special interest: montmorillonite (MMT) $[Al_{1.67}Mg_{0.33}(Na_{0.33})]Si_4O_{l0}(OH)_{2,}$ and hectorite (HT), $[Mg_{2.67}Li_{0.33}(Na_{0.33})]Si_4O_{10}(OH,F)_{2.}$ During flow, their platelets orient with the major axis in the flow direction and surface usually parallel to the shear plane [Kojima et al., 1995; Varlot et al., 2001; Lele et al., 2002; Bafna et al., 2003; Galgali et al., 2004]. Upon cessation of flow in low-viscosity media, the Brownian motion leads to a randomization of the flow-imposed orientation. For PNCs the randomization process may require hours [Utracki and Lyngaae-Jørgensen, 2002; Ren and Krishnamoorti, 2003].

Commercial organoclays are preintercalated clays, mainly MMT. Quaternary ammonium chloride of the type $R_1R_2(CH_3)_2N^+Cl^-$ [R_1 is usually a long paraffinic chain (e.g., octadecyl) and R_2 a functional group that is supposed to ameliorate miscibility with the polymer] represents the main class of intercalants [Utracki, 2008].

TABLE 16.1 Layered Minerals for Use in PNC

Smectite clays	Montmorillonite, bentonite, nontronite, beidellite, volkonskoite, hectorite, saponite, sepiolite, stevensite, sauconite, sobockite, svinfordite, kenyaite
Synthetic clays	E.g., hectorite, $MgO(SiO_2)_s(Al_2O_3)_a(AB)_b(H_2O)_x$ (where AB is a ion pair, e.g., NaF)
Layered silicic acids	Kanemite, makatite, octosilicate, magadiite, kenyaite, layered organosilicates
Other clays	Mica, vermiculite, illite, ledikite, tubular attapulgite, etc.
Layered hydroxides	Brucite: $Mg(OH)_2$ or gibbsite: $Al(OH)_3$
Layered double hydroxides	$[M^{2+}_{1-X}M^{3+}_X(OH)_2]^{Y+}(A^{n-Y/n})$. mH_2O, e.g., $Mg_6Al_{3.4}(OH)_{18\cdot8}(CO_3)_{1.7}.H_2O$; or $Zn_6\ Al_2\ (OH)_{16}\ CO_3.nH_2O$
Layered aluminophosphates	E.g., mineral AlPO (berlinite), $Al_4(PO_4)_3(OH)_3\cdot9H_2O$ (vantasselite), or from hydrothermal synthesis of $H_3PO_4 + Al(OH)_3$ with structure-directing agents
M^{4+} phosphates or phosphonates	M^{4+} = Ti, Zr, or Sn; e.g., α -form: $Zr(HPO_4)\cdot2H_2O$; γ-form: $ZrPO_4O_2P(OH)_2\cdot2H_2O$; λ-form: $ZrPO_4XY$ (X and Y are anionic or neutral ligands), etc.
Chlorides	$FeCl_3$, FeOCl, CdI_2, $CdCl_2$
Chalcogenides	TiS_2, MoS_2, MoS_3, $(PbS)_{1.18}(TiS_2)_2$
Cyanides	$Ni(CN)_2$
Oxides	$H_2Si_2O_5$, V_6O_{13}, HtiNbO$_5$, $Cr_{0\cdot5}V_{0\cdot5}S_2$, $W_{0\cdot2}V_{2\cdot8}O_7$, Cr_3O_8, $MoO_3(OH)_2$, V_2O_5, $VOPO_4\cdot2H_2O$, $CaPO_4CH_3\cdot H_2O$, $MnHAsO_4\cdot H_2O$, $Ag_6Mo_{10}O_{33}$, etc.
Others	Graphite, graphite oxide, boron nitride, etc.

Source: Adapted from Utracki et al. [2007].

16.1.3 Diversity of PNCs

PNC have been prepared with virtually all polymers, from water-soluble macromolecules to polyolefins and high-temperature specialty resins such as polyimide (PI). Elastomer-based PNCs with large clay platelets have been commercialized for improved barrier properties in automotive tires or sport balls. Elastomeric epoxy resins with clays demonstrate substential improvement in mechanical properties (e.g., tensile modulus and strength) [Varghese and Karger-Kocsis, 2005; Utracki, 2008]. In this chapter we focus primarily on clay-containing PNCs, the CPNCs.

For PNCs, the layered double hydroxides (LDHs) constitute a new class of mainly synthetic, reinforcing nanoparticles. During synthesis, LDHs may be preintercalated with organic anions. Unfortunately, most LDH platelets are thin, $t = 0.6 \pm 0.1$ nm, small in diameter, $d = 30$ to 40 nm [Wu et al., 2007]), and decompose thermally at $T \approx 207°C$ [Camino et al., 2001]); consequently, their main application has been for absorption of HCl during dehydrochlorination of poly(vinyl chloride) (PVC) and halogenated polymers, or as flame retardants. The flow behavior of polyethylene (PE) with LDHs was reported to be similar to that of CPNCs [Costa et al., 2006]. There are no commercial PNCs with LDHs on the market, but experimental products such as Perkalite, a preintercalated aluminum–magnesium (Al-Mg) LDH, have been

announced for use with elastomers and polyolefins [Akzo Nobel, 2007]. Costa et al. [2008] reviewed LDH-based PNCs.

Besides clays and LDHs, carbon nanotubes (CNTs) are recognized as potentially valuable nanofillers. They have been known since the early 1990s and are being produced as multiwalled nanotubes (MWNTs) or single-walled nanotubes (SWNTs). More than 10,000 research papers have been published on CNTs, but their PNC technology is still in its infancy. SWNTs are expensive (2009 prices: $200–2500/g); they are produced with variable diameters (0.7 to 1.4 nm) and different chiral numbers, thus conductance. The product may contain up to 30 wt% catalytic impurity. Because of the cost involved, CNTs are being in situ polymerized into high-performance polymeric matrices such as poly(*p*-phenylene benzobisoxazole). Since SWNTs enhance not only mechanical and thermal properties, but offer unique enhancement of the resistance to the electron radiation (by a factor of $> 10^5$), they are being explored for use in aerospace. However, the optimistic assessment still projects 5 to 10 years of development before commercial applications [Huber, 2004; Smith et al., 2004]. Considering our limited space here, the rheology of PNCs with CNTs is not discussed.

16.1.4 Model Suspension for PNCs

CPNCs constitute a new class of materials, made of a viscoelastic matrix containing a low concentration of disk-shaped nanofiller particles. Compared to polymers with microsized filler particles, these materials show significantly different dynamics and flow behavior. The main source of the difference is the nanosize, which is related to its large specific surface area with high surface energy, responsible for adsorption of nanosized solidified layers of organic molecules, which increases the solid loading to the extend that about. 1 vol% clay might reduce the chain mobility of 99 vol% of the matrix. Other sources for the difference are related to the specific type of aggregation of clay platelets, (i.e., the house-of-cards and stack domains) [Okamoto et al., 2001b]. The specificity of CPNCs and their different behavior notwithstanding, one might gain insight into their mechanism and structure by comparison with model systems.

At a vanishing deformation rate ($\dot{\gamma} \to 0$) and concentration ($\phi \to 0$), the hydrodynamic volume as expressed by $[\eta]$ increases linearly with the aspect ratio, p. When concentration reaches $\phi_{\max,}$ the disks are no longer able to rotate in shear but form locally oriented stacks; hence, the flow behavior changes. The stacks may show an apparent yield stress and present a smaller resistance to flow, as observed for PE with phlogopite mica. For this system the relative viscosity at $\dot{\gamma} \to 0$ followed two Lingard–Whitmore proportionalities: $\ln\eta_r \propto \phi$, with $[\eta] = 51.6$ and 8.5 for the free and hindered rotation regions, respectively. Substituting the former value into Eq. (16.7) leads to $p = 92 \pm 1$ [Fisa and Utracki, 1984].

As the rate of deformation increases, the flow fields affect the morphology of the dispersed particles (orientation, dispersion, aggregation, etc.) as well as the structure of the flowing body (e.g., skin-core effect, weld lines, flow encapsulation). Evidently, orientation is engendered more efficiently in irrotational flows, but even in shear, an increasing shear rate causes a progressive alignment of clay platelets [Utracki and Lyngaae-Jørgensen, 2002].

The behavior known from the studies of microcomposites was also observed in the flow of a commercial, fully exfoliated CPNC from Ube (1015C2; PA-6 with 2 wt% MMT-ω-aminododecyl acid). By comparison with microcomposites, in CPNCs other processes may be taking place. Of these, the most important is the change for better or worse of the platelet dispersion. For example, Bousmina [2006] recorded variations of XRD diffractograms during steady-state shearing. The data indicated that to achieve exfoliation the strain rate and total strain, γ, are important. Only for $0.2\,s^{-1} < \dot{\gamma}_c < 0.6\,s^{-1}$, the clay dispersion was found to increase with γ. It was also observed that shearing for a long time at $\dot{\gamma} = 0.6\,\mathrm{s}^{-1}$ caused twisting and folding of MMT platelets. The well-known thermal degradation of ammonium intercalant at $T > 150^{\circ}\mathrm{C}$ affects the clay dispersion in the opposite direction; elimination of the intercalant causes a progressive collapse of the spacing back to inorganic stacks.

Nanocomposites with spherical silica particles (mesosized; $D = 10$ to 80 nm) have been of industrial and academic interest. Large differences in the degree of dispersion in poly-ε-caprolactam (PA-6) matrix were reported; silica spheres with $D = 17$ nm aggregated, whereas those with $D = 80$ nm were fully dispersed [Reynaud et al., 2001]. A similar observation was reported by Oberdisse and Boué [2004]. The yield stress versus concentration curves were significantly higher for particles with $D \leq 25$ nm than for those with is $D = 50$ nm. This coincides with the earlier report by Pukánszky [1990] that incorporation of nanoparticles increases the tensile strength only if their diameter is $D < 50$ nm.

Colloidal silica ($\phi = 0$ to 0.04; $D = 12$ nm) was dispersed in polyethylene glycol (PEG) with a number-average molecular weight $M_n = 45$ to 292 kg/mol [Zhang and Archer, 2002]. The dynamic viscoelastic data indicated a transition from liquidlike to solidlike behavior at $0.01 < \phi < 0.02$, about one order of magnitude smaller than the three-dimensional percolation threshold, $\phi_\mathrm{p} = 0.156$. The effect depends not only on the particle content and surfactant, but also on the PEG molecular weight—larger M_n engendered stronger solidlike effects (see also [Zhu et al., 2005]). The proposed mechanism postulated that the silica particles are surrounded by immobilized shells of PEG that are bridged by macromolecules. Bartholome et al. [2005] confirmed this mechanism indirectly; the solidlike behavior was reduced by grafting the silica particles.

Utracki and Lyngaae-Jørgensen [2002] observed several common aspects of exfoliated CPNCs and liquid-crystal polymers (LCPs). Similar six-phase structures are predicted for CPNCs and observed in LCPs: isotropic, nematic, smectic-A, columnar, house of cards, and crystal [Porter and Johnson, 1967; Balazs et al., 1999; Ginzburg et al., 2000]. These phases in CPNCs originate in a balance between the thermodynamic interactions, clay concentration, and platelets orientation, while in LCPs they depend mainly on temperature. Since it is more difficult on the one hand to prepare disk-shaped than rigid-rod molecules, and on the other to develop flow theory for LCPs with disk moieties, the number of publications on the latter systems is small [Ciferri, 1991].

The LCP rheology usually describes the material behavior in a specific form, mainly nematic, which shows flow behavior similar to that of CPNC. This phase morphology is characterized by local orientation, evident in rheooptical studies. As

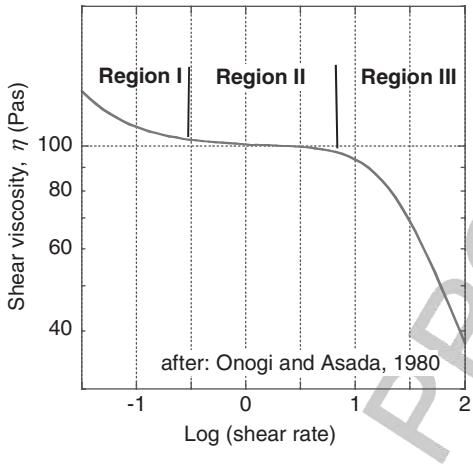

FIGURE 16.3 Schematic of viscosity versus shear rate dependence for nematic LCP. (After Onogi and Asada [1980].)

shown in Figure 16.3, there are three regions of flow for the nematic LCP [Onogi and Asada, 1980; Wissbrun, 1981]: (I) a shear-thinning region at low deformation rates, (II) a plateau region, and (III) a power-law shear thinning region. The structure in region I is highly variable, dependent on the specimen history and resulting polydomain morphology. There are strong interactions between nematic domains that resemble the yield stress behavior but with a slope of $-1/2$ instead of -1. In region II, rheooptics indicates systematic rotation of nematic domains; hence, here these domains are dispersed in a continuous matrix. The latter structure dominates region III, where initially, the domains tumble and then, at high enough deformation rates, become aligned in the flow direction. Figures 16.3 and 16.4 demonstrate that the three regions of LCP flow are duplicated by such exfoliated CPNCs as 1015C2. Evidently, owing to the size difference of oriented LCP mesogens and CPNC platelets, the time required for domain orientation is significantly different.

One of the most intriguing characteristics of nematic LCP is the behavior of the first normal stress difference, N_1. The experiment and theory indicate that for the flow of nematic LCP there is a region of the deformation rates where $N_1 < 0$ [Kiss and Porter, 1980; Marrucci, 1991]. The change from tumbling to flow-aligned stationary monodomain flow takes place at shear rates in the middle of the negative N_1 range. Some theories also predicted negative values of N_1 for the transitory response after startup at low shear rates.

Another similarity in the rheological response between CPNCs and LCPs is the stress growth behavior at startup [Metzner and Prilutski, 1986; Utracki, 2004]. For a constant applied shear rate, the shear stress, σ_{12}, goes through a maximum. Its magnitude depends on the shear history; the longer the specimen is undisturbed, t_{rest}, the larger is the stress overshoot:

$$\Delta\sigma \equiv (\sigma_{12,\max} - \sigma_{12,\infty})_{\dot{\gamma}=\text{const}} \propto \Delta\eta_{t\to\infty}\exp(-\tau_\sigma/t_{\text{rest}}) \qquad (16.10)$$

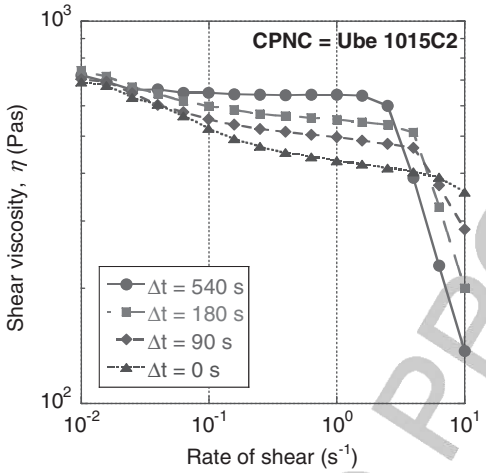

FIGURE 16.4 Shear viscosity of CPNC (Ube 1015C2) with indicated wait time between consecutive shear rate experiments. (From Utracki [2004].)

where at the constant rate of shearing the shear stresses are taken, respectively, at maximum, $\sigma_{12,\max}$, and at equilibrium, $\sigma_{12,\infty}$, and $\tau\sigma$ is an average relaxation time of the mesogens or clay platelets (i.e., the time required for randomization of fully shear-oriented mesogens). Thus, the behavior is explained by the orientation and interaction of anisometric particles [Viola and Baird, 1986]. Similar stress growth behavior is expected in extensional flow, but there the changes should be faster.

The domain flow theory of LCP assumes a balance between the alignment tendency under a velocity field and the elastic resistance to deformation of the director field [Marrucci, 1984]. The average value of the Eriksen distortion stress, σ_E, was taken as proportional to the elastic constant, K, and inversely proportional to the domain size. The flow behavior should depend on the local orientation: for high velocity in the region where the orientation director and velocity vector are parallel to each other, with low velocity for the opposite direction. As a result, the relation between the stress and the deformation rate might be scaled by the domain size:

$$\left.\begin{aligned} \sigma_E &\cong K\left(\frac{1}{a^{*2}} - \frac{1}{a_0^{*2}}\right) \\ \sigma &= \frac{\eta_{\text{equil}}\,\dot{\gamma} a_0^*}{a^* - a_0^*} \end{aligned}\right\rangle \quad \Rightarrow \quad \left\langle \begin{aligned} \eta_{\text{reduc}} &\equiv \frac{\eta}{\eta_{\text{equil}}} = \frac{1}{1-x^*} \\ \dot{\gamma}_{\text{reduc}} &= \dot{\gamma}\frac{a_0^{*2}\eta_{\text{equil}}}{K} = \frac{(1+x^*)(1-x^*)^2}{x^{*3}} \\ x^* &\equiv \frac{a^*}{a_0^*} \end{aligned}\right. \tag{16.11}$$

where $a_0{}^*$ and a^* are domain sizes in region I and during the flow, respectively. The reduced viscosity, η_{reduc}, and the reduced domain size, x^*, within LCP regions

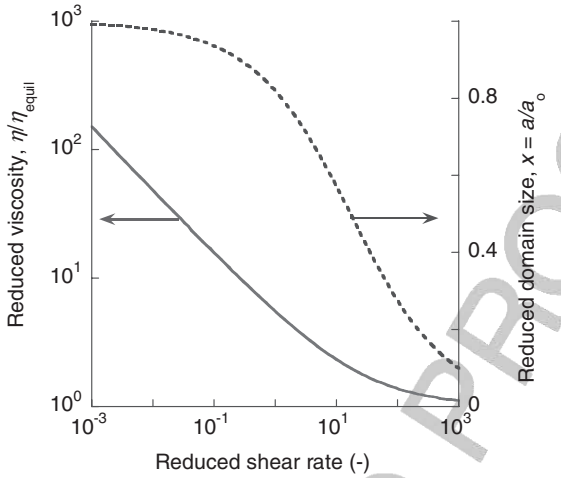

FIGURE 16.5 Reduced viscosity and domain size versus reduced shear rate in regions I and II for LCP. (After Marrucci [1984].)

I and II are displayed in Figure 16.5. The reduced viscosity, η_{reduc}, versus reduced deformation rate has two asymptotic limits; at low rates the initial log-log slope $= -\frac{1}{2}$, whereas at high rates in region II the log-log slope $= 0$. Thus, the derivation provides explanations for the shape of the flow curves of LCPs. Since the theory postulates the presence of large domains with aligned particles, it may be useful for interpreting the flow behavior of CPNC systems as well.

The van der Waals interactions between flat circular platelets of diameter D and thickness t separated by distance d were described by Russel et al. [1989]:

$$U_A = 64k_BTn_0\bar{\lambda}^2 \exp\{-\kappa d\} + \frac{A_H D^2}{12\pi}\left[\frac{1}{d^2} + \frac{1}{(2t+d)^2} - \frac{2}{(t+d)^2}\right] + \frac{m_1^2\Pi_2 + m_2^2\Pi_1 + (m_1m_2)^2/3k_BT + 3h\Pi_1\Pi_2\nu_1\nu_2/2(\nu_1+\nu_2)}{\left(4\pi\varepsilon_0 d^3\right)^2} \tag{16.12}$$

where $\bar{\lambda} = \tanh\{1.6 \times 10^{-19}\psi_s/4k_BT\}$. In Eq. (16.12), ψ_s is the surface energy, m_i ($i = 1, 2$) are the permanent dipole moments of platelets $i = 1$ and 2, Π_i their polarizabilities, ν_i ionization frequencies, $2\pi h = 6.6256 \times 10^{-34}$ J·s (Planck constant), and the permittivity in vacuum, $\varepsilon_0 = 8.854 \times 10^{-12}$ C^2/J·m. The Hamaker constant, $A_H = 2 \times 10^{-21}\ \Psi_s$ (mJ/m^2); thus, for clays, $A_H \approx 2 \times 10^{-20}$ J. Figure 16.6 shows U_A versus d dependence for interacting platelets. It is noteworthy that when platelets are at a distance <3.75 nm, the van der Waals forces are larger than those of C–C bonds and attempts at mechanical exfoliation would lead to matrix degradation. Fortunately, the presence of an adsorbed organic layer moderates these forces significantly [Bousmina, 2006].

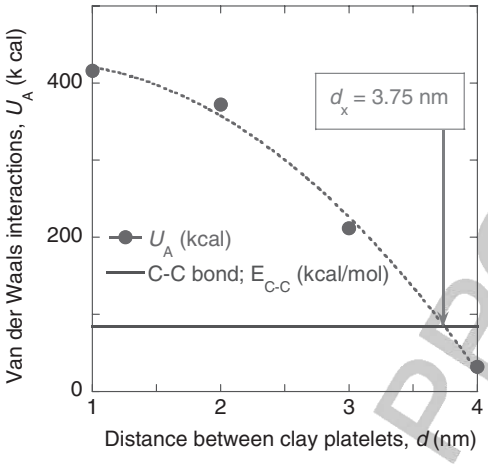

FIGURE 16.6 Interactions between two clay platelets of diameter 100 nm and thickness 1 nm, separated by a distance d. (Calculated from Bousmina [2006].)

For colloidal suspensions of spherical particles the concentration changes their separation d uniformly. Thus, one might predict the phase transitions between diluted, caged, or close-packed structures by calculating the attractive interactions from Eq. (16.12) and postulating a specific type of repulsive interactions. The transitions are detectable in plots of η_r versus the reduced stress:

$$\sigma_r = \frac{\sigma_{12}}{\sigma_C}\,\sigma_C = \frac{D^3}{8k_BT} \tag{16.13}$$

where σ_C is the critical stress and D is the particle diameter. The non-Newtonian viscosity ratio depends on concentration and stress in the full range, $\sigma = 0 - \infty$ [Quemada and Berli, 2002]:

$$\frac{\eta(\sigma)}{\eta(\sigma \to \infty)} = \frac{1+\sigma_r}{\Upsilon + \sigma_r} \tag{16.14}$$

where

$$\Upsilon \equiv \frac{1-\phi/\phi_0}{1-\phi/\phi_\infty} = \begin{cases} \dfrac{\eta_\infty}{\eta_0} & \text{for} \quad \phi < \phi_0 \\ \dfrac{-\sigma_Y}{\sigma_C} & \text{for} \quad \phi \geq \phi_0 \end{cases}$$

with σ_y the apparent yield stress. The flow of CPNCs is more complex, as the structure involves free rotation, the formation of rotating domains, both sensitive to stress and strain.

Mobuchon et al. [2007] studied the viscoelastic properties of a model system comprising 4 wt% C15A† (Cloisite C15A = MMT intercalated with a 25% excess of dimethyl dihydrogenated tallow ammonium, MMT-2M2HT) in a nonpolar Newtonian fluid consisting of a blend of two miscible low-molecular-weight poly(butane-*co*-ethylene), with $\eta = 28.5$ Pa·s at 25°C. The system was not exfoliated, although some individual platelets were seen between stacks. The authors analyzed the effects of flow history on the linear and nonlinear viscoelastic properties. They found that different pre-shear rates created different structures, but with similar recovery kinetics. As reported for a number of nonexfoliated systems, at low frequency the suspension exhibited a solidlike behavior, also dependent on flow history. A low pre-shear rate caused development of stronger pseudoequilibrium structures. The authors also reported that stress overshoots in reversed stress experiments could be scaled with strain, although the maximum overshoot increased with shear rate and rest time.

In summary, the model systems discussed in this part were zero-shear suspensions of disk-shaped particles in Newtonian liquids, mica-filled polymeric composites, LCPs and colloidal suspensions. The LCP model offers a good understanding of the flow behavior of exfoliated CPNCs. In the case of intercalated systems similar behavior is expected but is complicated by stress-induced changes in the degree of the dispersion and aspect ratio, as well as other possible modifications, such as the thermal decomposition of intercalant.

16.2 MELT RHEOLOGY

The rheological studies of PNCs are discussed in a sequence starting with the flow behavior in steady-state shearing, then in small-amplitude oscillatory and elongation flows, and terminating with mathematical modeling. Most studies on PNC flow have focused on the linear viscoelastic behavior. The attention is drawn to the solidlike behavior at small deformation rates, claiming that the nonterminal flow region is the most important PNC characteristic. However, such behavior has been observed in all MPSs having a percolated three-dimensional network i.e., in suspensions, ionomers, polymer alloys (e.g., compatibilized, low concentration blends [Utracki and Kamal, 2002]), composites, and foams [Utracki, 1988, 1995, 2004; Krishnamoorti and Yurekli, 2001; Solomon et al., 2001]. Thus, such behavior is not unique for PNCs, but related to the presence of three-dimensional structures. Furthermore, the argument that in PNCs the percolation threshold is reached at lower volume loading than for spheres is only partially correct. The situation is more complex in multicomponent PNCs (e.g., in those that contain compatibilizers with strongly polar end groups, which might form dispersed dipole–dipole or ionic micelles). It seems that stress overshoots at the startup of steady-state shearing, and studies of the time lag for the randomization of particle orientation, constitute a better diagnostic tool.

†In this chapter the customary abbreviations for Cloisites are used: C15A, C20A, C25A, C30B, and so on.

16.2.1 Stress Overshoots in Shear

Measurements of the transient rheological properties started in 1964 when the Weissenberg rheogoniometer became available. The device was modified by Meissner, and network theories of entangled polymers have been used to interpret the observations [Carreau, 1972; Meissner, 1972; Stratton and Butcher, 1973; Murayama, 1981]. Characteristically, the magnitude of N_1 overshoot is larger and delayed in comparison to that of σ_{12}. A plot of $\sigma_{12}(t)/\sigma_{12}(\infty)$ versus $\gamma = \dot{\gamma}t$ resulted in a master curve characteristic of the melt. Typical relaxation times for N_1, and σ_{12} and for melt reentanglement have been reported as 54, 3.6, and 385 s, respectively [Dealy and Tsang, 1981]. The stress overshoot, $\sigma_{12}(t)$, reached a maximum at a strain, $\gamma \approx 5$. Stress overshoot, flow reversal and relaxation experiments have been carried out on LCP solutions [Walker et al., 1995]. The master curve reached a maximum at $\gamma \approx 22$. It is noteworthy that while LCP is a model for PNCs, owing to differences in size between mesogens and clay platelets, the time scale for the orientation–disorientation of particles is expected to be different.

Solomon et al. [2001] studied the flow-induced structural changes in polypropylene (PP)–based PNCs by measuring the stress growth and flow reversal behavior. The CPNCs contained 2.03 to 4.8 wt% MMT-ODA and PP-MA compatibilizer. The stress growth was measured at shear rates of $\dot{\gamma} = 0.005$ to $1.0\,s^{-1}$. As shown in Figure 16.7, the overshoot went through a maximum at $\dot{\gamma} = 0.5\,s^{-1}$. The stress versus strain curves reached a maximum at $\gamma \approx 0.6 \pm 0.3$. Measurements of the flow reversal stress overshoot were carried out at $\dot{\gamma} = 0.1\,s^{-1}$. The overshoot increased regularly with the rest time, t_{rest} (interval between preshearing and flow reversal). The data followed the scaled relation $[\sigma_{12}(\max)/\sigma_{12}(\infty) - 1]/w\,(\text{MMT})$ versus t_{rest}. The authors observed that the structures relaxed faster than expected. The system was not totally exfoliated, but it contained compatibilized clay stacks. The stress responses have been controlled

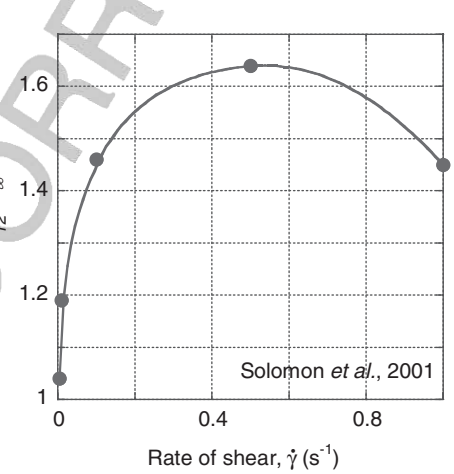

FIGURE 16.7 Scaled stress growth at startup versus shear rate for PP-based PNC containing 4.8 wt% MMT-ODA and maleated-PP as compatibilizer. (From Solomon et al. [2001].)

by hydrodynamics, while the fast disorientation was driven by stress relaxation and randomizing Brownian motion.

A similar relaxation of orientation for PP-based CPNCs with PP-MA was reported by Lele et al. [2002]. The authors presheared the system and then followed the disorientation with XRD. Again, the relaxation time was faster than expected from the theory of Brownian motion. Ren et al. [2000, 2003] studied polystyrene (PS) and poly(isobutylene-*co*-*p*-methyl styrene)–based CPNCs. The interlayer spacing in the system was $d_{001} = 2.1$ to 2.5 nm; thus, it was intercalated only. The authors assumed that the disorientation observed was not governed by Brownian motion but by the stress relaxation of macromolecules.

Thorough rheological studies have been carried out using a commercial, fully exfoliated CPNC from Ube (1015C2 = PA-6 with 2 wt% MMT–dodecyl ammonium acid) [Utracki and Lyngaae-Jørgensen, 2002; Utracki, 2004]. During the reactive preparation of this CPNC, about one-third of MMT anions were neutralized by ammonium cations, which resulted in a CPNC with direct bonding between clay and the matrix through about 30,000 dodecyl paraffinic links. It is noteworthy that the inorganic volume content in these nanocomposites was $\phi = 0.0064$. Specimens prepared by diluting this CPNC with the PA-6 resin matrix to an organoclay content of 0, 0.5, 1.0, 1.5, and 2 wt% were also tested. Even at such a low loading, the dynamic and steady-state flow curves resembled the dependence illustrated in Figure 16.3. Within regions II and III ($\omega > \omega_c = 1.4 \pm 0.2$ rad/s), at strains $\gamma \leq 0.10$ the rheological signals were the same for scans up or down in frequencies, indicating no structural changes. However, at higher strains the shearing up and down in frequencies resulted in different rheological signatures. At high strains and deformation rates, the flow curves for different concentrations of organoclay collapsed onto the dependence characteristic of neat matrix, indicating orientation of clay platelets in the flow direction.

To verify this postulate, two CPNC specimens were prepared, one sheared dynamically between parallel plates (disks) at $\omega = 100$ rad/s and $\gamma = 40\%$ for 15 min, and another just inserted into the rheometer, melted, but not sheared. To determine the clay orientation, the specimens were microtomed close to the disk border (maximum shear strain) in the planar and perpendicular directions and then observed under the high-resolution transmission electron microscope [Perrin, 2002]. In the first specimen the well-dispersed clay platelets (see Figure 16.8) were found to be oriented perpendicular to the stress direction, while in the second, unsheared specimen, the exfoliated, often bent platelets were randomly oriented.

Startup tests for 1015C2 at $T = 240°C$ and $\dot{\gamma} = 0.003$ to $0.01\ s^{-1}$ showed an initial stress growth followed by the signal increase caused by polycondensation. For $\dot{\gamma} > 0.03\ s^{-1}$, stress overshoots were observed. Their magnitude increased consistently with the rate of shearing. Next, interrupted stress growth experiments have been carried out in three stages: (1) preshearing (see the first superimposed peaks in Figure 16.9 for 3 runs), (2) allowing for t_{rest}, and (3) shearing *either in the same or the opposite direction*. Except for the data for $t_{rest} \leq 25$ s (a small effect on the imperfect flow orientation), the platelet randomization during t_{rest} generated the same rheological signal when the shearing was imposed in the preshearing or reversed direction. The overshoot peaks (see Figure 16.9) followed the distribution equation,

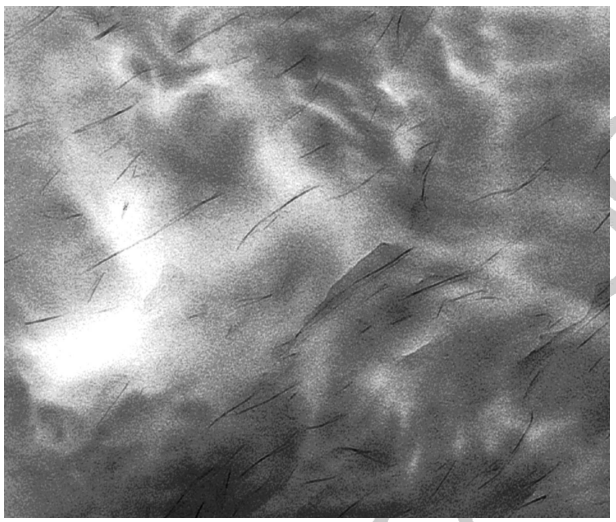

FIGURE 16.8 TEM of PNC from Ube shows "in-plane" orientation of MMT platelets. Orientation in an unsheared specimen was random, with many bent clay platelets. (From Perrin [2002].)

$$\Delta\eta \equiv \eta - \eta_\infty = a_0 t^b (a_1)^t \qquad t = \text{total time} - t_{\text{rest}} \tag{16.15}$$

where $b \approx$ ½is a measure of the width of $\Delta\eta$ distribution, a_0 that of the orientation, and $a_1 \approx 1$ that of the overshoot dissipation rate. Equation (16.15) fitted the data with the correlation coefficient squared (r^2) and the coefficient of determination, both greater than 0.999.

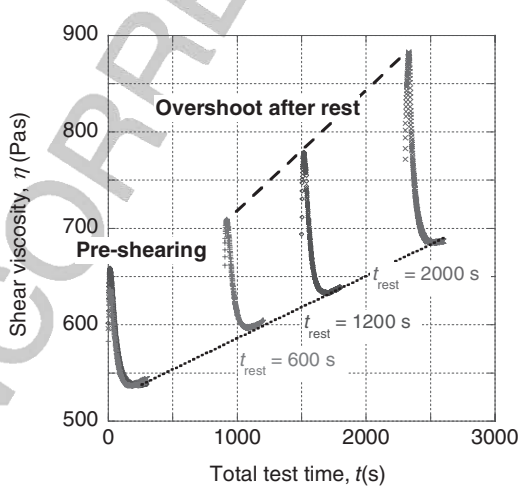

FIGURE 16.9 Transient viscosity responses for PNC presheared at $\dot{\gamma} = 0.1\,\text{s}^{-1}$ for 300 s, relaxed for $t_{rest} = 600$, 1200, and 2000 s, then sheared for 300 s at the same rate. The baseline reflects polycondensation of the PA-6 matrix. (From Utracki [2004].)

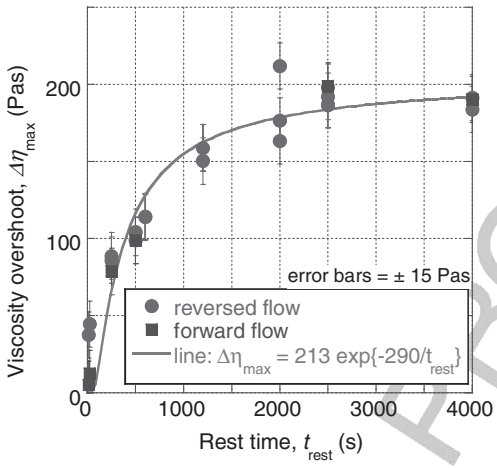

FIGURE 16.10 Viscosity overshoot versus rest time expressed as incremental (over the baseline) shear viscosity for CPNC calculated from the experiments exemplified in Figure 16.9. Utracki [2004].)

Figure 16.10 illustrates the relation between the maximum of the stress overshoot and the rest time, t_{rest}. The maxima, $\Delta\eta_{max}$, were computed as the extrema of Eq. (16.15), setting $d\Delta\eta/dt = 0$. The data follow a single exponential curve:

$$\Delta\eta_{max} = a \exp\left(\frac{-b}{t_{rest}}\right); \quad a = 213 \pm 7, \quad b = 290 \pm 29, \quad r^2 = 0.997 \quad (16.16)$$

Letwimolnun et al. [2007] studied the stress overshoot of PP-based CPNCs with 5 to 30 wt% PP-MA and 5 wt% MMT-2M2HT (C20A). Composition and melt compounding in an internal mixer or a twin-screw extruder (TSE) affected the degree of dispersion, from poor intercalation to exfoliation. The authors presheared the CPNC (forward shearing) and then after t_{rest}, sheared it in the reverse direction, observing increases of the stress overshoot with t_{rest} and with the degree of clay dispersion (estimated from the melt yield stress). Comparing the dependencies in Figures 16.10 and 16.11 it is evident that randomization of orientation in diluted, exfoliated PA-6-based CPNC [Utracki, 2004] is about twice as fast as that of PP/PP-MA/C20A: 1 h versus > 2 h. The slower randomization in the latter system might originate in more massive intercalated stacks and/or higher matrix viscosity.

In the case of intercalated nanocomposites with aggregates, the reversed and forward flows after preshearing might lead to different responses: for example, for PP with 17 wt% ethylene–propylene copolymer, 3.6 wt% PP-MA and 2.4 wt% C20A [Vermant et al., 2007]. After a short rest time, the stress overshoot obtained in forward flow was prominent, whereas no overshoot was seen in the reversed flow. The authors suggested that in the presence of aggregates, the forward flow makes them interlock, whereas the reverse flow disentangles them. By increasing the rest time, flow

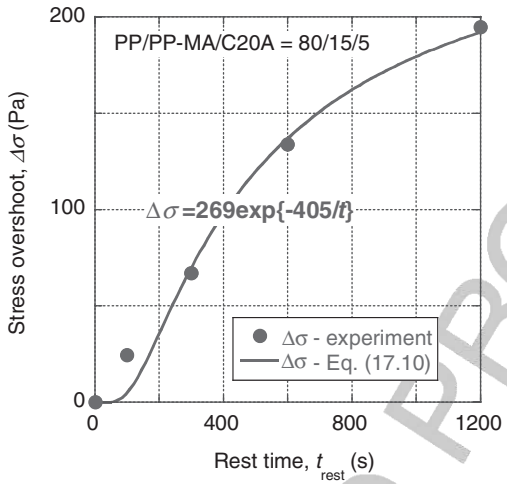

FIGURE 16.11 Stress overshoot in reversed direction versus rest time for CPNC of PP/PP-MA/C20A = 80/15/5 prepared in a TSE; the solid line represents Eq. (16.10). (From Letwimolnun et al. [2007].)

in either direction resulted in similar overshoot. This was explained by the attractive interparticle forces, which create a more uniform particle network, and the differences between structures in the two directions diminish. Because of the tendency for the creation of three-dimensional structures, the linear viscoelastic behavior of CPNC is usually limited to a low deformation rate and/or strain (e.g., nonlinearity at 1% strain has been reported) [Solomon et al., 2001; Lee and Han, 2003a,b].

Li et al. [2003] postulated that the storage modulus of CPNCs, G', is a sum of three contributions: these of the polymer matrix (G'_p), the confinement in the intercalated stacks (G'_c), and the interparticle frictional interactions between tactoids (G'_i):

$$G'_{\text{CPNC}} = G'_p + G'_c + G'_i \tag{16.17}$$

The latter contribution is the most sensitive to concentration, sharply increasing above the percolation threshold, $\phi > \phi_p$. Experimentally, ϕ_p was determined by plotting low-frequency G' values versus clay content. At $\phi < \phi_p$, liquidlike rheological behavior was observed, whereas above it, $\phi > \phi_p$, the behavior was solidlike. The stress overshoot at startup increased with clay loading and deformation rate, and it was scaled by strain. Similarly, the stress overshoot after a rest period in the intercalated CPNC also scaled with strain; hence, the randomizing Brownian motion has a small effect on the behavior of these systems.

Poly(butylene terephthalate) (PBT) was melt compounded at 230°C with C10A (MMT preintercalated with dimethyl benzyl hydrogenated tallow ammonium) [Wu et al., 2005a]. The clay concentration was 0 to 8 wt% and $d_{001} = 3.4$ to 3.7 nm; thus, CPNC was only intercalated. The linear viscoelastic region was observed for $\gamma < 0.01$

and $\phi_p \approx 0.03$, but the stress overshoot at startup or after flow reversal was observed only for clay loading of $\phi \geq 0.06$. As reported for other intercalated systems, the overshoot scaled with strain, indicating a LCP-type phase behavior, with interactions between the tactoids.

During the last few years, in addition to natural and synthetic layered silicates (such as clays) other layered inorganics have been used in PNCs (e.g., LDH) [Utracki et al., 2007]. The rheological studies of these systems are scarce. Costa et al. [2005, 2006, 2008] used Mg–Al-based LDH for reducing the flammability of low-density polyethylene (LDPE). PNCs with or without maleated LDPE (LDPE-MA) were studied. LDH platelets had hexagonal or circular disk geometry with diameter of less than 60 nm and were 0.76 nm thick. In LDPE they mainly formed aggregates up to a few hundred nanometers thick and up to 3 μm long, with few individual platelets. Because of the cationic nature of LDH, these particles interacted with LDPE-MA, which in turn increased the non-Newtonian behavior at low frequency. PNCs with 5 or 10 wt% LDH were rheologically nonlinear with a strong influence of concentration on the stress overshoot in flow reversal. As for clay-containing PNC, the overshoot also increased with rest time. The behavior was interpreted as caused by the presence of three-dimensional structures formed by the aggregation of LDH stacks, which could be ruptured by shear and re-formed during the rest.

In summary, two mechanisms are responsible for stress overshoots after rest. The first is based on randomization of the orientation imposed by Brownian motion and relaxation of the matrix, whereas the second assumes that a three-dimensional structure is broken by shearing and re-forms under quiescent conditions. The former mechanism is expected to be applicable to LCP and exfoliated PNC, where platelets are still able to rotate freely. The second mechanism dominates the intercalated systems, especially those with large low-aspect-ratio stacks. The probability of the Brownian force contribution might be assessed from the rotary diffusivity coefficient and the diffusion time [Larson, 1999]:

$$D_r = \frac{3k_B T}{4\eta_m D^3} \quad \Rightarrow \quad t_D \simeq \frac{(\pi/2)^2}{D_r} = \frac{\pi^2 \eta_m D^3}{3k_B T} \tag{16.18}$$

Equation (16.18) postulates that platelets are circular with diameter D, rotating in a matrix of viscosity η_m, at temperature T ($k_B = 1.381 \times 10^{-23}$ J/K is the Boltzmann constant). The time required for a disk to rotate by $\pi/2$ is t_D. For PA-6-based CPNC, substituting into Eq. (16.18) the average clay platelet diameter, $D = 300$ nm, and the matrix viscosity at the processing temperature $T = 500$ K of $\eta_m = 300$ Pa·s, gives $t_D \approx 3800$ s, a value close to the approximate 3600 s determined for the randomization of orientation in Figure 16.11. Thus, Brownian forces may indeed be responsible for the kinetics observed for structural changes in fully exfoliated, diluted CPNC. Evidently, the calculations are only approximate and do not take into account grafting of clay platelets by PA-6 macromolecules, which on one hand increases the effective clay platelet diameter, and on the other hand increases the effective viscosity of the matrix.

A comment regarding intercalated PNC is needed. According to Eq. (16.18), the rate-controlling parameters are D^3 and η_m. The intercalated stacks of even

small-diameter platelets (e.g., $D < 60$ nm) may form aggregates ≤ 3 μm in size [Costa et al., 2005, 2006]. In consequence, t_D calculated for intercalated systems might be five orders of magnitude larger than that calculated for exfoliated PNC; hence precluding the Brownian motion as the randomization mechanism.

16.2.2 Steady-State Shear Flow

Steady-state shearing is important for predicting processability and performance of PNC. After discussing the transient effects and stress overshooting, it is evident that steady-state shearing might seriously affect the structure of extruded or injection-molded PNC articles. Thus, it is expected that shearing from a low to a high deformation rate will engender different flow curves than that from a high to a low shear rate. There are many reports on the effects of flow-induced changes of morphology, such as orientation of clay platelet or the flow effects on the matrix crystallinity [Kojima et al., 1994]. For example, during flow through a die and the subsequent stretching between chilled rolls, the clay platelets in PA-6 matrix became oriented in-plane, while PA-6 crystallized with the chain axes *parallel* to the clay surface. Injection molding of the same CPNC engendered five layer orientations: skin with in-plane orientation for the macromolecules and clay platelets, an intermediate layer with chains oriented *perpendicularly* to the clay surface, and a center layer with clay platelets oriented perpendicular to the flow direction and the macromolecules oriented parallel to it [Kojima et al., 1995]. Thus, during film stretching by rolls or during the fountain flow within the mold cavity, the macromolecular chains are oriented in-plane and crystallize with the chain axes parallel to the clay surface, but at lower stresses the crystal lamellae are laying on the clay surface with chains oriented perpendicularly to it.

Medellin-Rodriguez et al. [2001] studied the orientation of Ube CPNC (with 0, 2, and 5 wt% of organoclay) during steady-state shearing between parallel plates at $\dot{\gamma} = 60\,\mathrm{s}^{-1}$ and $T = 240^{\circ}\mathrm{C}$ for up to 20 min. Under these conditions there was a gradual change in platelet alignment reflected in the increased scattering intensity perpendicular to the shear plane. Tumbling of clay platelets took place at $\phi < \phi_m$, but since the motion was periodic with long residence time in the preferred direction, the overall platelet orientation was in the flow direction [Goldsmith and Mason, 1967]. After stopping the flow, the randomization of orientation was slow (e.g., at $T = 240^{\circ}\mathrm{C}$ it took more than 12 min to randomize the platelets, whereas the PA-6 relaxation time was ≈ 0.4 s).

Since the commercial 1015C2 is exfoliated, well characterized, and available in large quantities, it has been used in a diversity of tests, including melt rheology. For example, it was sheared under steady state in a cone-and-plate geometry, increasing the shear rate from the initial value with "preshearing time" between the consecutive data acquisition points of $\Delta t = 0$ to 540 s (see Figure 16.4). Starting at $\dot{\gamma} = 0.01\,\mathrm{s}^{-1}$ the viscosity, η, decreased from a plateau toward a power-law region [Sammut and Utracki, 2004]. The first normal stress difference of these experiments are presented in Figure 16.12. The value of N_1 is increasing with preshearing time. Two further aspects are noteworthy:

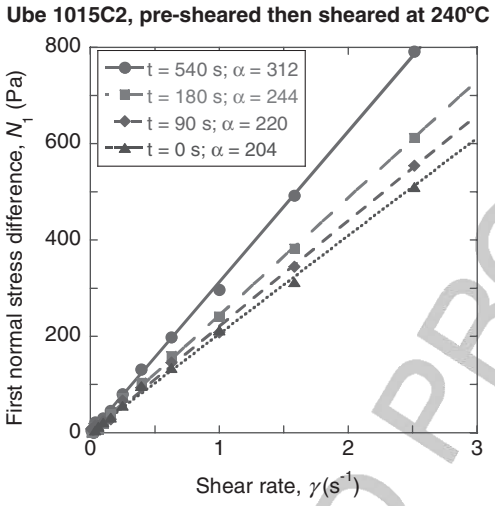

FIGURE 16.12 First normal stress difference, N_1, of Ube 1015C2 PNC versus shear rate; α is the slope of the dependence. (See the text.)

1. N_1 is proportional to the rate of shear, $N_1 = \alpha\dot{\gamma}$, with the α -parameter increasing with the rest time, $\alpha = 205 + 0.206t_{\text{rest}}$ (the correlation coefficient $r = 0.996$).
2. There is a significant difference in the N_1 and η dependencies on $\dot{\gamma}$; in the full range of the accessible variables, $N_1 \propto \dot{\gamma}$, while η shows a more complex behavior.

The proportionality between N_1 and $\dot{\gamma}$ has been observed at low deformation rates for concentrated LCP solutions in cresol [Kiss and Porter, 1980; Moldenaers and Mewis, 1992], for colloidal and noncolloidal suspensions, and fiber suspensions in a Newtonian matrix [Zirnsak et al., 1994], as well as for block copolymers and multibranched star polymers [Brady and Bossis, 1985; Kotaka and Watanabe, 1987; Masuda et al., 1987; English et al., 1997]. For LCP this behavior was considered originating in polydomain flow [Larson and Doi, 1991], while for rigid fiber suspensions in interparticle interactions [Zirnsak *et al.*, 1994]. It is tempting to postulate that the clay platelet orientation is the origin of the difference. Evidently, the scan direction and the pre-shearing time between data points affect the orientation, but the proportionality $N_1 = \alpha\dot{\gamma}$ and complexity of the $\eta = f(\dot{\gamma})$ dependence remain. The Larson–Doi [1991] theory of polydomain flow leads to

$$\frac{N_1}{\sigma_{12}} = 2(\lambda_p^2 - 1)^{-1/2} \qquad \lambda_p = \frac{p'^2 - 1}{p'^2 + 1} \tag{16.19}$$

where λ_p is a characteristic parameter of the system dependent on the domain aspect ratio, p'. Since λ_p is constant, Eq. (16.19) predicts that in domain flow there is proportionality between N_1 and σ_{12}. Unfortunately, such proportionality does not exist for the CPNC studied.

The orientational effects of flow when increasing or decreasing shear rate are not limited to PA-6-based systems, although in PA-6 the exfoliation makes the effects particularly large. By contrast to clay behavior in PA-6, in PS, clay platelets are notoriously difficult to disperse. However, even for these systems, different flow curves were reported for shearing up and down the $\dot{\gamma}$ scale [Hyun et al., 2001; Kim et al., 2002]. The authors named the phenomenon *hysteresis loops*. Figure 16.13 presents the dynamic viscosity, η', and dynamic elasticity, G'/ω^2, versus ω, thus, a similar dependence as that for steady-state shearing displayed in Figure 16.4 for $\Delta t = 0$ s. Two specimens were sheared, one for increasing ω and the other for decreasing ω. The results are different, despite the significantly weaker orientational effects of small-amplitude oscillatory flow than that of steady-state shearing. Similar observations were reported for flow of polyamide-12 (PA-12) with 2.5 wt% C30B [Médéric et al., 2006].

Results from the capillary flow of CPNCs are less interesting. Since the nature minimizes the expenditure of energy, during MPS flow the less viscous phase migrates to the high-stress areas, hence toward the wall [Utracki and Kamal, 2002]. During the flow of suspensions through tubes the solid particles migrate away from the wall, either to the tube axis, or to an annulus midway between the tube wall and the axis [Whitmore, 1962]. In consequence, in capillary flow clay platelets migrate away from the wall and the viscosity decreases to the level of the matrix polymer. However, since migration takes time, the closeness of the flow curve of CPNCs to that of the matrix depends on several factors (i.e., the capillary length-to-diameter ratio, the stress level, composition, etc. [Aalaie et al., 2007]. The steady-state shear flow curves obtained for PS with $w = 0$ to 9 wt% organoclay in parallel-plate experiments merged to a common dependence at high $\dot{\gamma}$ [Han et al., 2006].

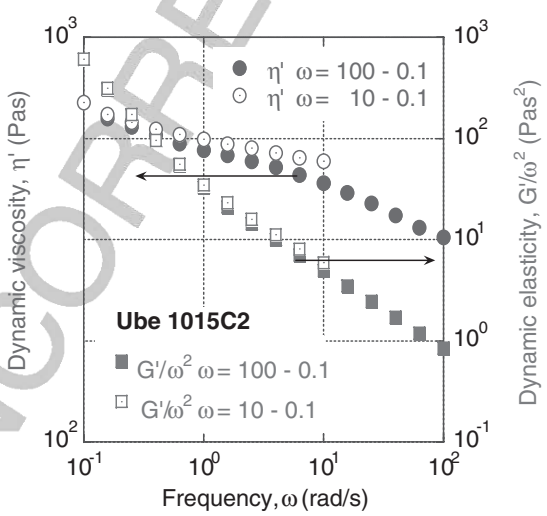

FIGURE 16.13 Dynamic viscosity and elasticity of 1015C2 versus frequency. Two samples were sheared, one with increasing ω and the other one with decreasing ω. (From Sammut and Utracki [2004].)

In the case of compatibilized systems it may be the low-viscosity compatibilizer that is forced to migrate toward the wall. In such a case, the CPNC viscosity at low $\dot{\gamma}$ are larger than that of neat polymer, but smaller at high $\dot{\gamma}$. Numerous examples of this behavior have been reported [Wang et al., 2003; Gu et al., 2004]. Manifestly, the magnitude of the effect depends on the relative (to the matrix) viscosity of the compatibilizer and its concentration [Lee *et al*., 2006].

Lee *et al.* [2007] studied the rheological behavior of poly(ethylene-*co*-vinyl acetate) (EVAc; 40 wt% VAc) and its CPNC with $\leq$ 10 wt% C30B; the tests were conducted under steady-state and small oscillatory shear flow. The samples were prepared by melt compounding at 110°C for 25 min, which resulted in a high degree of dispersion. The flow behavior was quite regular, well described by the Carreau-Yasuda equation [Carreau, 1968, 1972; Yasuda, 1979]:

$$\frac{\eta - \eta_\infty}{\eta_0 - \eta_\infty} = \left[1 + (\tau\dot{\gamma})^a\right]^{(n-1)/a} \tag{16.20}$$

where η_0 and η_∞ are the viscosities at $\dot{\gamma} \to 0$ and $\dot{\gamma} \to \infty$, respectively, while τ and n are, respectively, the primary relaxation time, and the power-law index. The variations of these parameters with C30B content are displayed in Figure 16.14; the dependencies are similar to those for a series of polymers with increasing molecular weight. One might suppose that clay platelets are grafted by EVAc, forming multibranched copolymer molecules with polar center and nonpolar skin, behaving as a homopolymer and unable to form three-dimensional structures.

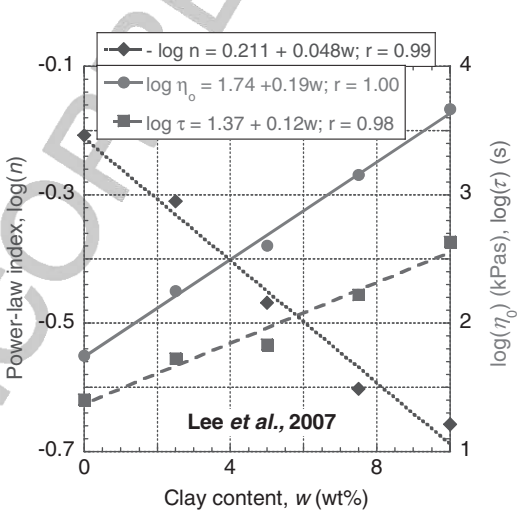

FIGURE 16.14 Semilogarithmic plot of the zero-shear viscosity, maximum relaxation time, and the power-law index versus clay concentration for EVAc–C30B. (From Lee et al. [2007].)

16.2.3 Small-Amplitude Oscillatory Shear Flow

Because of the complications caused by the stress-induced orientation of clay platelets resulting in different rheological responses, the studies of CPNC flow focus on small-amplitude oscillatory shear flow (SAOS). As the discussion on the steady-state flow indicates, there is a great diversity of structures within the CPNC family. Whereas some nanocomposites form strong three-dimensional structures, others do not; thus while nonlinear viscoelastic behavior is observed for most CPNCs, some systems can be studied within the linear regime.

SAOS tests of CPNC should start with strain sweeps to determine the range of variables where the linear viscoelasticity is to be found. The strain sweep data might be described by KBKZ-type nonlinearity expression [Utracki and Lyngaae-Jørgensen, 2002]:

$$G'(\gamma) = \frac{G'_0}{1 + G'_1\gamma_f^2 - G'_2\gamma_f^3}$$

$$G''(\gamma) = \frac{G''_0}{1 + G''_1\gamma_f^2 - G''_2\gamma_f^3} \tag{16.21}$$

where G' and G'' represent the storage and loss shear modulus, respectively; the strain fraction is $\gamma_f = \gamma/100$, and G_i are equation parameters with G_0 defining the linear viscoelastic values of G' and G''. One of the advantages of the linear region is the validity of the time–temperature (t–T) superposition principle—thus the possibility of extending the studies over many decades of frequency [Ferry, 1980].

Krishnamoorti et al. [1996] reported the t–T superposition for the end-tethered CPNCs of PA-6 and poly(ε-caprolactone). The authors observed that orientation of clay platelets depends on the amplitude of dynamic stress. The alignment changed the slope within the terminal zone, reduced the dynamic moduli, and affected the complex viscosity, η^*, at $\omega \leq 3$ rad/s. The effects were related primarily to changes in G', caused by enhanced interactions between the flow domains. Utracki [2004] reported good t–T superposition for the PA-6-based CPNC, 1015C2. Presheared samples were scanned from $\omega = 100$ to 0.1 rad/s at $T = 230$ to 260°C; as shown in Figure 16.15, good superposition was obtained. It is noteworthy that whereas 1015C2 is exfoliated, the CPNCs based on PS are not. However, the t–T superposition was also obtained for the latter, having large stacks and behaving like diluted suspensions [Sepehr et al., 2005].

The frequency shift factor, a_T, has been related to the free-volume fraction, f [Ferry, 1980]. There is a direct correlation between f and the Simha–Somcynsky (S-S) hole fraction, h [Utracki and Simha, 2001b]. Under ambient pressure, h depends on the reduced temperature [Utracki and Simha, 2001a]:

$$\begin{aligned} h &= a_0 + a_1\widetilde{T} + a_2\widetilde{T}^2\,; \quad \text{where} \quad \widetilde{T} \equiv \tfrac{T}{T*} \\ a_0 &= -0.0921; \quad a_1 = 4.89; \quad a_2 = 12.56; \quad r^2 = 0.99999 \end{aligned} \tag{16.22}$$

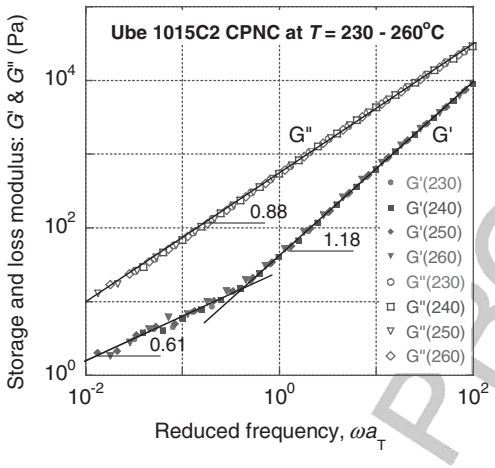

FIGURE 16.15 Time–temperature superposition: dynamic moduli versus reduced frequency for 1015C2. Slopes of the three lines are indicated. (From Utracki [2004].)

with T^* being the characteristic for a given substance temperature-reducing parameter (see Chapter 6). Equation (16.22) leads to a general expression for the shift factor between two reduced temperatures, $\widetilde{T}$ and $\widetilde{T}_0$:

$$\ln a_T = B\left(\frac{1}{a_0 + a_1\widetilde{T} + a_2\widetilde{T}^2} - \frac{1}{a_0 + a_1\widetilde{T}_0 + a_2\widetilde{T}_0^2}\right) \tag{16.23}$$

where $B \approx 2.21$. Alternatively, one may cast Eq. (16.23) into Williams–Landel–Ferry (WLF) form [Williams et al., 1955]:

$$\ln a_T = \frac{-(B/h_0)\{(\widetilde{T} - \widetilde{T}_0)[1 + (a_2/a_1)(\widetilde{T} + \widetilde{T}_0)]\}}{(h_0/a_1) + (\widetilde{T} - \widetilde{T}_0)[1 + (a_2/a_1)(\widetilde{T} + \widetilde{T}_0)]} \simeq \frac{-(B/h_0)(T - T_0)}{(h_0/a_1)T^* + T - T_0} \tag{16.23a}$$

For $(a_2/a_1)(\widetilde{T} + \widetilde{T}_0) \simeq 0.18 < 1$, the classical WLF dependence in reduced-temperature form is recovered. Similarly, Eq. (14.23) transforms into an Arrhenius-type expression:

$$\log a_T = a_o + \frac{\Delta H_\eta}{RT} \tag{16.24}$$

For Ube 1015C2 the experimental value of the activation energy of flow, $\Delta H_\eta = 18$ kJ/mol, agrees with the value calculated from Eq. (16.24) with $T^* = 11{,}307$ K computed from the pressure–volume–temperature (PVT) measurements for the matrix PA-6 [Utracki et al., 2003].

Within the linear viscoelastic region the modified Krieger–Dougherty [1959] dependencies might be used [Utracki, 1988; Utracki and Lyngaae-Jørgensen, 2002]:

$$\eta' \equiv \frac{G''}{\omega} = \eta_0 \left[1 + \frac{G''}{G_\eta}\right]^{-m_1} \qquad \psi \equiv \frac{G'}{\omega^2} = \psi_o \left[1 + \left(\frac{G''}{G_\psi}\right)^2\right]^{-m_2} \tag{16.25}$$

where η_o, Ψ_o, G_η, and G_Ψ are constants. Equation (16.25) is valid at clay content $\phi < \phi_m$; for $\phi > \phi_m$ the three-dimensional structure engenders the apparent yield stress, which follows the relation [Utracki, 1989]

$$\sigma_y(\omega) = \sigma_y^0[1 - \exp(-\tau_y \omega)]^u \tag{16.26}$$

where the strength of domain interactions is σ_y^o, the relaxation time of the aggregate is τ_y, and the exponent u accounts for the aggregate size polydispersity.

As shown in Figure 16.16, Eqs. (16.25) and (16.26) with $u \simeq 1$, well describe the dynamic behavior with yield of the end-tethered CPNC 1015C2 [Utracki and Lyngaae-Jørgensen, 2002]. By diluting this CPNC it was found that at $\gamma = 0.40$ the yieldlike behavior occurs at $\phi > \phi_m \simeq 0.12$. Thus, according to Eq. (16.9), the effective aspect ratio of the interacting entities is $p \approx 200$. Independent of dilution, the onset of the yieldlike behavior occurred at $\omega_c \approx 1.4 \pm 0.2$ rad/s, related to the relaxation time of the aggregate, $\tau_y = 4.5$ s. At given T and γ, the aggregates are destroyed at frequencies above ω_c. This relaxation time is significantly longer than that for PA-6: $\tau_{PA} = 0.2$ s. If ω_c reflects the transition from region I to II of the LCP-type behavior, then the domain size, calculated from the expression [Marrucci, 1984],

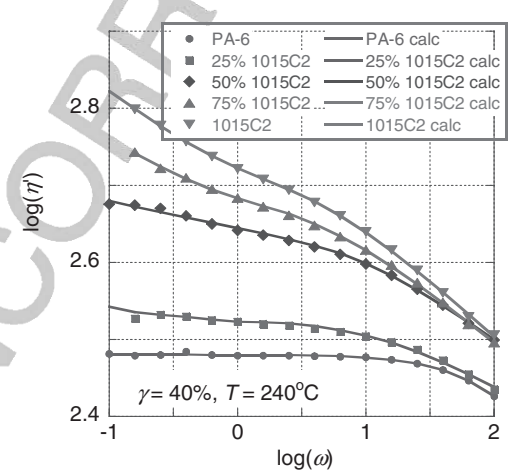

FIGURE 16.16 Frequency scans for diluted 1015C2. Points are experimental; lines computed from Eqs. (16.25) and (16.26). (From Utracki and Lyngaae-Jørgensen [2002].)

$$\dot{\gamma} \simeq \frac{K}{a_0^2 \eta_{\text{equil}}} \tag{16.27}$$

is $a_o \approx 300$ nm for the three compositions with 100, 75, and 50 wt% of 1015C2 and comparable to the nominal value, $a_o \approx d = 286 + 2z_1 = 298$ nm, where $z_1 = 6$ nm is the thickness of solidified layer on the clay surface.

It has been shown that for an incompressible linear viscoelastic liquid there is an interrelation between G' and G'' through the frequency relaxation spectrum, $H(\lambda)$ [Utracki, 2004]:

$$\frac{G'}{\omega^2} = \lambda \left(\frac{G''}{\omega} \right) \quad \text{or} \quad \psi(\omega) = \lambda \eta'(\omega) \tag{16.28}$$

with λ being a relaxation time. A relation between G' and G'' might also be obtained from Doi–Edwards theory as log (G'/G''), usually plotted versus log G'' [Doi and Edwards, 1978]. Figure 16.17 illustrates the Eq. (16.28) dependence for PA-6 containing 0, 25, 50, 75, and 100% of 1015C2. The data for PA-6 have a slope of –0.23, originating in polycondensation (the test was run from the highest to the lowest frequency). The λ value for PNC systems is larger and more sensitive to frequency. The increase is due not only to PA-6 polycondensation but also to structural changes up to the critical frequency $\omega_c \simeq 1.4 \pm 0.2$ rad/s. It is noteworthy that the slopes for the lower frequencies, $\omega < \omega_c$, are significantly smaller and similar for all the dilutions, indicating similar structure for the CPNC samples.

An early review on PNC reported that with clay loading the slopes at low-frequency dynamic storage and loss moduli change, from liquidlike to solidlike [Giannelis

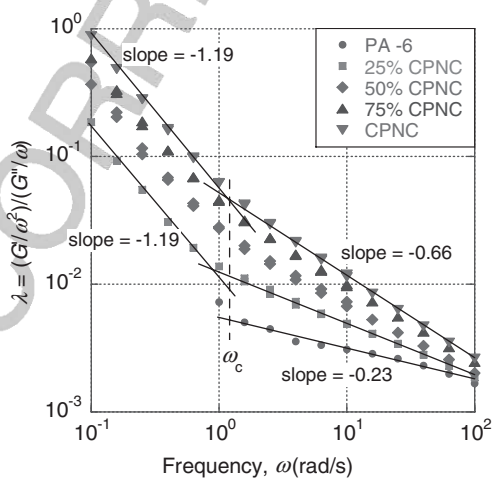

FIGURE 16.17 Frequency dependence of the parameter λ for PA-6 and its mixtures with Ube 1015C2 CPNC. (See the text.)

et al., 1999]:

$$g' \equiv \frac{d\log G'}{d\log\omega} \qquad g'' \equiv \frac{d\log G''}{d\log\omega} \tag{16.29}$$

Thus, for PCL-based CPNCs, g' decreased from 2 to 0.5 (PCL + 5 wt% organoclay), and g'' from 1 to 0.65. Similar changes were observed for other CPNCs. More recently, Wagener and Reisinger [2003] related the slopes in Eq. (16.29) to the degree of clay dispersion in polybutylene terephthalate (PBT containing 4 wt% MMT). The slope g'' decreased from 0.98 (PBT) or 0.96 (PBT + Na-MMT) to 0.11 (PBT + organoclay). This change was accompanied by an increase in the tensile modulus from 2.5 to 3.5 GPa.

Lim and Park [2001] studied the SAOS behavior of polyethylene (PE)-based CPNCs containing C6A. Within the terminal region the dynamic moduli and their slopes increased with increasing clay content, while the ratio G'(CPNC)/G'(matrix) decreased with increasing frequency. The authors reported that while the noncompatibilized systems were intercalated, addition of maleated-PE (PE-MA) resulted in a high degree of exfoliation even at 5 wt% C6A. With increasing frequency the storage modulus of CPNC drifted toward that of the matrix. Wang et al. [2002] also studied CPNC containing PE-MA but with three silicates: C20A, Laponite SCPX2231, and synthetic SiO_2, having the aspect ratio $p = 100$ to 200, 20 to 30, and 1, respectively. Since XRD did not show diffraction peaks down to $2\theta = 2^{o}$, the systems were well dispersed with $d_{001} \geq 4.4$ nm. The low-frequency slope, $g' \equiv d \ln G'/d \ln \omega$, decreased with silicate loading and their p from g' (matrix) ≈ 1.2 to 0.3, 0.62, and 0.82, respectively. It is noteworthy that exfoliation is not the only mechanism leading to slope reduction (e.g., formation of clay aggregates, phase separation, or presence of compatibilizer micelles leads to similar effects) [Lepoittevin et al., 2002]. Similarly, melt blending PP: PP-MA = 0: 1 or 1: 1 with C6A resulted in intercalated CPNC with $d_{001} = 3.3$ nm [Galgali et al., 2001]. The low-frequency ($\omega = 0.06$ to 1 rad/s) "terminal" slope was analyzed using the dependence

$$\begin{aligned} g'_o &\equiv \lim_{\omega\to 0}\frac{d\log G'}{d\log\omega} = a_o + a_1 w_{PP-MA} + a_2 w_{\text{clay}} + a_3 t \\ a_{\text{o}} &= 1.48 \pm 0.09 \qquad a_1 = -0.085 \pm 0.013 \qquad a_2 = -0.043 \pm 0.015 \\ a_3 &= -0.028 \pm 0.027 \qquad \text{standard deviation } \sigma = 0.15 \end{aligned} \tag{16.30}$$

where w represents wt% of compatibilizer and clay. The parameters indicate that the strongest influence was that of PP-MA, next was the clay content, and then the time under stress ($t = 0$ to 3 h). The dynamic yield stress was observed only after compatibilization. Since PP-MA had a small influence on d_{001}, it was probably located outside the clay stacks, and reduction of g' was caused by the formation of interactive three-dimentional structures. The compatibilized CPNC also showed lower creep compliance than that for PP or noncompatibilized CPNC; PP-MA enhanced three-dimentional solidlike structures to a level similar to that observed for end-tethered PA-6-based systems. The zero-shear viscosity, $\eta 0$, increased

with PP-MA or clay loading, while the activation energy of viscosity remained constant.

PS-based CPNCs were prepared by melt compounding preintercalated synthetic fluoromica (Somasif ME-100) [Hoffmann et al., 2000]. The latter was intercalated with either amine-terminated PS (ATPS) or 2-phenylethylamine (PEA), expanding the interlayer spacing from $d_{001} = 0.95$ nm to >4 and 1.4 nm, respectively. The SAOS rheological behavior of these systems was quite different; the presence of 5 wt% PEA caused a slight (in comparison to the matrix) increase of $G' = G'(\omega)$ with the gradient $g'_0 \approx 2$, while CPNC containing ATPS was exfoliated — its $g'_0 \approx 0.5$. These experiments confirmed the theoretical conclusions by Balazs and her colleagues that amine-terminated macromolecules are efficient intercalants [1998, 1999].

Okamoto et al. [2000] preintercalated Na-MMT with oligo(propylene glycol) diethyl methyl-ammonium chloride, or methyl-trioctyl-ammonium chloride (SPN and STN, respectively), dispersed the organoclays thus obtained in methyl methacrylate (MMA) or styrene (St) and then polymerized. The interlayer spacing indicated intercalation. The frequency sweeps showed frequency-independent dynamic moduli, indicating a three-dimensional solid for MMA/STN and St/SPN systems. In a better dispersed MMA/SPN system, strong frequency dependence was observed (i.e., exfoliation apparently eliminated the three-dimensional structures).

16.2.4 Extensional Flows

The extensional flow behavior should be determined under well-controlled conditions, recording the stress growth function at a constant Hencky deformation rate, $\dot{\varepsilon}(s^{-1})$, and temperature [i.e., $\log\eta_E^+(\dot{\varepsilon}, T)$ versus $\log t$]. The stress growth function may show either behavior similar to that of steady-state shear, $3\eta_S^+$, or it might show strain hardening (SH)-a nonlinear viscoelastic behavior. SH is defined as a logarithm of a ratio of the stress growth function in elongation to three times that for the linear viscoelastic response in shear, with both values taken at the same T and t. [Sammut, 2007]:

$$\mathrm{SH} \equiv \log\left(\frac{\eta_E^+}{3\eta_S^+}\right)_t \tag{16.31}$$

Thus, for linear viscoelastic materials, SH = 0. SH has been reported for entangled, highly branched, long-chain-branched, or polydispersed resins as well as for the more recent bimodal metallocene polyolefins. Partially cross-linked polymers or blends of standard resins with ultrahigh-molecular-weight homologs may also show SH. For these single-phase polymeric systems all SH functions at a different strain rate plotted versus the Hencky strain, $\varepsilon = \dot{\varepsilon}t$, fall on a single line:

$$\mathrm{SH} = \mathrm{SH}_0 + \varepsilon \cdot \mathrm{SSH} \tag{16.32}$$

where SSH is the slope of SH versus ε. Noteworthy, SSH is a characteristic material parameter; experimentally, its value, SSH ≈ 0.2, was calculated for long-chain

branched polymers as well as calculated for PP-MA-based CPNCs from data by Okamoto et al. [2001 b,c]. Equations (16.31) and (16.32) demonstrate that changes from linear to nonlinear flows originate in the strain-induced structural changes.

Multiphase polymeric systems respond differently to extensional stresses. For example, exceptionally, diluted suspensions show strain softening, SS [Utracki, 1984; Takahashi, 1996]. This behavior was traced to a disturbance of the stress distribution around solid particles during extensional flow. However, when the concentration of filler particles was large enough to engender three-dimensional structures, the apparent yield stress was seen to affect the level of the stress growth function (i.e., at a low strain rate, the signal was significantly higher than at a high rate). Because of the yield stress effects, the superposition of the stress growth function usually observed [Eq. (16.32)], is absent [Mutel et al., 1984]. For short glass fiber (≤ 40 wt%)–filled PP, neither SH nor SS was observed. However, the question is whether CPNCs with the hairy clay platelet (HCP) morphology will show either SH or SS.

The first report of the elongational flow behavior of CPNCs came from Okamoto's laboratory [Okamoto et al., 2001a–c; Nam et al., 2001, 2002]. The authors studied the flow of melt-compounded CPNC of PP-MA with 0, 2, 4, and 7.5 wt% of MMT-ODA. The silicate stacks were 193 to 127 nm long and 5 to 10.2 nm thick, with $d_{001} \simeq 2.31$ to 3.24, 3.03, and 2.89 nm, respectively. The measurements were carried out in a Meissner-type elongational rheometer (RME) at $T = 150°C$ and $\dot{\varepsilon} = 0.001$ to $1.0\,s^{-1}$. The SH behavior was quite unique; since PP-MA melt did not show SH, its presence in CPNCs must have originated from grafting clay platelets by PP-MA. At 4 wt% organoclay loading, the effect was large (see Figure 16.18), decreasing regularly as the strain rate increased. Figure 16.19 shows that at constant Hencky strain, $\varepsilon = 0.3$; SH followed the power-law dependence: $SH_\varepsilon \approx a_0\dot{\varepsilon}^{-a_1}$. The authors traced the strong

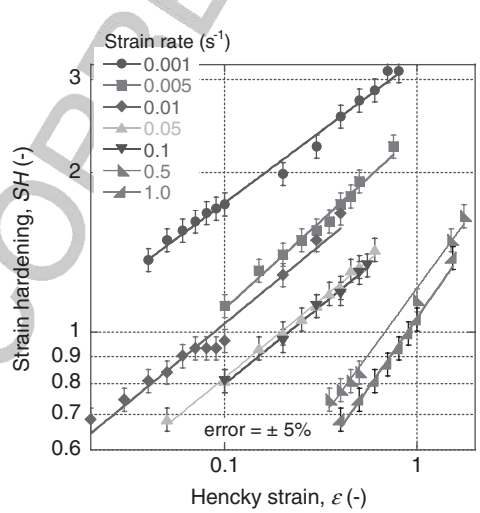

FIGURE 16.18 Strain hardening for CPNC of PP-MA with 4 wt% C18-MMT ($d_{001} = 3.03$ nm). (Data from Okamoto et al. [2001b,c].)

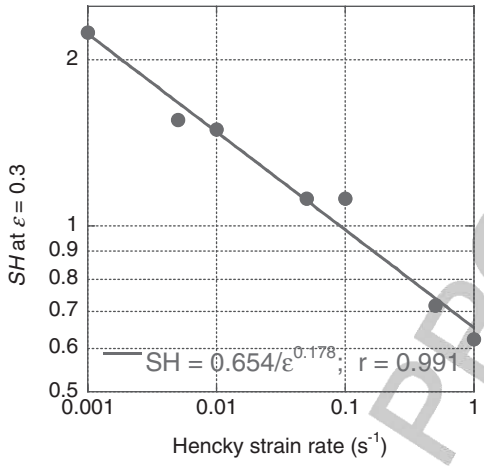

FIGURE 16.19 Cross-plot of SH from Figure 16.18 at the Hencky strain $\varepsilon = 0.3$ vs. Hencky strain rate, $\dot{\varepsilon}$. See text.

SH for CPNCs containing a small amount of clay to the presence of house-of-cards structures, resulting in the yield behavior. The flow-induced structures were different in shear and elongation.

One of the consequences of the high SH value of CPNCs is its foamability, expected in multiphase systems from the yield stress behavior [Utracki, 1995]. Furthermore, owing to high SH, the foams should have good dimensional stability. It is noteworthy that SH stabilizes such processes as film blowing, blow molding, wire coating, and extrusion foaming. More recently, SH was reported for PP as well as its CPNC with 5 wt% C15A and PP-MA [Lee et al., 2006]. In the Meissner-type Rheometrics elongational rheometer (RME) at $\dot{\varepsilon} = 0.05$ to 1 s^{-1} the maximum SH was obtained at $\varepsilon = 3$ to 5; SH was absent for noncompatibilized systems, the observation confirmed by Lee and Youn [2008].

High SH values were reported for PS-based CPNCs with 2 or 10 wt% C10A [Tanoue et al., 2004a,b]. Münstedt-type rheometrics extensional rheometer (RER) and RME instruments were used, but deformations in the former were not uniform. The data from RME (at $\dot{\varepsilon} = 0.1$ to 1 s^{-1} and $\varepsilon \leq 4.4$) were corrected for clamp slippage. SH was observed for neat PS ($SSH = 0.12 \pm 0.03$) and that containing 2 or 10 wt% organoclay.

CPNCs with SH were prepared with other polymer matrices, but the effects were smaller than those reported for PP-MA-based CPNC. Thus, PMMA with 10 or 15 wt% smectite preintercalated with methyl diethyl propylene glycol ammonium showed enhancement of the SH above the effect observed for the matrix [Kotsilkova, 2002]. A correlation between SH and birefringence was reported.

Several CPNCs were tested by Sammut [2007], who in addition to RER and RME (equipped with optical interferometry for simultaneous measuring of the width and thickness of deformed specimen, thus the true strain) also used the

Sentmanat extensional rheometer (SER), an add-on to the advanced rheometrics expansion system (ARES; now from TA Instruments). The maximum Hencky strain was about 4. Neither PP nor its CPNC with 5 wt% C15A and PP-MA compatibilizer showed any SH. Also, tests of PA-6 and 1015C2 gave negative results. Only preliminary tests of Toyota experimental 1022C5 (containing 4.91 ± 0.24 wt% MMT, $d_{001} = 5.62 \pm 0.28$ nm, exfoliation degree $= 39 \pm 16\%$) indicated the presence of a small amount of SH at $\varepsilon \approx 1$ and $\dot{\varepsilon} = 0.5$ to $1\,s^{-1}$. These careful measurements indicate that in CPNCs true SH occurs less frequently than one might have expected.

16.2.5 Fourier Transform Analysis of CPNCs

Fourier transform rheology (FTR) [Wapner and Forsman, 1971] was used for the analysis of CPNCs. The experiments were performed in the ARES using the software developed by Wilhelm [2002]. It was expected that the method may be suitable for characterization of the nonlinear viscoelastic response of CPNC. The FTR analysis is based on the expression

$$\sigma \propto A_1 \cos \omega t + A_3 \cos 3\omega t + A_5 \cos 5\omega t + \cdots \tag{16.33}$$

Usually, the FTR signal is plotted as the relative magnitude of the odd harmonic peaks divided by that of the first peak: $R_n(\omega) = I_n(\omega)/I_1(\omega)$, with $n = 3, 5, 7, \ldots$. Since harmonics occur only for nonlinear viscoelastic systems, $R_n(\omega) = 0$ evidences the linear viscoelastic behavior. As $I_n(\omega)$ decreases with n, the strongest third harmonic peak, $R_3(\omega)$, has been used primarily.

Experiments were performed on several CPNCs with PA-6, PP, or PS matrix. The large-amplitude oscillatory shear (LAOS) was conducted at the injection frequency of $\nu_0 \leq 10$ Hz and strain $\gamma \leq 70\%$. The results confirmed that the nonlinearity increases with strain and frequency. The FTR advantage rests in the quantification of these influences, as well as in that of the shearing time [Debbaut and Burhin, 2002; Utracki, 2004]. An example of data is presented in Figures 16.20 and 16.21. At constant $\gamma = 40\%$, the degree of exfoliation affects the R_3 signal. With all other independent variables being constant (e.g., 1015C2, T, γ), R_3 increases at increasing frequency.

Unfortunately, because of the clay platelet alignment in the stress field, the method did not fulfill expectations. To obtain a strong enough signal, large strains and frequencies had to be used, but these destroy the characteristic LCP-type structure, and the rheological behavior was controlled by the matrix. As evident from data in Figure 16.21, the melt-compounded PA-PNC samples with good and poor clay dispersion showed behavior similar to that of the matrix. However, the CPNC with clay grafted by PA-6 (1015C2 in Figures 16.20 and 16.21) was found to have a higher degree of nonlinearity, revealing the effects of clay–matrix interactions, which resulted in a high degree of dispersion.

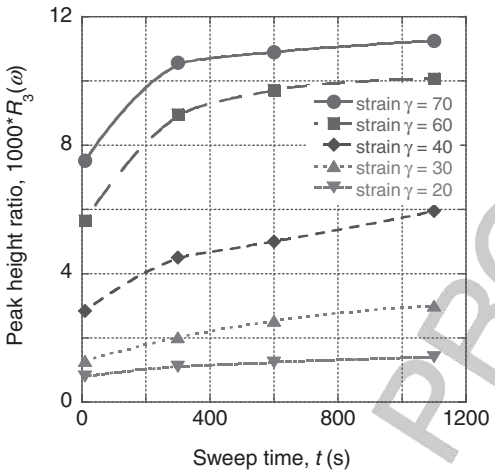

FIGURE 16.20 FTR data for 1015C2 at $\omega = 1$ Hz and the strain ranging from 0.20 to 0.70. (From Sammut et al. [2007].)

16.2.6 Free-Volume Effects on Flow

The experiments showed that for a great diversity of low-molecular-weight liquids (solvents), there is a singular relationship between the zero-shear viscosity, η_0, and density, ρ [Batchinski, 1913]:

$$\eta_{0,P,T} \propto \rho_{P,T} \tag{16.34}$$

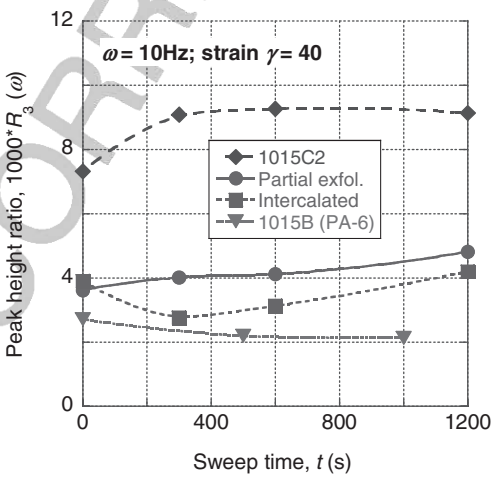

FIGURE 16.21 $R_3(\omega)$ vs. shearing time at $\omega = 10$ Hz and $\gamma = 0.4$, for PA-6 and PA-6 based CPNC. (From Sammut et al. [2007].)

The theoretical explanation for these observations was based on the concept of free volume that upon changes of P and T affects density and viscosity similarly [van der Waals, 1873]. Doolittle modified Eq. (16.34) to read [Doolittle 1951a, b, 1952, 1954; Doolittle and Doolittle, 1957]

$$\ln \eta_{0,P,T} = a_0 + \frac{a_1}{f} \qquad f = \frac{V - V_0}{V} \tag{16.35}$$

where f is the free-volume fraction, V the total volume (at given P and T), and V_0 the occupied volume.

The Simha–Somcynsky (S-S) [Simha and Somcynsky, 1969; Somcynsky and Simha, 1971] equation of state incorporates the hole fraction, h, a direct measure of f (for details, see Chapter 6). Thus, it was natural to modify empirical equation (16.35) by replacing f calculated from the density by h computed from the equation of states, as well as replacing η_0 by its more general, constant stress homolog, η_σ [Utracki, 1974, 1983a,b, 1985, 1986; Utracki and Simha, 1981, 1982, 2001b; Utracki and Ghijsels, 1987]:

$$\ln \eta_\sigma(P, T) = a_0 + a_1 Y_S \qquad Y_S \equiv \frac{1}{a_2 + h(P, T)} \tag{16.36}$$

The relation predicts that $\eta_\sigma(P, T)$ is a function of T and P only through $h = h(T, P)$. The parameter a_0 reflects the effect of molecular weight, a_1 is related to the segmental friction coefficient, and a_2 only linearizes the dependence. The procedure is to measure the PVT surface of a given liquid, and from the S-S equation of state extract $h = h(P, T)$ at the same P and T as those used for the viscosity measurements. For n-paraffins and their mixtures and lubricating silicone oils (viscosity spans about six decades), good superposition was obtained in a wide range of variables, [e.g., $20 \leq T\ (^\circ\text{C}) \leq 204$ and $0.1 \leq P\ (\text{MPa}) \leq 500$]. Furthermore, for these nonpolymeric liquids the universality of the parameters $a_1 = 0.79 \pm 0.01$ and $a_2 = 0.07$ was observed.

However, application of Eq. (16.36) to molten polymers has been less straightforward. No "master curve" could be defined for a given series of polymers, as the molecular-weight distribution affected the magnitude of the a_1 parameter. Furthermore, as discussed in Chapter 14, the melts undergo a secondary liquid–liquid transition at $T_T/T_g \geq 1.20 \pm 0.05$ [Boyer, 1985, 1987; Bicerano, 2003; Ngai, 2000, 2003]. Thus, not only did different pressure parameters have to be used below and above T_T, but to achieve superposition of the rheological data onto a master curve, the characteristic pressure–reducing parameter, P^*, had to be redefined as $P^*{}_R = \xi_p P^*$, where the factor ξ_p depends on the substance. Evidently, the different sources of the rheological and PVT data could have introduced extra errors. Fortunately, Sedlacek et al. [2004, 2005] reported η and PVT data for eight commercial polymers measured within the same range of T and P. The authors observed that Eq. (16.36) was not followed: At high P the viscosity data were below the master curve defined by low-pressure data.

The data and procedures were reevaluated carefully [Utracki and Sedlacek, 2007], but the plots of η versus h still did not result in superposition; for superposing the data, $P_R^* = \xi_p P^*$, with $\xi_p = 1$ to 2.1, had to be used. These results imply that at lower temperatures the free-volume cells are smaller than required for segmental jumps. The nonuniversality of the η versus h dependence is related to the diversity of liquid structures. It is noteworthy that as T increases, the magnitude of ξ_p decreases. Amorphous polymers at $T > 1.52T_g$ are expected to follow Eq. (16.36), which has been proven valid for low-molecular-weight solvents and silicone oils [Utracki and Simha, 1981, 1982, 2001b]. It is interesting to recall that Boyer [1985, 1987] postulated that "true liquid" behavior of amorphous polymer occurs at $T \geq T_L\rho = T_{\mathrm{LL}} + 50^\circ C$, with $T_{\mathrm{LL}} \geq 1.20T_g$ being the liquid–liquid transition temperature; for PS ($M_n = 390$ kg/mol), $T_L\rho/T_g \approx 1.27$ to 1.38. However, in amorphous–atactic polymers with traces of tacticity [e.g., poly(vinyl chloride)] with melting-point temperature $1.5 \leq T_m/T_g \leq 2.0$, the true liquid behavior should be expected at even higher T. Thus, the departures from the flow behavior predicted by Eq. (16.36) observed for molten polymers must be considered not an exception but a rule.

The necessity of using different ξ_p values for different polymers means that the empirical Eqs. (16.36) to (16.37) are nonuniversal. In addition, since the William–Landel–Ferry (WLF) relation is based on Eq. (16.37), its applicability is not general. These dependencies might be used as empirical, with parameters to be determined for each system within the range of independent variables. However, judging by the success of WLF dependence at ambient pressure, it might be that under this condition the superposition is more common. This is also illustrated in Figure 16.22, where the ambient pressure dynamic viscosity at 240°C (i.e., $T/T_g = 1.62$) is plotted versus $1/h$ for CPNC 1015C2; both the zero-shear and constant stress data follow a straight line: $\log \eta' \propto 1/h$.

16.2.7 Modeling of PNC Flows

Mathematical modeling of PNC rheological behavior is essential for understanding the nanocomposites. Models predicting the flow of materials might be used for estimating the structure and thus the performance of the final products [i.e., mechanical or barrier (permeability) properties]. Scores of papers have been published on the rheological behavior of nanocomposites, but only a few research teams have developed predictive models. Different approaches have been used to describe PNC thermodynamics and rheology: a self-consistent field (SCF) lattice model, molecular dynamic (MD) and Monte Carlo simulations, continuum mechanics, molecular network–based models, and the GENERIC approach (dynamic equations compatible with thermodynamics) [Vaia and Giannelis, 1997a,b; Balazs et al., 1998, 1999; Zhang and Archer, 2004; Anderson et al., 2005; Gu and Grmela, 2008].

MD was used for idealized nanocomposites containing 5 vol% of differently shaped model nanoparticles: rodlike, compact (icosahedral, or 20-sided), and sheetlike [Knauert et al., 2007]. The authors computed the relative shear viscosity, η_r, and the tensile strength, τ, of the melt (see Figure 16.23). The one-order-of-magnitude increase in η_r was explained by chain bridging between nanoparticles. The largest

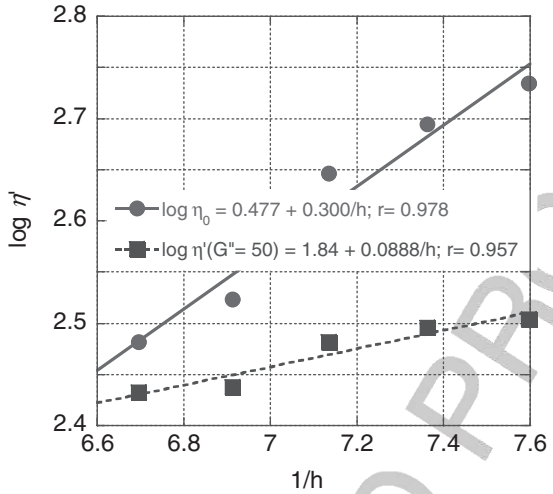

FIGURE 16.22 Dynamic viscosity of PA 6 based CPNC at $T = 1.62T_g$ vs. inversed hole fraction from the S-S eos. Circles are for zero-shear, squares for constant stress ($G'' = 50$ Pa). (Data from Utracki and Lyngaae-Jörgensen [2002] and Utracki et al. [2003].)

increase η_r and parallel to it, the number of bridging molecules was computed for rods and the smallest for sheets. However, for η_r the shape of nanoparticles had a relatively small effect. For τ the order was reversed and the effect of nanoparticle shape was more pronounced. The sheets provided the largest increases in tensile strength, while the other particles (especially rods) reduced the strength below the matrix value. Since bridging could not explain these effects, the authors postulated that deformability of nanoparticle sheets contributed to the strength by reducing the Poisson ratio. Simulations were carried out for polymer–particle interactions that would favor dispersion. However, even in such a case, MD suggested that aggregation of sheets is more severe than that of other shapes.

Kairn et al. [2005] used coarse-grained MD for predicting the rheological behavior of $CaCO_3$ ($D = 70$ nm)-filled PP. Although there were some differences in scale between the simulated composite and the experimental data, qualitative similarities were noted in the shear behavior. Starr et al. [2003] investigated the effect of particle clustering on the PNC rheological behavior. Systems with well-dispersed particles showed higher η, especially at low $\dot{\gamma}$, which increased with concentration ($\phi \geq 0.15$). From the hydrodynamic point of view, an opposite effect could be expected i.e., that large rigid particles would provoke greater η than a collection of small ones, [Bicerano et al., 1999]. However, the simulation indicated that clusters formed were dynamic, not rigid. Moreover, the reduced molecular mobility of polymer near the particle surface also increased viscosity. These results have been confirmed for PP-based PNC with the same composition but a different degree of clay dispersion [Sepehr and Utracki, 2006].

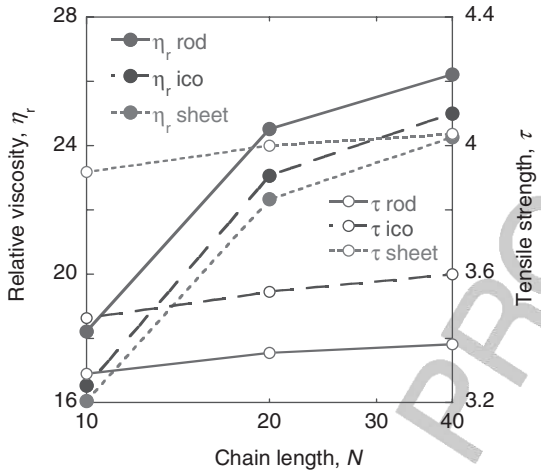

FIGURE 16.23 MD computed relative viscosity, η_r, and the tensile strength, τ, vs. chain length for rod-like, compact (icosahedra), and sheet-like particles. (From Knauert et al. [2007].)

MD simulations, suitable for predicting the viscosity and time-dependent shear modulus of PNC with nonentangled or weakly entangled polymers, are limited to systems that have only a few nanoparticles. Borodin et al. [2005] used a multiscale modeling of PNC mechanical properties consisting of three steps: (1) creating MD simulations of viscoelastic properties of the matrix and cylinder-filled composites, then postulating the position-dependent shear modulus; (2) starting with the MD-simulated bulk– and interfacial–polymer properties, calculating the viscoelastic properties of PNC using the material-point method (MPM); and (3) comparing the viscoelastic properties obtained for a composite from the MPM with those from MD. This strategy could be used for highly concentrated systems, complex geometries, and a diverse level of attractive interactions between the matrix and filler particles. The computing time was also reduced. The multiscale modeling of PNC properties is a popular and useful approach discussed in many reviews (see, e.g., [Zeng et al., 2008]).

Pryamitsyn and Ganesan [2006] reviewed and suggested new uses for the coarse-grained, momentum-conserving dissipative particle dynamic (DPD) method. The model assumes spherical nanofillers of a fixed size radius, $R = 2.5$ units of the polymer segment diameter, dispersed at $\phi = 0$, 0.007, 0.11, 0.33, 0.43, and 0.5. The polymer matrix was modeled as a beadstring of FENE type, with a chain length N_P. The concentration was varied by changing the number of the dispersed particles, N_C, while keeping the number of polymer segment units constant. In simulations the shear rate ranged from $\dot{\gamma} = 5 \times 10^{-4}$ to $1\ s^{-1}$. To prevent particle aggregation a weak attractive force was assumed between nanoparticles. The simulation suggested that the shear flow of PNC is similar to that of colloidal suspensions, provided that the particle-induced changes in the polymer rheology and polymer slip effects are accounted for. At low nanoparticle loadings, matrix shear thinning dominates. At higher loadings, the

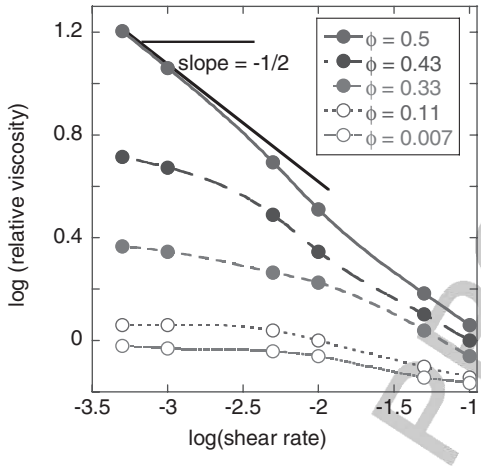

FIGURE 16.24 Relative viscosity vs. shear rate for model suspensions in matrix containing $N_P = 16$. See text. (From pryamitsyn and Ganesan [2006].)

flow is controlled by the particle–particle interactions. An example of the computed relative viscosity versus deformation rate is shown in Figure 16.24. It is noteworthy that at the highest clay concentration, the initial slope $\partial \log \eta_r / \partial \log \dot{\gamma} \Rightarrow -\frac{1}{2}$.

Several authors used the continuum mechanics for modeling conventional polymer composites as well as PNC. Ren and Krishnamoorti [2003] used a K-BKZ integral constitutive model to predict the steady-state shear behavior of a series of intercalated nanocomposites containing an organo-MMT and a disordered styrene–isoprene diblock copolymer. The model predicts the low-$\dot{\gamma}$ shear stress properties calculated from the experimental linear stress relaxation and the relaxation-based damping behavior. However, as it does not take into account the effect of clay platelet orientation, it is unable to predict the shear stress behavior at intermediate $\dot{\gamma}$ and the normal stress behavior at all $\dot{\gamma}$ and clay contents.

Letwimolnun et al. [2007] used two models to explain the transient and steady–state shear behavior of PP nanocomposites. The first model was a simplified version of the structure network model proposed by Yziquel et al. [1999] describing the nonlinear behavior of concentrated suspensions composed of interactive particles. The flow properties were assumed to be controlled by the simultaneous breakdown and buildup of suspension microstructure. In this approach, the stress was described by a modified upper-convected Jeffery's model with a modulus and viscosity that are functions of the suspension structure. The Yziquel et al. model might be written:

$$\frac{1}{G(\xi)}\frac{\delta \boldsymbol{\sigma}}{\delta t} + \frac{\boldsymbol{\sigma}}{\eta(\xi)} = \left(1 + \frac{\eta_\infty}{\eta(\xi)}\right)\dot{\boldsymbol{\gamma}} + \frac{\eta_\infty}{G(\xi)}\frac{\delta \dot{\boldsymbol{\gamma}}}{\delta t} \tag{16.37}$$

$$G(\xi) = G_0 \xi + G_\infty \tag{16.38}$$

$$\eta(\xi) = \eta_0 \left(\frac{1}{\xi} - 1 \right)^{(n-1)/(n+1)} \tag{16.39}$$

where $\delta/\delta t$ is the upper-convected derivative; $\boldsymbol{\sigma}$ and $\dot{\gamma}$ are the stress and rate of deformation tensors, ξ is the structure parameter, varying between 0 and 1; $G(\xi)$ and $\eta(\xi)$ are the elastic modulus of the structured material and its power-law viscosity (n being the power-law exponent); G_∞ and η_∞ are the elastic modulus and the viscosity of the "destroyed" structure (here the matrix filled with noninteractive particles), $G_0 + G_\infty$ is the elastic modulus of the structured material at equilibrium; and η_0 is a characteristic viscosity.

For $\xi = 1$ the viscosity goes to infinity and the behavior is that of a solid or of a material with yield stress. Hence, the model describes a transition from solid- to liquidlike behavior as ξ decreases under applied stress from 1. The evolution of the structure parameter ξ with time is described by a kinetic equation, where the structure breakdown is related to the energy dissipated by the flow process:

$$\frac{\partial \xi}{\partial t} = \frac{k_1}{\lambda_0}(1 - \xi) - k_2 \frac{\lambda_0}{\eta_0} \xi \, |\boldsymbol{\sigma} : \dot{\boldsymbol{\gamma}}| \tag{16.40}$$

where $\lambda_0 = \eta_0/(G_0 + G_\infty)$ is a characteristic relaxation time (assumed to be constant). The first term on the right side of Eq. (16.40) accounts for the effects of Brownian motion, responsible for the structure buildup at rest. In this model, n and η_∞ are determined by steady-state shearing. $G_0 + G_\infty$ and G_∞ are obtained from the plateau values of G' at small deformation for the nanocomposite and binary blend (PP/PP-MA), respectively. The kinetic constants k_1 and k_2 and the characteristic time λ_0 (or η_0) are taken as adjustable parameters. The model predicted the values of stress overshoot and the steady shear viscosity of PP/PP-MA/C20A as well as the effect of structure reorganization during rest time and breakdown under flow. However, the stress overshoot and steady-state plateau predicted were reached too rapidly.

The second model used by Letwimolnun et al. [2007] is an extension of that used by Sepehr et al. [2004] for short fiber suspensions. A hydrodynamic diffusive term related to the Brownian motion, D_r, was added to the diffusive term of the Folgar and Tucker [1984] equation as $\widetilde{D}_r = C_I \bar{\dot{\gamma}} + D_r$ in

$$\dot{\boldsymbol{a}}_2 = \frac{D\boldsymbol{a}_2}{Dt} = \frac{1}{2}(\boldsymbol{\omega}\boldsymbol{a}_2 - \boldsymbol{a}_2\boldsymbol{\omega}) + \frac{\lambda}{2}(\dot{\boldsymbol{\gamma}}\boldsymbol{a}_2 + \boldsymbol{a}_2\dot{\boldsymbol{\gamma}} - 2\dot{\boldsymbol{\gamma}} : \boldsymbol{a}_4) + 2\widetilde{D}_r(\mathbf{I} - 3\boldsymbol{a}_2) \tag{16.41}$$

where $\mathbf{a_2}$ and $\mathbf{a_4}$ are second- and fourth-order orientation tensors as defined by Advani and Tucker [1987], with the trace of $\mathbf{a_2}$ equal to 1. A closure approximation is necessary for evaluating the fourth-order orientation tensor as a function of the second-order tensor. In this study the natural closure approximation of Verleye and Dupret [1994] was used; λ is a function of p' (aspect ratio of oblate ellipsoid) [i.e., $\lambda = (p'^2 - 1)/(p'^2 + 1)$]; $\dot{\boldsymbol{\gamma}}$ and $\boldsymbol{\omega}$ are the rate-of-strain and vorticity tensors, defined by $\dot{\boldsymbol{\gamma}} = \boldsymbol{\kappa} + \boldsymbol{\kappa}^t$ and $\boldsymbol{\Omega} = \boldsymbol{\kappa} - \boldsymbol{\kappa}^t$, where $\boldsymbol{\kappa}$ is the velocity gradient tensor, $\bar{\dot{\gamma}}$ is the effective deformation rate, and C_I is a phenomenological interaction diffusion

coefficient; D_r defined in Eq. (16.18) is related to the Brownian motion [Larson, 1999; Ren et al., 2003a,b]. The constitutive equation used for particle suspensions had the general form [Lipscomb et al., 1988]

$$\boldsymbol{\sigma} = -P\mathbf{I} + \eta_s\,\dot{\boldsymbol{\gamma}} + \boldsymbol{\sigma}^m + \boldsymbol{\sigma}^p \tag{16.42}$$

where P is the hydrostatic pressure, σ the sum of the contribution of the stress tensor due to the viscoelastic matrix, σ^m, and the clay platelets, σ^p, defined as

$$\boldsymbol{\sigma}^p = [\eta_s + \eta(\dot{\boldsymbol{\gamma}})]\,\phi\,[A\,\dot{\boldsymbol{\gamma}} : \boldsymbol{a}_4 + B(\dot{\boldsymbol{\gamma}}\cdot\boldsymbol{a}_2 + \boldsymbol{a}_2\cdot\dot{\boldsymbol{\gamma}}) + C\,\dot{\boldsymbol{\gamma}} + FD_r\boldsymbol{a}_2] \tag{16.43}$$

where $\eta(\dot{\gamma})$ is the matrix viscosity, η_s is the Newtonian solvent viscosity, ϕ is the particle volume fraction, and *A, B, C,* and F are rheological coefficients dependent on p'. In this work the matrix was assumed to be Newtonian with a viscosity of η_s [$\boldsymbol{\sigma}^m$ and $\eta(\dot{\gamma})$ excluded]. The particle aspect ratio and the interaction coefficient (p', C_I) were used as fitting parameters; p' controls the overshoot amplitude and C_I the steady-state value [Sepehr et al., 2004].

The model predicted stress overshoot and steady state η of PP-based PNC. However, it was unable to predict the effect of $\dot{\gamma}$ on the overshoots (i.e., the growth of stress overshoot amplitude with increasing $\dot{\gamma}$). The structure reorganization of particles was predicted qualitatively and the kinetics for the particle disorientation based on the Brownian motion was too slow in comparison with experimental results [Solomon et al., 2001; Lele et al., 2002; Ren et al., 2003a,b], which might imply that the matrix recovery affects the clay orientation.

Sepehr et al. [2008] are investigating the viscoelastic Giesekus model [Giesekus, 1982, 1983; Bird et al., 1987] coupled with Eq. (16.41), with $\widetilde{D}_r$ described by Doi [1981]. The interactions between polymer and particles were incorporated following suggestions by Fan [1992] and Azaiez [1996]. These authors used Eq. (16.42) with the contribution to stress tensor caused by clay platelets [Eq. (16.43)] and viscoelastic Giesekus matrix expressed as [Fan, 1992]

$$\beta\chi\boldsymbol{\sigma}^m + \beta\frac{\alpha\tau}{\eta_0}\boldsymbol{\sigma}^m\cdot\boldsymbol{\sigma}^m + \tau\boldsymbol{\sigma}^m_{(1)} + \frac{M\beta(1-\chi)}{2}(\boldsymbol{a}_2\cdot\boldsymbol{\sigma}^m + \boldsymbol{\sigma}^m\cdot\boldsymbol{a}_2) = 2\eta_m\dot{\boldsymbol{\gamma}} \tag{16.44}$$

where η_0 is the polymer zero-shear viscosity, α the mobility factor, τ the polymer relaxation time, and $M = 3$ (for three-dimensional flows); β and χ, are the friction coefficient and the particle–matrix interaction parameter, respectively. The original Giesekus model might be recovered by setting β and $\chi = 1$. The simulation results of this model, considering the effect of diffusive terms, $\widetilde{D}_r \neq 0$, with β and $\chi \neq 1$, were compared with the experimental results for 1015C2. The model predicted correctly the shear and normal stress overshoots that occur at the same strain. The relaxation behavior after the cessation of flow was also well described, providing a good prediction of the subsequent stress growth behavior. Similarly, the increasing magnitude of the shear stress overshoot peak with rest time was well described, and the negative values of N_1 were qualitatively predicted. However, the model overestimated

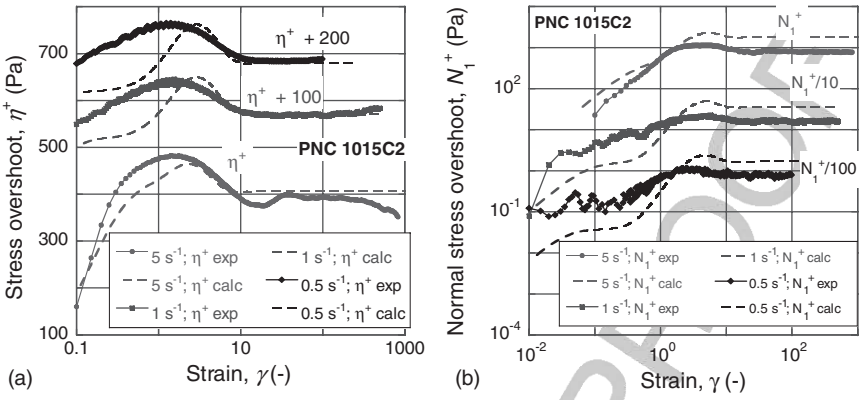

FIGURE 16.25 Stress overshoot for PA-6 based CPNC (Ube 1015C2): (a) shear stress; (b) first normal stress difference behavior. The data measured (solid lines) or calculated (dashed lines) for $\dot{\gamma} = 5\,s^{-1}$ are in absolute values, while those at two other rates are displaced for clarity by the value indicated in the figure [Sepehr et al., 2008].

the steady-state value of N_1. The experimental and simulation data are compared in Figure 16.25.

A similar model with different diffusive terms was used by Wang et al. [2006b] for PS/CNT nanocomposites by neglecting the Brownian motion and assuming that β and $\chi = 1$. In that work, the steady shear viscosity was predicted correctly, but N_1 was not.

A mesoscopic rheological model based on the GENERIC framework [Grmela, 1984, 1990, 1991, 2002; Grmela and Carreau, 1987; Grmela and Ottinger, 1997] was recently proposed for CPNCs [Eslami et al., 2007; Gu and Grmela, 2008]. The authors considered exfoliated CPNC with homogeneously dispersed platelets in a viscoelastic FENE-P polymer matrix. The mesoscopic level of description implies that the matrix macromolecules are characterized by a conformation tensor, **c**, and clay lamellae by another conformation tensor, **a**. Having chosen the state variables, the model is formulated by writing down a framework for the governing equations and then filling the framework by specifying the kinematics of the state variables, the free energy, Φ, and the dissipation potential, Ξ. For viscoelastic matrix and clay platelets, the authors generalized the FENE-P and Jeffery models [Jeffery, 1922; Bird et al., 1980] using a formulation with free energy and specifying the dissipation potential as:

$$\frac{\partial \mathbf{c}}{\partial t} = -\nabla(\mathbf{c}\cdot\Phi\mathbf{u}) - \frac{1}{2}(\boldsymbol{\omega}\cdot\mathbf{c} - \mathbf{c}\cdot\boldsymbol{\omega}) + \frac{1}{2}(\dot{\boldsymbol{\gamma}}\cdot\mathbf{c} - \mathbf{c}\cdot\dot{\boldsymbol{\gamma}}) - \frac{\partial \Xi}{\partial \Phi_c} \tag{16.45}$$

$$\frac{\partial \mathbf{a}}{\partial t} = -\nabla(\mathbf{a}\cdot\Phi\mathbf{u}) - \frac{1}{2}(\boldsymbol{\omega}\cdot\mathbf{a} - \mathbf{a}\cdot\boldsymbol{\omega}) + \left(-\frac{1}{2}(\dot{\boldsymbol{\gamma}}\cdot\mathbf{a} - \mathbf{a}\cdot\dot{\boldsymbol{\gamma}}) + \frac{1}{A_0}tr(\mathbf{a}\cdot\dot{\boldsymbol{\gamma}})\mathbf{a}\right) - \frac{\partial \Xi}{\partial \Phi_a} \tag{16.46}$$

with the constitutive equation

$$\boldsymbol{\sigma} = -2\mathbf{c}\cdot\Phi_c + 2\xi\mathbf{a}\cdot\Phi_a - \frac{2}{A_0}\xi\mathbf{a}\ \mathrm{tr}(\mathbf{a}\cdot\Phi_a) \tag{16.47}$$

where $\mathbf{u}$ is the momentum field of the fluid per unit volume and $A_0 = tr\,\mathbf{a}$ is the surface area of the platelet. The first term in Eqs. (16.45) and (16.46) was added to include the case when $\mathbf{a}$ and $\mathbf{c}$ depend on the position coordinate r. In this approach, the arbitrariness of closure approximation had been avoided by formulating the governing equations directly on the conformation tensor level. By appropriate choice of Ξ and Φ, the model is able to express important physical features (e.g., polymer–platelet and platelet–platelet interactions). The dissipation potential chosen was assumed to be a function of free energy and the mobility tensors of polymer, platelet, and their coupling. The authors compared the experimental data from the literature in steady and transient shear flows with the model predictions. The results showed a qualitative agreement for startup flows at high $\dot{\gamma}$ but less satisfactory at low flows. Moreover, the stress overshoot predicted reached a steady-state plateau sooner than the experimental overshoot, indicating faster orientation of clay particles in the flow direction. For steady shear flow, model predictions and experimental data were in good qualitative agreement, especially for PNC with low nanofiller content.

Sarvestani and Picu [2004] proposed a molecular network model of nonentangled polymer matrix with less than 10 wt% of nanofiller particles. The model assumed the creation and destruction of loops, tails, and bridges between nanoparticles. The stress tensor contains contributions pertaining to bridging and dangling segments (B and D, respectively):

$$\boldsymbol{\sigma} = \sum_i (\langle \mathbf{F}_i^B \mathbf{R}\rangle_B + \langle \mathbf{F}_i^D \mathbf{R}\rangle_D) \qquad \mathbf{F}_i(\mathbf{R}) = \frac{-3k_BT}{il^2}\frac{\mathbf{R}}{1-(R/il)^2} \tag{16.48}$$

The relation was solved by MC lattice simulations of the steady shear flow. Several levels of polymer–filler interactions and concentrations were explored. The viscoelastic response was found to depend on the lifetime of the polymer–filler junctions. As expected, the largest effect of the nanofiller was found at low strain rates or frequencies. Solidlike behavior was predicted for systems in which the polymer molecules interact strongly with the nanoparticles (i.e., with the network of bridging segments). Next, the authors extended the model to PNC with an entangled polymer matrix [Sarvestani and Picu, 2005]. Entanglement effects were introduced by assuming that diffusion in the chain contour (tube) direction is larger than that in the transverse direction. Owing to the strong polymer–filler interactions, incorporation of particles reduced the macromolecular mobility in both tube directions. The authors assumed that only frictional interactions affect chain dynamics and stresses. The effects of such model parameters as polymer–filler affinity, anisotropy of diffusion in the longitudinal and transverse tube directions, and the polymer–filler attachment fraction were

evaluated. The model simulation was compared successfully with experimental data of shear viscosity and alignment angle versus $\dot{\gamma}$.

The model was extended to suspensions of monodispersed nonaggregating rigid spherical particles in diluted solution of unentangled monodispersed macromolecules [Sarvestani and Jabbari, 2007]. The viscoelastic response postulated depended on the monomer–filler interactions, concentration of particles, and surface friction. These factors increased the shear viscosity, shear thinning, and solidlike behavior at low frequency. For example, the low-frequency G' plateau increased with increasing interactions, friction coefficient, and volume fraction of solid particles, but decreased with increasing particle size. Next, Sarvestani [2008] presented a theory for the linear viscoelastic behavior of entangled polymeric liquids reinforced with low filler of nonaggregating colloidal nanoparticles. The model assumes that a fraction of entangled chains is adsorbed reversibly on the particle surface. The onset of solidlike behavior at low frequency originates in sluggish relaxation of adsorbed chains.

Since nanoparticles in PNC are orders of magnitude smaller than conventional reinforcements, the models developed for composites are not applicable to nanocomposites. However, development of a universal model for PNC is challenging since the shape, size, and dispersion of the nanoparticles vary widely from one system to another. On the one hand, exfoliated clay provides vast surface areas of solid particles (ca. 800 m^2/g) with a large aspect ratio that adsorb and solidify a substantial amount of the matrix polymer, but on the other hand, the mesoscale intercalated clay stacks have a much smaller specific surface area and small aspect ratio. However, in both these cases the particle–particle and particle–matrix interactions are much more important than in conventional composites, affecting the rheological and mechanical behavior. Thus, the PNC models must include the thermodynamic interactions, often neglected for standard composites.

16.3 SOLID-STATE VISCOELASTIC BEHAVIOR

The viscoelastic behavior of molten CPNC has been discussed as part of the melt rheology. At present the focus will be on the solid-state behavior (e.g., below the melting point, T_m, or the glass transition temperature, T_g). This division for the melt and solid viscoelasticity is artificial, motivated on the one hand by different instruments and on the other by the lack of systematic studies spanning liquid and solid states of PNC, as has been done for neat polymers [Ferry, 1980]. The dynamic tests are usually carried out as a temperature scan at a low heating rate (e.g., 1 to 5°C/min and at constant frequency, usually $\upsilon = 0.1$, 1.0, or 10 Hz). The results are expressed as either absolute or relative (to the matrix) storage modulus, showing strong temperature dependence. There are attempts to replace the steady-state mechanical testing of CPNC by dynamic scans, but the moduli obtained from these two tests often differ. However, since the relative quantities [e.g., G'(PNC)/G' (matrix)] correlate closely with the steady-state tensile modulus, E(PNC)/E(matrix), the problem might be related to the instrument calibration and experimental procedure, not to the fundamentals.

16.3.1 Nanocomposites with an Elastomeric Matrix

Viscoelastic properties of elastomer-based CPNCs were measured at a constant frequency of 1 Hz as a temperature sweep of the dynamic moduli. Exfoliated CPNCs with polybutadiene (BR) or polyisoprene (IR) matrix were prepared by in situ anionic polymerization, with T_g increasing by about 10°C upon incorporation of 6.2 wt% organoclay [Liao et al., 2005, 2006]. However, contrary to expectations, these CPNCs did not show improved dynamic tensile storage modulus, E'.

A recent review summarized the preparation and properties of CPNCs with an elastomeric matrix [Utracki, 2008]. As in the case of CPNCs with a thermoplastic matrix, the enhancement of properties depends on (1) clay volume fraction, (2) degree of clay dispersion, (3) clay aspect ratio, and (4) clay–matrix interactions. During melt mixing the degree of dispersion as well as attrition of clay platelets and loss of intercalant occur simultaneously. In consequence, there is an optimum mixing time and temperature for the desired set of properties. Throughout the process the macromolecules must diffuse into interlayer spacing in clay stacks. For this reason, addition of inorganic clay (e.g., Na-MMT) to molten rubber leads to microcomposites with clay particles dispersed in the matrix, resulting in poor performance. By contrast, preparation of exfoliated CPNCs starting with rubber latex and mineral clay has been reported. The process involves: (1) dispersion of Na-clay in water, possibly with a stabilizer; (2) preparation of rubber latex; (3) combining the two suspensions; (4) coagulation; and (5) vulcanization. Since the ammonium intercalants are thermally unstable at $T > 130\,^{\circ}\mathrm{C}$, the use of nonintercalated clay is beneficial.

The degree of clay dispersion in the final product depends on the clay content, additives, and procedure (i.e., addition of vulcanization ingredients, coagulation, vulcanization, etc.). Usually, incorporation of a solid filler increases the modulus and tensile strength, but at the expense of the elongation at break. By contrast, the addition of clay to rubber often shows the increased modulus and tensile strength of vulcanized CPNCs with about constant elongation at break. Full exfoliation is possible at $w \leq 1.14$ wt% MMT; above this limit, locally, platelets form stacks with the d_{001} decreasing with increasing w. In consequence, the performance parameters of CPNCs, even under the most ideal conditions, go through a maximum; in most cases the optimum clay content ranges from 2 to 5 wt%. Even at poor clay dispersion, as judged from the d_{001}, the inorganic clay in latex shows a good performance. This may indicate that even in the presence of clay stacks there is a high concentration of individual clay platelets. Their dispersion is stabilized by adsorbed macromolecules, and then by vulcanization. In many cases the semisynthetic FM with aspect ratio $p \leq 6000$ engenders better performance than does MMT. It is noteworthy that the enhancement of matrix stiffness (or relative tensile modulus) by incorporation of 5 wt% clay (inorganic) is $E_r \equiv E(\mathrm{CPNC})/E(\mathrm{matrix}) = 1.15$, 2.0, and 5.5 for glassy, semicrystalline thermoplastic, and elastomeric matrix, respectively. In other words, at 5 wt% clay loading, the CPNC modulus increases by up to 15, 100, and 450% over the matrix modulus, respectively [Utracki, 2009].

Dielectric relaxation spectroscopy (DRS) was used for studies of the effects of confinement, the type and concentration of clay, and the molecular weight of

elastomers. CPNCs with polyisoprene (IR) as the matrix were prepared by a solution with ≤ 10 wt% C25A or C30B. The tests showed that the average relaxation time for normal and segmental modes was independent of clay loading of $w \leq 10\%$, but the dc conductivity and interfacial polarization increased with it. The authors concluded that the type of clay, its concentration, or the unentangled matrix molecular weight affects the segmental dynamics, indicating that the time and length scales of the α -process remain unaffected. The average relaxation time of CPNCs with high-molecular-weight IR has increased, as expected [Mijović et al., 2006].

Styrenic thermoplastic elastomers (TPSs) are block or random copolymers with "soft" and "rigid" parts [Legge et al., 1987]. Their temperature sweeps at constant rate are expected to show two T_g's (e.g., at -80 and $+100^\circ$C), corresponding to the two components modified by the degree of domain dispersion (alternating and most random copolymers show a single T_g). However, CPNCs prepared by the co-dissolution of poly(styrene-*b*-butadiene) (SBS) with up to 7.5 wt% organoclay, showed no change in the rubber T_g's, a small decrease of PS-block T_g, and an increase of E' by about 25% [Liao et al., 2004]. By contrast, anionically polymerized SBS in the presence of ≤ 4 wt% organoclay was found to display both effects: small increases in T_g's and increased modulus [Zhang et al., 2006]. Similar behavior was reported for maleic anhydride (MA)–compatibilized systems [Chang et al., 2004].

Another segmented elastomer, the thermoplastic urethane (TPU), is one of the most versatile materials, due to its biocompatibility, elasticity, and abrasion resistance. The segmental flexibility, chain entanglement, and cross-linking influence the properties and determine application of the end products. TPUs are block copolymer with alternating soft and rigid blocks, separated into two phases. Jin et al. [2006] investigated the viscoelastic properties of CPNCs, comprising organoclay dispersed in TPU with different hard segment contents. The TPU/C20A nanocomposites were prepared by in situ polymerization, molded, and cured. Unfortunately, no information was reported about the degree of clay dispersion. The dynamic temperature scan was performed in the bending mode from -80 to 200°C at 10 Hz, heating at 3°C/min. The addition of organoclay increased the TPU elasticity, decreased its damping property, and significantly improved the thermal stability, but the effects on the tensile modulus were small, dependent on the hard segment content (i.e., incorporation of 3 wt% of organoclay to TPU containing 18, 26, 32, and 36 wt% hard segments changed the matrix modulus by -19, -17, $+7$, and $+5\%$, respectively). The dynamic testing yielded similar results. While below $T_g \approx -30^\circ$C, the E' of neat PU and its nanocomposites was about the same, above T_g the addition of organoclay had different effects on E', depending on the hard segment content: At low temperature the relative modulus decreased and at high temperature it increased, but as for E the changes for E'_r were small.

Navarro-Bañón et al. [2005] reported a similar decrease for TPU with nanosilica ($D = 7$ nm) having different degrees of silanization from 15.5 to 100%. In that study, the T_g of TPU soft segments ($\approx -22\ ^\circ$C) did not vary with nanosilica content. The authors reported that initially, at $T = -80$ to $-30\ ^\circ$C, E' increased, but then it decreased at $T = 10$ to 50°C. More recently, elastomeric TPU was prepared by dispersing C30B in polyol and polymerizing the system [Berta et al., 2009]. The dynamic

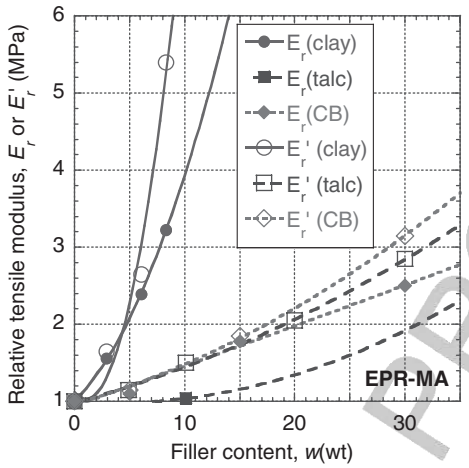

FIGURE 16.26 Relative tensile moduli, static and dynamic, for lightly maleated ERP with clay (circles), talc (squares), and carbon black (diamonds). (From Hasegawa et al. [2004].)

moduli, Young's modulus, and flammability all increased with improved degree of dispersion.

Mousa et al. [2006] used an internal mixer for compounding PVC nitrile rubber(NBR) with 50 phr of DOP and up to 10 phr of MMT preintercalated with trimethyl amine. No information about the clay dispersion was reported, but its addition increased the storage and loss moduli by a factor of 16 to 35, supposedly caused by the interactions between the intercalant ammonium groups and the PVC/NBR matrix.

Ethylene–propylene–rubber (EPR) and ethylene–propylene–diene–rubber (EPDM) constitute another large group of TPOs (olefinic thermoplastic elastomers). For CPNCs there is a need for compatibilization with maleated compounds (e.g., EPR-MA). For example, melt-compounded EPR-MA (0.42 wt% MA) with MMT-octadecyl amine (ODA) was compared to EPR compounds containing carbon black or talc [Hasegawa et al., 2004; Ahmadi et al., 2005]. The organoclay was found to be exfoliated and dispersed homogeneously. As shown in Figure 16.26, the CPNC had higher relative tensile moduli than those of conventional composites. A difference between the moduli measured under steady state and dynamic deformation was noted. The difference originated not only in the method of deformation but also in temperature. Although the difference in temperature was not large (20°C for E' versus 25°C for tensile test), the plot of E_r' versus T showed a broad maximum plateau at $\Delta T = 0 \pm 50$°C.

Gatos and Karger-Kocsis [2005] studied the clay dispersion and viscoelasticity of CPNC based on sulfur-cured EPDM. The organoclays MMT-ODA or MMT-3MODA were incorporated at 10 phr. The resulting CPNCs were intercalated or exfoliated, respectively. The dynamic temperature scan was performed at 2°C/min and 10 Hz. At $T = -80$ to -40°C the E' of both CPNCs was about the same, about 25% higher than that of the matrix. Significant differences were reported for $T > -10$°C, E_r's of the exfoliated and intercalated CPNC was $E'_r \approx 2.3$ and 1.7, respectively.

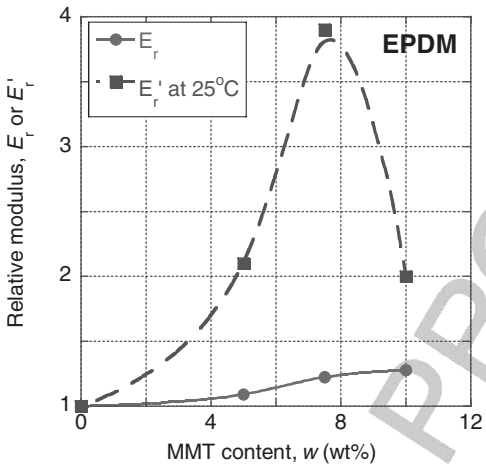

FIGURE 16.27 Relative moduli, E_r and E'_r, vs. clay content at about the same temperature. Circles, Young modulus; squares, storage modulus. (From Liu et al. [2006].)

Nanocomposites with EPDM have been compatibilized with EPDM-MA. The viscoelastic data resembled those observed for the styrene copolymers: small changes in T_g and modulus [Li et al., 2004]. However, the effect of MMT-ODA on E'_r depended strongly on T: In CPNC with 5 wt% organoclay at $-100\,^\circ$C, $E'_r \approx 1$, while at 25°C it reaches a maximum value of 2.6, compared with $E_r = 1.4$ at this temperature. According to x-ray diffraction and transmission electron microscopy the CPNC was exfoliated and dispersed uniformly.

EPDM-based nanocomposites were melt-compounded with MMT preintercalated with MA that compatibilized the system and accelerated curing [Liu et al., 2006]. The CPNC comprising < 10 wt% MMT was exfoliated. The mechanical properties were measured under steady state and dynamic conditions (at 3°C/min and 10 Hz). Figure 16.27 displays the relative moduli versus clay content. Manifestly, there is a significant difference between E_r and E'_r. The absolute values of E range from 1.9 to 2.4 MPa, while those of E' from 1 to 3.9 MPa; reversed difference was reported by Mishra et al. [2005] for TPO-based PNC. There E ranged from 13.2 to 22.6 MPa, in comparison to E' which varied from 47 to 137 MPa.

There is a growing tendency to incorporate nanofillers into polymer blends. When the two polymers differ significantly in rigidity, their behavior resembles that of TPE. For example, a blend of PA-6 with PP (PA-6/PP = 70/30) compatibilized with EPR-MA was melt-compounded with 4 phr of MMT-ODA [Chow et al., 2005]. The CPNC had a high degree of clay dispersion and distribution. The dynamic mechanical thermal analyzer (DMTA) data (at 10 Hz) showed a tendency opposite to that observed for TPE: The largest enhancement of E' was obtained for non-compatibilized CPNC at the lowest temperature of $-100\,^\circ$C (by about 25%); the addition of EPR-MA reduced this effect by one-half, up to $+100\,^\circ$C. However, for these systems the tensile moduli measured in steady state and dynamic mode at 23°C were comparable (i.e.,

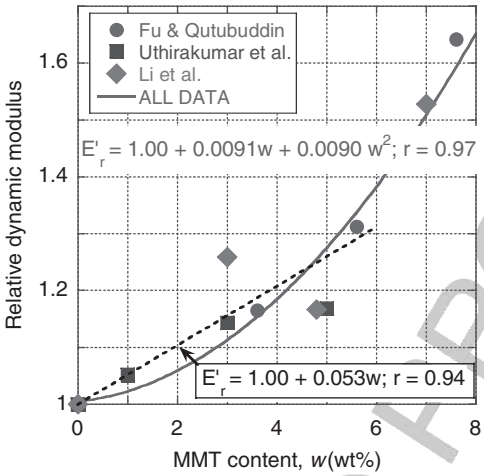

FIGURE 16.28 Relative dynamic moduli of PS CPNC vs. MMT content. (Data from Fu and Qutubuddin [2001], Uthirakumar et al. [2004], and Li et al. [2005].)

$E = 1.99$ and 2.25 GPa for the compatibilized matrix and CPNC, whereas $E' = 1.62$ and 1.97 GPa, respectively). The matrix T_g of the compatibilized CPNC increased by about 10 °C. Review of polymer blends rheology (with or without nanoparticles) was recently published [Utracki, 2010].

16.3.2 Nanocomposites with a Vitreous Matrix

Fu and Qutubuddin [2001] prepared exfoliated CPNC with PS as the matrix. Systems containing $\leq$ 7.6 wt% MMT were analyzed using a dynamic mechanical analyzer (DMA) with a three-point bending fixture at 1 Hz and a 5°C/min heating rate from $T = -25$ to 100°C. The values of the shear storage modulus, G', were reported to be comparable to those of the flexural modulus. Up to $T \approx 60$°C the G'_r value was constant, increasing with MMT content (see the dotted line in Figure 16.28). Similarly, exfoliated PS/MMT was prepared reactively and tested in DMA at 1 Hz and 5°C/min [Uthirakumar et al., 2004]. The relative dynamic modulus is also displayed in Figure 16.28, along with values calculated from Li et al. data [2005]. Results from these three sources follow a similar dependence. Considering the high modulus of the polymer matrix, the enhancement of rigidity observed upon incorporation of clay is impressive [Utracki, 2008].

In contrast with the results obtained for elastomers, incorporation of clay into vitreous PS-type matrix has a significantly smaller effect on the modulus. From a physical point of view, there is a large difference of molecular mobility between these two types. Whereas in elastomers the reinforcement takes place in a high-mobility liquidlike environment above T_g, in the vitreous systems represented by PS the tests are conducted at $T < T_g$. It would be expected that during the steady-state deformation of elastomeric CPNC, the clay platelets might orient in the stress direction and thus lead to lower modulus than that measured at low strain in dynamic mode.

In their review, Schmidt et al. [2002] focused on the dynamics of the clay–matrix interface. The MD simulation revealed the presence of three-layer intergallery structures with intercalant molecules close to the clay surface and macromolecules in the central layer. In the case of PS-based CPNC, because of interactions between the clay surface and aromatic rings, the polymer might diffuse toward the silicate. Furthermore, the model suggested that adjacent layers might have different densities. Within a specific range of temperature and pressure, the high- and low-density layers show solid and liquidlike dynamics, observed by cross-polarization spin-echo nuclear magnetic resonance (NMR) spectroscopy [Zax et al., 2000].

Okamoto et al. [2000, 2001a] investigated the dispersed structures in PNC with PMMA or its copolymers (MMA with polar monomers) as the matrix. The PNC was prepared by in situ polymerization with 10 wt% of organically modified smectic clay, obtaining intercalated nanocomposites. The storage tensile modulus E' and tan δ of PMMA–clay and PMMA–intercalant were similar. However, when copolymers were used as the matrix, the E' of PNC increased over the entire temperature range, but tan δ peaks shifted to lower T.

Hsieh et al. [2004] investigated the mechanical and flow behavior of polycarbonate (PC)-based CPNC, prepared in a corotating TSE with 1.5 to 5 wt% C25A. The rubbery plateau modulus of PNC with finely dispersed intercalated clay decreased significantly. PNC with 5 wt% clay had T_g lower by about 10°C than neat PC, traced to the degradative reduction of its M_w by 43%.

16.3.3 Nanocomposites with a Semicrystalline Matrix

CPNCs with a semicrystalline matrix have complex morphology and diverse mobility, as the type and level of crystallinity varies and the T_g of the matrix polymer may be below or above the ambient temperature. There is also a greater diversity of chemical composition of these polymers. Considering the industrial importance of CPNC with PA-6 and PP matrices, only these two types are discussed.

PA-6-Based CPNC Polyamides are hygroscopic and their performance depends on the amount of absorbed moisture. PA-6 may be plasticized with up to 6 wt% H_2O, which reduces the modulus and lowers the transition temperatures. Dry polymer melts at $T_m = 219$°C and has three lower transition temperatures: $T_g \approx 60$, $T_\beta \approx -60$, and $T_\gamma \approx -130$°C, well defined in the loss modulus versus T plots.

Vlasveld et al. [2005] investigated the viscoelastic properties of melt-compounded PA-6 with 1 to 20 wt% nano- and microparticles: fluoromica ME-100 and its organically modified MEE grade, nanosilica ($D = 20$ to 50 nm), fiber-shaped nanoparticles ($D = 10$ to 30 nm, $L - a$ few hundred nanometers), and then glass beads ($D = 30$ μm), glass fibers ($D = 10$ μm, $L = 4$ mm), and glass flakes ($t = 2.5$ μm, $L = 50$ to 1800 μm). DMA tests at 1 Hz and heating rate of 5°C/min ($T = -130$ to 200°C) showed that the modulus of PNC with 1 to 20 wt% ME-100 increased with silicate concentration over the entire temperature range, while T_g remained constant. PNC with MEE clay had a good dispersion of high-aspect-ratio platelets, which resulted in higher E' values than those of inorganic ME-100. The particle shape also affected the performance. Thus,

spherical particles showed the smallest modulus enhancement and platelets the largest. For microparticles the shape at a constant filler content of 5 wt% showed a trend similar to that seen for nanoparticles (except that at high temperatures, where glass fibers were more effective than flakes). The test results confirmed that microparticles are significantly less effective than nanoparticles.

Winberg et al. [2005] investigated how the incorporation of clay into PA-6 affects the free-volume cavity size and the viscoelastic properties. The CPNC contained 4 to 35 wt% C20A. DMA tests were performed using an automated torsion pendulum while heating at 2°C/min from 173 to 473 K at 1 Hz. The authors reported enhancement of E' with clay content (i.e., $E'_r = 1.3$ to 1.6 at $T < T_g$ and $E'_r = 1.3$ to 3.3 at $T_g < T = 373$ K). Furthermore, at $= 0$ to 120°C, the loss modulus, E'' increased with increasing clay content.

Incarnato and co-workers [2004] reported that at constant clay content the CPNC modulus increases with the extrusion rate. Addition of clay shifted the main E'' peak position by about 60 to 70°C. The same authors [2003] also investigated the viscoelastic properties of a PA-6 and its statistical, partially aromatic copolymer, ADS, with 3, 6 and 9 wt% C30B. In tensile mode the low-T relative modulus, E'_r increased from 1.15 to 1.54 (at 1 Hz and 5°C/min). The influence of clay on T_g might be attributed to the confinement of polymer chains in silicate galleries, which partially hinders the molecular motion [Ash et al., 2002]. It is significant that T_g does not always increase with organoclay content, as the outcome is influenced by the type, quantity, and miscibility of the plasticizing intercalant.

PA-6-based CPNCs with up to 10 wt% MMT-ODA were analyzed in DMA (at 1 Hz and 3 K/min; $T = 143$ to 383 K) [Pramoda and Liu, 2004; Li et al., 2007]. The melt-compounded nanocomposites were exfoliated at $w < 5$ wt% MMT-ODA. The organoclay presence affected PA-6 crystallinity and crystalline morphology (e.g., change from α- to γ-crystalline form). The dependence E' versus T increased with clay loading. At least up to T_g, the curves for different clay concentrations were parallel to each other, similar to PS-based PNC, where the relative tensile modulus was T-independent. Plots of E' and T_g versus organoclay content showed the opposite tendency: $dE/dw = 0.06$ and $dT_g/dw = -1.03$, with correlation coefficients of 0.93 and 0.98, respectively. However, as shown in Figure 16.29, E' strongly decreased with increasing T_g, indicating that the scatter of the data was related to the variability of CPNC morphologies. This behavior is not unusual, indicating the reduction of molecular mobility by solidification on a clay surface and possible reduction of crystallinity in the presence of immiscible ODA intercalant. It is noteworthy that CPNC type and performance depends on the type and quantity of intercalant and other additives [Chiu et al., 2005].

PP-Based CPNC In PP, $T_g \approx 0$°C, and at $T < T_g$, as for PS or PA-6. for different clay loadings the dynamic moduli of CPNC versus T nearly parallel each other; hence, the relative moduli $E'_r = E'$ (CPNC)/E' (matrix) is almost constant. Wu et al. [2005b] prepared PP-based CPNC by solution blending of PP + PP-MA with MMT preintercalated with cetyl pyridinium and hexamethylene diamine (HMDA)–modified PP-MA. The nanocomposites contained 0 to 5 wt% of well-dispersed organoclay. DMA

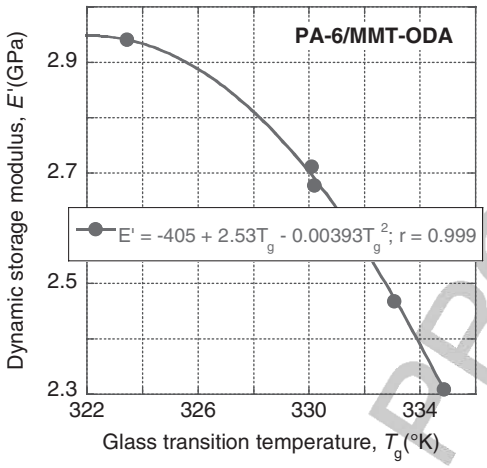

FIGURE 16.29 Dynamic storage modulus vs. T_g for PA-6 with 0–10 wt% MMT-ODA.

analysis (1 Hz, 2°C/min from −80 to 90°C) showed significant increases of modulus at $T < T_g$: $E'_r = 1.09$, 1.48, and 1.67 for 1, 3, and 5 wt% organoclay, respectively. At $T_g < T = 80$°C the relative modulus increased even more rapidly: $E'_r \approx 4.1$, 7.1, and 7.9. However, as in other publications, the dynamic behavior was found to depend on the type of intercalant and compatibilizer as well as their amounts. Thus, the relative storage modulus of PP-based CPNC (with 5 wt% MMT-ODA and 0 to 20 wt% compatibilizer) was: $E'_r = 0.89$ to 1.2 and 0.95 to 1.6 at −68 and +124°C, respectively [Zhong et al., 2006]. Similarly, E'_r of CPNC of PP + PP-MA + 10 wt% MMT-ODA decreased with T, converging from widely different values at −30 to a single value at 170°C [Wang et al., 2006]. At $T < T_g$, the magnitude of $E'_r \approx 1.08$ to 1.4 depended on the PP-MA molecular weight (M_w), while at $T > T_g$, E'_r reached a maximum at $T \approx 58$°C. Incorporation of 10 wt% TPO [poly(ethylene-*co*-octene) with $T_g \approx -50$°C] significantly affected the relative moduli below and above T_g [Lim *et al.*, 2006]. Thus, at 1Hz and 5 K/min, in the absence of TPE, $E'_r = 1.57$ and 1.38 at 193 and 293 K, respectively, while in its presence $E'_r = 1.38$ and 1.13, respectively, at these temperatures. The tensile modulus of these CPNC (at room temperature?) without and with the TPE was smaller: $E_r = 1.23$ and 1.11, respectively.

Modesti et al. [2006] investigated the effects of processing on the thermal behavior of PP-based CPNC. The authors used a homopolymer, compatibilizer (PP-MA), and 3.5 or 5 wt% organoclay. The composition was melt-compounded in a corotating TSE ($D = 42$ mm, $L/D = 40$). The CPNC storage modulus increased less rapidly in PP without than with PP-MA. Furthermore, the modulus enhancement increased with increasing clay content, especially at low temperature. At $T < T_g$, the PP-PNC and PP-MA-PNC showed $E'_r = 1.05$ to 1.13 and $E'_r = 1.2$ to 1.25, respectively; these values changed to 1.2 and 1.5 at $T = 80$°C. Processing also affected clay dispersion and the dynamic-mechanical properties. The best results were obtained using low barrel temperature and high shear stress.

Kim et al. [2006] investigated a novel fabrication method by applying an electrical field to enhance the clay dispersion. Melt compounding with an electrical field of PP/PP-MA with 5 wt% C20A improved the clay dispersion. The treated electrically PP-clay showed larger storage and loss moduli over the entire temperature range. However, the T_g value of PP was unaffected by compounding and addition of clay.

Wang and Sheng [2005] prepared a PP-based PNC by using 1 to 7 wt% organically modified attapulgite clay, which has a three-dimensional structure and fibrous morphology. The zeolite-like clay channels could be filled with water or organic molecules. The viscoelastic properties of these materials showed remarkable enhancements of E' at low temperature, with the largest increase at 2 wt% clay loading: $E'_r = 2.7$ for 2 wt% compared with $E'_r = 1.4$ for 3 wt%. The PNC with 1 and 5 wt% clay had comparable stiffness ofver the entire temperature range. An increase of T_g for PNC with 2 wt% clay was also noted.

Liu and Wu [2001] investigated PP-based PNC prepared by melt compounding with clay preintercalated with unsaturated monomer, capable of tethering onto PP backbone. The resulting CPNCs were intercalated. At low T the relative storage modulus, E'_r increased with organoclay loading from 1.37 for 1 wt% to 1.59 for 7 wt%, and at $T = 135^\circ$C from 1.36 to 2.0. The E'' also increased at $T > T_g$. The T_g of PP initially decreased with organoclay content, reaching a minimum at 3 wt% clay.

The dynamic mechanical behavior of PP-PNC was studied by Kawasumi et al. [1997]. The CPNCs contained PP with 5 wt% of two types of clay (a MMT Kunipia-F and a fluoromica ME-100), and two types of PP-MA. Owing to the high aspect ratio of ME-100, it enhanced E' more than MMT; the relative modulus at $T = 80$ to 90°C was $E'_r = 2.4$. Below T_g, $E'_r \approx 1.3$ to 1.4; then it increases with T to 1.7 to 2 before decreasing near T_m.

Few reports compared the dynamic and steady-state moduli. Figure 16.30 shows the dynamic storage plotted versus the steady-state Young's modulus for three different families of CPNC based on PA-6, PP, and PS with 2 wt% MMT-ODA. The tensile and dynamic tests were conducted at room temperature using the same injection-molded dogbones (ASTM D638). At 1 Hz and 2°C/min, the dynamic tests were within the linear viscoelastic zone. The value of Young's modulus was larger than the storage value, but a linear correlation was observed.

In CPNCs the improvement in the steady-state and dynamic moduli depends on the matrix modulus, the clay aspect ratio, its degree of dispersion, and interaction between the clay and the matrix. Furthermore, the reinforcement (expressed by the relative modulus, E_r or E'_r) depends on the T distance from T_g. The largest improvement in the storage modulus belongs to PNC with the lowest T_g, hence to elastomer-based CPNC with $T_g < 25^\circ$C, and the smallest to glassy (e.g., PS-based) CPNC with $T_g > 25^\circ$C; the reinforcement of dried PA-6-based CPNC was moderate. A comparison of published steady-state and dynamic moduli shows some differences between these two sets of data, whereas the new values determined for the three types of CPNCs under controlled conditions show acceptable agreements. The relative modulus in Figure 16.31, $E'_r = E'_c/E'_m$ provides a more relevant measure of clay addition effects than that of the absolute values. Furthermore, the relative moduli seem to have a smaller standard deviation, and its values in dynamic and steady-state tests are more compa-

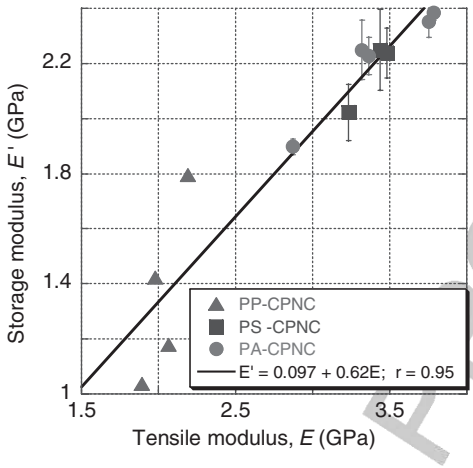

FIGURE 16.30 Dynamic storage modulus vs. steady state Young modulus for three different families of PNC based on PA-6, PP and PS with 2-wt% MMT-ODA and their matrix at $T = 25^{\circ}$C.

rable. The differences often noted may be due to the nature of the matrix, nonlinear viscoelastic response, difference of the rate and magnitude of applied strain that may orient the platelets, miscalibration of instrument, and so on. Therefore, before the dynamic tests are used as a convenient replacement of the standard tensile or flexural method, a systematic study is needed to optimize the test procedures [Utracki, 2009].

There is a need for thorough studies of the solid viscoelastic properties of CPNCs. A single sweep of temperature at a single arbitrarily selected frequency and heating

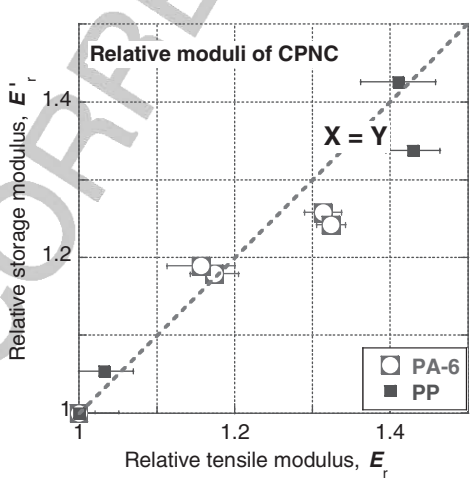

FIGURE 16.31 Relative storage vs. relative tensile modulus for PA, PP and their melt compounded CPNC at $T = 25^{\circ}$C with different degree of clay dispersion. (From Sepehr and Utracki [2006].)

rate, or the reverse of frequency at a constant T, are insufficient for correlating with the standard tensile test results. Since these two types of measurements gave similar results for CPNCs with a rigid matrix (vitreous or semicrystalline polymers at ambient T), the differences reported between E and E' may originate from the different clay platelets orientations imposed by sample preparation and test conditions, especially at $T > T_g$.

16.4 SUMMARY AND OUTLOOK

The rheological studies of CPNCs in shear and elongation demonstrate that even at low clay loading the flow might be complex. Nanofiller orientation, crowding during solidification, and the seldom considered chemical changes (e.g., decomposition of intercalant) might affect the interlayer spacing and performance. CPNCs show a range of performances, starting with the traditional behavior of filled systems and ending with end-tethered nanocomposites having distinct flow characteristics. For end-tethered CPNCs, at low or moderate clay concentrations, the shear flow may be interpreted using LCP theories. Following the Onogi and Asada [1980] classification, three regions of flow might be identified:

1. At low deformation rates, there is a solidlike yield stress behavior with the slope $-1/2$, caused by disintegration of a three-dimensional structure.
2. At middle strain rates, assemblies of clay platelets undergo either a tumbling (in shear) or stretching (in elongation).
3. At high deformation rates, the platelets become oriented in the stress direction, which causes the viscosity to decrease almost to the matrix level.

In end-tethered systems, three-dimensional structures are observed at about 0.5 vol% clay. These are responsible for nonlinear viscoelastic flow behavior, which may be characterized by stress overshoot or FTR experiments. These methods are well suited for quantification of the nonlinear effects as a function of composition, strain rate, strain, temperature, and so on. The unique character of CPNCs is evident in extensional flow. The still infrequent studies of these flows lead to the conclusion that the presence of exfoliated clay platelets able to interact with the matrix (e.g., in end-tethered systems) might enhance the strain hardening. This effect agrees well with the hairy clay platelet (HCP) model of CPNC. Accordingly, in analogy to the improved processability of some resins by blending them with branched homolog (e.g., industrial blends of LLDPE with LDPE), one may use the CPNC technology to improve film blowing, blow molding or foaming, and microfoaming of difficult-to-process resins. At high extensional flow rates, the platelets may be oriented perpendicularly to the stretch direction, which causes the transient viscosity to move into the strain-hardening region. Both effects are stronger for end-tethered than for free platelets systems, especially at higher levels of clay loading.

More work is required to resolve several rheological problems of PNC flow in shear and elongation. Conventional elongational measurements need to be combined with the structure-characterizing methods, such as light, x-ray, or neutron scattering, to record changes in orientation and degree of clay dispersion during flow. Finally, as illustrated in Section 16.2.7, modeling of the rheological properties of PNC is still in its infancy. Molecular dynamics approaches appear to be promising, as computers are faster and better performing and the possibility of simulating the behavior of millions of particles in three-dimensional flows using parallel computers opens up new frontiers for MD. Nevertheless, better, more realistic phenomenological models need to be developed. Such models incorporated in a simulation software package will be useful not only for characterization, but primarily for predicting correct behavior (stresses, structure, orientation) under real processing conditions as encountered, for example, during injection molding.

REFERENCES

Aalaie, J., Khanbabaie, G., Khoshniyat, A. R., and Rahmatpour, A., Study on steady shear, morphology and mechanical behavior of nanocomposites based on polyamide 6, *J. Macromol. Sci. B*, **46**, 305–316 (2007).

Advani, S. G., and Tucker, C. L., The use of tensors to describe and predict fiber orientation in short fiber composites, *J. Rheol.*, **31**, 751–784 (1987).

Ahmadi, S. J., Huang, Y., and Li, W., Fabrication and physical properties of EPDM–organoclay nanocomposites, *Compos. Sci. Technol.*, **65**, 1069–1076 (2005).

Akzo Nobel Chemicals BV, Tech. Bull. PA 07.415.01, June 2007; Perkalite® F100, Product Data Sheet PA 61451.02/, Nov. 2007; PowerPoint presentation, www.nrk.nl/Scripts/Download.aspx.

Anderson, K. L., Sinsawat, A., Vaia, R. A., and Farmer, B. L., Control of silicate nanocomposite morphology in binary fluids: coarse-grained molecular dynamics simulations, *J. Polym. Sci. B*, **43**, 1014–1024 (2005).

Ash, B. J., Schadler, L. S., and Siegel, R. W., Glass transition behavior of alumina/polymethylmethacrylate nanocomposites, *Mater. Lett.*, **55**, 83–87 (2002).

Azaiez, J., Constitutive equations for fiber suspensions in viscoelastic media, *J. Non-Newtonian Fluid Mech.*, **66**, 35–54 (1996).

Bafna, A., Beaucage, G., Mirabella, F., and Mehta, S., 3D hierarchical orientation in polymer–clay nanocomposite films, *Polymer*, **44**, 1103–1115 (2003).

Balazs, A. C., Singh, C., Zhulina, E., and Lyatskaya, Y., Modeling the phase behavior of polymer/clay nanocomposites, *Acc. Chem. Res.*, **32**, 651–657 (1999).

Bartholome, C., Beyou, E., Bourgeat-Lami, E., Cassagnau, Ph., Chaumont, Ph., David, L., and Zydowicz, N., Viscoelastic properties and morphological characterization of silica/polystyrene nanocomposites synthesized by nitroxide-mediated polymerization, *Polymer*, **46**, 9965–9973 (2005).

Batchelor, G. K., Slender-body theory for particles of arbitrary cross-section in Stokes flow, *J. Fluid Mech.*, **44**, 419–440 (1970).

Batchelor, G. K., The stress generated in a non-dilute suspension of elongated particles by pure straining motion, *J. Fluid Mech.*, **46**, 813–829 (1971).

Batchelor, G. K., Transport properties of 2-phase materials with random structure, *Annu. Rev. Fluid Mech.*, **6**, 227–255 (1974).

Batchelor, G. K., The effect of Brownian motion on the bulk stress in a suspension of spherical particles, *J. Fluid Mech.*, **83**, 97–117 (1977).

Batchinski, A. J., Untersuchungen über die innere Reibung der Flussigkeiten, *Z. Phys. Chem.*, **84**, 643–706 (1913).

Berta, M., Saiani, A., Lindsay, C., and Gunaratne, R., Effect of clay dispersion on the rheological properties and flammability of polyurethane–clay nanocomposite elastomers, *J. Appl. Polym. Sci.*, **112**, 2847–2853 (2009).

Bicerano, J., Glass transition, in Encyclopedia of Polymer Science and Technology, 3rd ed., Vol. 2, Mark, H. F.,Ed., Wiley, Hoboken, NJ, 2003.

Bicerano, J., Douglas, J. F., and Brune, D. A., *Rev. Macromol. Chem. Phys.*, **C39**, 561–642 (1999).

Bird, R. B., Dotson, P. J., and Johnson, N. L., Polymer solution rheology based on a finitely extensible bead–spring chain model, *J. Non-Newtonian Fluid Mech.*, **7**, 213–235 (1980).

Bird, R. B., Hassager, O., Armstrong, R. C., and Curtiss, C. F., Dynamics of Polymeric Fluids, Wiley, New York, 1987.

Borodin, O., Bedrov, D., Smith, G. D., Nairn, J., and Bardenhagen, S., Multiple modeling of viscoelastic properties of polymer nanocomposites, *J. Polym. Sci. B*, **43**, 1005–1013 (2005).

Bousmina, M., Study of intercalation and exfoliation processes in polymer nanocomposites, *Macromolecules*, **39**, 4259–4263 (2006).

Boyer, R. F., T_{LL} and related liquid state transitions—relations: a review, in Polymer Yearbook 2, Pethrick, R. A.,Ed., Harwood Academic, New York, 1985.

Boyer, R. F., Evidence from T_{LL} and related phenomena for local structure in the amorphous state of polymers in Order in the Amorphous State, Miller, R. L., and Rieke, J. K.,Eds., Plenum Press, New York, 1987.

Brady, J. F., and Bossis, G., The rheology of concentrated suspensions of spheres in simple shear flow by numerical simulations, *J. Fluid Mech.*, **155**, 105–129 (1985).

Camino, G., Maffezzoli, A., Braglia, M., De Lazzaro, M., and Zammarano, M., Effect of hydroxides and hydroxycarbonate structure on fire retardant effectiveness and mechanical properties in ethylene–vinyl acetate copolymer, *Polym. Degrad. Stabil.*, **74**, 457–464 (2001).

Carreau, P. J.,Rheological equations from molecular network theories, Ph.D. dissertation, University of Wisconsin, Madison, 1968.

Carreau, P. J., Rheological equations from molecular network theories, *Trans. Soc. Rheol.*, **16**, 99–127 (1972).

Chang, Y.-W., Shin, J.-Y., and Ryu, S. H., Preparation and properties of styrene–ethylene/butylenes–styrene (SEBS)–clay hybrids, *Polym. Int.*, **53**, 1047–1051 (2004).

Chiu, F.-C., Lai, S.-M., Chen, Y.-L., and Lee, T.-H., Investigation of the polyamide 6/organoclay nanocomposites with or without a maleated polyolefin elastomer as toughener, *Polymer*, **46**, 11600–11609 (2005).

Chow, W. S., Abu Bakar, A., Mohd Ishak, Z. A., Karger-Kocsis, J., and Ishiaku, U. S., Effect of maleic anhydride-grafted ethylene–propylene rubber on the mechanical, rheological and

morphological properties of organoclay reinforced polyamide 6/polypropylene nanocomposites, *Eur. Polym. J.*, **41**, 687–696 (2005).

Ciferri, A., Phase behavior of rigid and semirigid mesogens, in Liquid Crystallinity in Polymers, Ciferri, A.,Ed., VCH, New York, 1991.

Cohn, M. I.,Reducing particle size of clay and rheology control of clay–water systems, U.S. patent 3,348,778, Oct. 24, 1967, Appl. Mar. 4, 1966, to Mineral Industries Corp.

Costa, F. R., Abdel-Goad, M., Wagenknecht, U., and Heinrich, G., Nanocomposites based on polyethylene and Mg–Al layered double hydroxide: I. Synthesis and characterization, *Polymer*, **46**, 4447–4453 (2005).

Costa, F. R., Wagenknecht, U., Jehnichen, D., Abdel Goad, M., and Heinrich, G., Nanocomposites based on polyethylene and Mg–Al layered double hydroxide: II. Rheological characterization, *Polymer*, **47**, 1649–1660 (2006).

Costa, F. R., Saphiannikova, M., Wagenknecht, U., and Heinrich, G., Layered double hydroxide based polymer nanocomposites, *Adv. Polym. Sci.*, **210**, 101–168 (2008).

Dealy, J. M., and Tsang, W., Structural time dependency in the rheological behavior of molten polymers, *J. Appl. Polym. Sci.*, **26**, 1149–1158 (1981).

Debbaut, B., and Burhin, H., Large amplitude oscillatory shear and Fourier-transform rheology for a high-density polyethylene: experiments and numerical simulation, *J. Rheol.*, **46**, 1155–1176 (2002).

Doi, M., Molecular dynamics and rheological properties of concentrated solutions of rodlike polymers in isotropic and liquid crystalline phases, *J. Polym. Sci. B*, **19**, 229–243 (1981).

Doi, M., and Edwards, S. F., Dynamics of concentrated polymer systems, *J. Chem. Soc., Faraday Trans.*, **74** (2), 1802–1817 (1978).

Doolittle, A. K., Studies in Newtonian flow: I. The dependence of the viscosity on temperature, *J. Appl. Phys.*, **22**, 1031–1035 (1951a);**22**, 1471–1475, (1951b); **23**, 236–239 (1952).

Doolittle, A. K., The Technology of Solvents and Plasticizers, Wiley, New York, 1954.

Doolittle, A. K., and Doolittle, D. B., Studies in Newtonian flow: V. Further verification of the free-space viscosity relation, *J. Appl. Phys.*, **28**, 901–905 (1957).

English, R. J., Gulati, H. S., Jenkins, R. D., and Khan, S. A., Solution rheology of a hydrophobically modified alkali-soluble polymer, *J. Rheol.*, **41**, 427–444 (1997).

Eslami, H., Grmela, M., and Bousmina, M., A mesoscopic rheological model of polymer/layered silicate nanocomposites, *J. Rheol.*, **51**, 1189–1222 (2007).

Fan, X. J., *Theoretical and Applied Rheology*, *Proceedings of the XIth International Congress on Rheology*, Brussels, Elsevier, Amsterdam 1992, pp. 850–852.

Ferry, J. D., Viscoelastic Properties of Polymers, 3rd ed., Wiley, New York, 1980.

Fisa, B., and Utracki, L. A., Rheology of mica-reinforced polyethylene melts, *Polym. Compos.*, **5**, 36–43 (1984).

Folgar, F. P., and Tucker, C. L., Orientation behavior of fibers in concentrated suspensions, *J. Reinf. Plast. Compos.*, **3**, 98–119 (1984).

Frisch, H. L., and Simha, R., Viscosity of colloidal suspensions and macromolecular solutions, in Rheology, Vol. 1, Eirich, F. R.,Ed., Academic Press, New York, 1956.

Fu, X.-A., and Qutubuddin, S., Polymer–clay nanocomposites: exfoliation of organophilic montmorillonite nanolayers in polystyrene, *Polymer*, **42**, 807–813 (2001).

Galgali, G., Ramesh, C., and Lele, A., A rheological study on the kinetics of hybrid formation in polypropylene nanocomposites, *Macromolecules*, **34**, 852–858 (2001).

Galgali, G., Agarwal, S., and Lele, A., Effect of clay orientation on the tensile modulus of polypropylene–nanoclay composites, *Polymer*, **45**, 6059–6069 (2004).

Gatos, K. G., and Karger-Kocsis, J., Effects of primary and quaternary amine intercalants on the organoclay dispersion in a sulfur-cured EPDM rubber, *Polymer*, **46**, 3069–3076 (2005).

Giannelis, E. P., Krishnamoorti, R., and Manias, E., Polymer–silicate nanocomposites: model systems for confined polymer and polymer brushes, *Adv. Polym. Sci.*, **138**, 107–147 (1999).

Giese, R. F., and van Oss, C. J., Colloid and Surface Properties of Clays and Related Materials, Marcel Dekker, New York, 2002.

Giesekus, H., A simple constitutive equation for polymer fluids based on the concept of deformation dependent tensorial mobility, *J. Non-Newtonian Fluid Mech.*, **11**, 69–109 (1982).

Giesekus, H., Stressing behavior in simple shear flow as predicted by a new constitutive model for polymer fluids, *J. Non-Newtonian Fluid Mech.*, **12**, 367–374 (1983).

Ginzburg, V. V., Singh, C., and Balazs, A. C., Theoretical phase diagrams of polymer/clay composites: the role of grafted organic modifiers, *Macromolecules*, **33**, 1089–1099 (2000).

Goldsmith, H. L., and Mason, S. G., The microrheology of dispersions, in Rheology, Vol. 4, Eirich, F. R.,Ed., Academic Press, New York, 1967.

Grmela, M., Particle and bracket formulations of kinetic equations, *Contemp. Math.*, **28**, 125–132 (1984).

Grmela, M., Thermodynamic and rheological modeling: polymeric liquid crystals, in *Polymer Rheology and Processing*, Collyer, A. A., and Utracki, L. A.,Eds., Elsevier, Amsterdam, 1990, pp. 55–81.

Grmela, M., Mesoscopic dynamic and thermodynamic: application to polymer fluids, *Lect. Notes Phys.*, **381**, 99–126 (1991).

Grmela, M., Reciprocity relations in thermodynamics, *Physica A*, **309**, 304–328 (2002).

Grmela, M., and Carreau, P. J., Conformation tensor rheological models, *J. Non-Newtonian Fluid Mech.*, **23**, 271–294 (1987).

Grmela, M., and Ottinger, H. C., Dynamics and thermodynamics of complex fluids: I. Development of a general formalism, *Phys. Rev. E*, **55**, 6620–6632 (1997).

Gu, J. F., and Grmela, M., GENERIC model of active advection, *J. Non-Newtonian Fluid Mech.*, **152**, 12–26 (2008).

Gu, S.-Y., Ren, J., and Wang, Q.-F., Rheology of polypropylene/clay nanocomposites, *J. Appl. Polym. Sci.*, **91**, 2427–2434 (2004).

Han, S. S., Kim, Y.-S., Lee, S. G., Lee, J. H., Zhang, K., and Choi, H. J., Rheological properties of polystyrene–organophilic layered silicate nanocomposites, *Macromol. Symp.*, **245–246**, 199–207 (2006).

Happel, J., and Brenner, H., Low Reynolds Number Hydrodynamics, Nijhoff, The Hague, The Netherlands, 1983.

Hasegawa, N., Okamoto, H., and Usuki, A., Preparation and properties of ethylene propylene rubber (EPR)–clay nanocomposites based on maleic anhydride–modified EPR and organophilic clay, *J. Appl. Polym. Sci.*, **93**, 758–764 (2004).

Hashin, Z., Viscoelastic behavior of heterogeneous media, *J. Appl. Mech. Trans. ASME*, **32E**, 630–636 (1965).

Ho, D. L., Briber, R. M., and Glinka, C. J., Characterization of organically modified clays using scattering and microscopy techniques, *Chem. Mater.*, **13**, 1923–1931 (2001).

Hoffmann, B., Dietrich, C., Thomann, R., Friedrich, Ch., and Mülhaupt, R., Morphology and rheology of polystyrene nanocomposites based upon organoclay, *Macromol. Rapid Commun.*, **21**, 57–61 (2000).

Hofmann, A. W., Beiträ ge zur Kenntnifs der flüchtigen organischen Basen: X. Uebergang der flüchtigen Basen in eine Reihe nichtflüchtiger Alkaloï de, *Liebigs Ann. Chem.*, **78**, 253–286 (1851).

Hsieh, A. J., Moy, P., Beyer, F. L., Madison, P., Napadensky, E., Ren, J., and Krishnamoorti, R., Mechanical response and rheological properties of polycarbonate layered-silicate nanocomposites, *Polym. Eng. Sci.*, **44**, 825–837 (2004).

Huber, T. A., Polymer–Carbon Nanotube Composites:, A Literature Review, Tech. Memo ADA436227, Defense Research and Development Atlantic Dartmouth (Canada), 2004.

Hyun, Y. H., Lim, S. T., Choi, H. J., and Jhon, M. S., Rheology of poly(ethylene oxide)/organoclay nanocomposites, *Macromolecules*, **34**, 8084–8093 (2001).

Incarnato, L., Scarfato, P., Russo, G. M., Di Maio, L., Iannelli, P., and Acierno, D., Preparation and characterization of new melt compounded copolyamide nanocomposites, *Polymer*, **44**, 4625–4634 (2003).

Incarnato, L., Scarfato, P., Scatteia, L., and Acierno, D., Rheological behavior of new melt compounded copolyamide nanocomposites, *Polymer*, **45**, 3487–3496 (2004).

Israelachvili, J. N., Intermolecular and Surface Forces with Applications to Colloidal and Biological Systems, Academic Press, New York, 1985.

Jeffery, G. B., The motion of ellipsoidal particles immersed in a viscous fluid, *Proc. R. Soc.*, **A102**, 161–179 (1922).

Jin, J., Song, M., Yao, K. J., and Chen, L., A study on viscoelasticity of polyurethane–organoclay nanocomposites, *J. Appl. Polym. Sci.*, **99**, 3677–3683 (2006).

Jogun, S. M., and Zukoski, C. F., Rheology of dense suspensions of plate like particles, *J. Rheol.*, **40**, 1211–1232 (1996).

Jogun, S. M., and Zukoski, C. F., Rheology and microstructure of dense suspensions of plate-shaped colloidal particles, *J. Rheol.*, **43**, 847–871 (1999).

Kairn, T., Daivis, P. J., Ivanov, I., and Bhattacharya, S. N., Molecular-dynamics simulation of model polymer nanocomposite rheology and comparison with experiment, *J. Chem. Phys.*, **123**, 194905-1 (2005).

Kawasumi, M., Hasegawa, N., Kato, M., Usuki, A., and Okada, A., Preparation and mechanical properties of polypropylene–clay hybrids, *Macromolecules*, **30**, 6333–6338 (1997).

Keller, W. D.,in Kirk-Othmer Encyclopedia of Chemical Technology, 3rd ed., Vol. 6, Grayson, M., and Eckroth, D.,Eds., Wiley-Interscience, New York, 1979.

Kim, D. H., Park, J. U., Cho, K. S., Ahn, K. H., and Lee, S. J., A novel fabrication method for poly(propylene)/nanocomposites by continuous processing, *Macromol. Mater. Eng.*, **291**, 1127–1135 (2006).

Kim, T. H., Jang, L. W., Lee, D. C., Choi, H. J., and Jhon, M. S., Synthesis and rheology of intercalated polystyrene/Na^+ montmorillonite nanocomposites, *Macromol. Rapid Commun.*, **23**, 191–195 (2002).

Kiss, G., and Porter, R. S., Rheology of concentrated solutions of helical polypeptides, *J. Polym. Sci. Polym. Phys.*, **18**, 361–388 (1980).

Knauert, S. T., Douglas, J. F., and Starr, F. W., The effect of nanoparticle shape on polymer–nanocomposite rheology and tensile strength, *J. Polym. Sci. B*, **45**, 1882–1897 (2007).

Kojima, Y., Usuki, A., Kawasumi, M., Okada, A., Kurauchi, T., Kamigaito, O., and Kaji, K., Fine structure of nylon-6–clay hybrid, *J. Polym. Sci. B*, **32**, 625–630 (1994).

Kojima, Y., Usuki, A., Kawasumi, M., Okada, A., Kurauchi, T., Kamigaito, O., and Kaji, K., Novel preferred orientation in injection-molded nylon-6–clay hybrid, *J. Polym. Sci. B*, **33**, 1039–1045 (1995).

Kotaka, T., and Watanabe, H., Rheological and morphological properties of heterophase block copolymer solutions, in Current Topics in Polymer Science, Vol. II, Ottenbrite, R. M. Utracki, L. A., and Inoue, S.,Eds., Hanser-Verlag, Munich, 1987.

Kotsilkova, R., Rheology–structure relationship of polymer/layered silicate hybrids, *Mech. Time-Depend. Mater.*, **6**, 283–300 (2002).

Krieger, I. M., and Dougherty, T. J., A mechanism for non-Newtonian flow in suspensions of rigid spheres, *Trans. Soc. Rheol.*, **3** (1), 137–152 (1959).

Krishnamoorti, R., and Yurekli, K., Rheology of polymer layered silicate nanocomposites, *Curr. Opin. Colloid Interface Sci.*, **6**, 464–470 (2001).

Krishnamoorti, R., Vaia, R. A., and Giannelis, E. P., Structure and dynamics of polymer–layered silicate nanocomposites, *Chem. Mater.*, **8**, 1728–1734 (1996).

Larson, R. G., The Structure and Rheology of Complex Fluid, Oxford University Press, New York, 1999.

Larson, R. G., and Doi, M., Mesoscopic domain theory for textures liquid-crystalline polymers, *J. Rheol.*, **35**, 539–563 (1991).

Lee, H. M., Park, B. J., Choi, H. J., Gupta, R. K., and Bhattacharya, S. N., Preparation and rheological characteristics of ethylene–vinyl acetate copolymer/organoclay nanocomposites, *J. Macromol. Sci. B*, **46**, 261–273 (2007).

Lee, K. M., and Han, C. D., Effect of hydrogen bonding on the rheology of polycarbonate/organoclay nanocomposites, *Polymer*, **44**, 4573–4588 (2003a).

Lee, K. M., and Han, C. D., Rheology of organoclay nanocomposites: effects of polymer matrix/organoclay compatibility and the gallery distance of organoclay, *Macromolecules*, **36**, 7165–7178 (2003b).

Lee, S. H., and Youn, J. R., Properties of polypropylene/layered-silicate nanocomposites and melt-spun fibers, *J. Appl. Polym. Sci.*, **109**, 1221–1231 (2008).

Lee, S. H., Cho, E., and Youn, J. R., Rheological behavior of polypropylene/layered silicate nanocomposites prepared by melt compounding in shear and elongational flows, *J. Appl. Polym. Sci.*, **103**, 3506–3515 (2006).

Legge, N. R., Holden, G., and Schroeder, H. E.,Eds., Thermoplastic Elastomers, Hanser-Verleg, Munich, 1987.

Lele, A., Mackley, M., Ramesh, C., and Galgali, G., In situ rheo-x-ray investigation of flow-induced orientation in layered silicate–syndiotactic polypropylene nanocomposite melt, *J. Rheol.*, **46**, 1091–1110 (2002).

Lepoittevin, B., Devalckenaere, M., Pantoustier, N., Alexandre, M., Kubies, D., Calberg, C., Jérôme R., and Dubois, P., Poly(ε-caprolactone)/clay nanocomposites by in-situ intercalative polymerization catalyzed by dibutyl tin dimethoxide, *Polymer*, **43**, 4017–23 (2002).

Letwimolnun, W., Vergnes, B., Ausias, G., and Carreau, P. J., Stress overshoots of organoclay nanocomposites in transient shear flow, *J. Non-Newtonian Fluid Mech.*, **141**, 167–179 (2007).

Li, H., Yu, Y., and Yang, Y., Synthesis of exfoliated polystyrene/montmorillonite nanocomposite by emulsion polymerization using a zwitterion as the clay modifier, *Eur. Polym. J.*, **41**, 2016–2022 (2005).

Li, J., Zhou, C., Wang, G., and Zhao, D., Study on rheological behavior of polypropylene/clay nanocomposites, *J. Appl. Polym. Sci.*, **89**, 3609–3617 (2003).

Li, T. -C., Ma, J., Wang, M., Tjiu, W. C., Liu, T., and Huang, W., Effect of clay addition on the morphology and thermal behavior of polyamide 6, *J. Appl. Polym. Sci.*, **103**, 1191–1199 (2007).

Li, W., Huang, Y. D., and Ahmadi, S. J., Preparation and properties of ethylene–propylene–diene rubber/organo-montmorillonite nanocomposites, *J. Appl. Polym. Sci.*, **94**, 440–445 (2004).

Liao, M., Zhu, J., Xu, H., Li, Y., and Shan, W., Preparation and structure and properties of poly(styrene-b-butadiene)/clay nanocomposites, *J. Appl. Polym. Sci.*, **92**, 3430–3434 (2004).

Liao, M., Shan, W., Zhu, J., Li, Y., and Xu, H., Structure and properties of rubber/organic montmorillonite nanocomposites prepared by in situ anionic intercalation polymerization, *J. Polym. Sci. B*, **43**, 1344–1353 (2005).

Liao, M., Zhang, W., Shan, W., and Zhang, Y., Structure and properties of polybutadiene/montmorillonite nanocomposites prepared by in situ polymerization, *J. Appl. Polym. Sci.*, **99**, 3615–3621 (2006).

Lim, J. W., Hassan, A., Rahmat, A. R., and Wahit, M. U., Morphology, thermal and mechanical behavior of polypropylene nanocomposites toughened with poly(ethylene-*co*-octene), *Polym. Int.*, **55**, 204–215 (2006).

Lim, Y. T., and Park, O. O., Phase morphology and rheological behavior of polymer/layered silicate nanocomposites, *Rheol. Acta*, **40**, 220–229 (2001).

Lipscomb, G. G., Denn, M. M., Hur, D. U., and Boger, D. V., The flow of fiber suspensions in complex geometries, *J. Non-Newtonion Fluid Mech.*, **26**, 297–325 (1988).

Liu, B. L., Ding, Q. J., He, Q. H., Cai, J., Hu, B. X., and Shen, J., Novel preparation and properties of EPDM/montmorillonite nanocomposites, *J. Appl. Polym. Sci.*, **99**, 2578–2585 (2006).

Liu, X., and Wu, Q., PP/clay nanocomposites prepared by grafting–melt intercalation, *Polymer*, **42**, 10013–10019 (2001).

Luengo, G., Schmitt, F. -J., Hill, R., and Israelachvili, J. N., Thin film rheology and tribology of confined polymer melts: contrasts with bulk properties, *Macromolecules*, **30**, 2482–2494 (1997).

Marrucci, G., Remarks on the viscosity of polymeric liquid crystals, in Advances in Rheology, Mena, B., Garcia-Rejon, A., and Rangel-Nafaile, C.,Eds., Universided National Autónoma de México, 1984, pp. 441–448.

Marrucci, G., Rheology of nematic polymers, in Liquid Crystallinity in Polymers, Ciferri, A.,Ed., VCH, New York, 1991.

Masuda, T., Ohta, Y., and Onogi, S., Viscoelastic properties of multibranch polystyrenes, in Current Topics in Polymer Science, Vol. II, Ottenbrite, R. M., Utracki, L. A., and Inoue, S.,Eds., Hanser-Verleg, Munich, 1987.

Medellin-Rodriguez, F. J., Burger, C., Hsiao, B. S., Chu, B., Vaia, R., and Phillips, S., Time-resolved shear behavior of end-tethered nylon-6 clay nanocomposites followed by non-isothermal crystallization, *Polymer*, **42**, 9015–9021 (2001).

Médéric, P., Razafinimaro, T., and Aubry, T., Influence of melt-blending conditions on structural, rheological, and interfacial properties of polyamide-12 layered silicate nanocomposites, *Polym. Eng. Sci.*, **46**, 986–994 (2006).

Meissner, J., Modification of the Weissenberg rheogoniometer for measurement of transient rheological properties of molten polyethylene under shear: comparison with tensile data, *J. Appl. Polym. Sci.*, **16**, 2877–2899 (1972).

Metzner, A. B., and Prilutski, G. M., Rheological properties of polymeric liquid crystals, *J. Rheol.*, **30**, 661–691 (1986).

Mijović , J., Lee, H. K., Kenny, J., and Mays, J., Dynamics in polymer–silicate nanocomposites as studied by dielectric relaxation spectroscopy and dynamic mechanical spectroscopy, *Macromolecules*, **39**, 2172–2182 (2006).

Mishra, J. K., Hwang, K.-J., and Ha, C.-S., Preparation, mechanical and rheological properties of a thermoplastic polyolefin (TPO)/organoclay nanocomposite with reference to the effect of maleic anhydride modified polypropylene as a compatibilizer, *Polymer*, **46**, 1995–2002 (2005).

Mobuchon, Ch., Carreau, P. J., and Heuzey, M.-C., Effect of flow history on the structure of a non-polar polymer/clay nanocomposite model system, *Rheol. Acta*, **46**, 1045–1056 (2007).

Modesti, M., Lorenzetti, A., Bon, D., and Besco, S., Thermal behaviour of compatibilized polypropylene nanocomposite: effect of processing conditions, *Polym. Degrad. Stabil.*, **91**, 672–680 (2006).

Moldenaers, P., and Mewis, J., Parallel superposition measurements on polymeric liquid crystals, in Theoretical and Applied Rheology, Moldenaers, P., and Keunings, R.,Eds., Elsevier Science, Amsterdam, 1992.

Mousa, A., Halim, N. A., and Al-Robaidi, A., Rheological and mechanical properties of clay-thermoplastic elastomers derived from PVC and NBR, *Polym. Plast. Technol. Eng.*, **45**, 513–518 (2006).

Mukhopadhyay, A., and Granick, S., Micro- and nano-rheology, *Curr. Opin. Colloid Interface Sci.*, **6**, 423–429 (2001).

Murayama, N., Network theory of the nonlinear behavior of polymer melts., *Simple shear flow, Colloid Polym. Sci.*, **259**, 724–730 (1981).

Mutel, T., Kamal, M. R., and Utracki, L. A., Elongational behavior of short glass fiber reinforced polypropylene melts, *Polym. Compos.*, **5**, 289–298 (1984).

Nakajima, K., Watabe, H., and Nishi, T., Single polymer chain rubber elasticity investigated by atomic force microscopy, *Polymer*, **47**, 2505–2510 (2006).

Nam, P. H., Maiti, P., Okamoto, M., Kotaka, T., Hasegawa, N., and Usuki, A., A hierarchical structure and properties of intercalated polypropylene/clay nanocomposites, *Polymer*, **42**, 9633–9640 (2001).

Nam, P. H., Maiti, P., Okamoto, M., Kotaka, T., Nakayama, T., Takada, M., Ohshima, M., Usuki, A., Hasegawa, N., and Okamoto, H., Foam processing and cellular structure of polypropylene/clay nanocomposites, *Polym. Eng. Sci.*, **42**, 1907–1918 (2002).

Navarro-Bañón, V., Vega-Baudrit, J., Váquez, P., and Martín-Martinez, J. M., Interactions in naosilica–polyurethane composites evidenced by plate–plate rheology and DMTA, *Macromol. Symp.*, **221**, 1–10 (2005).

Ngai K. L., Dynamic and thermodynamic properties of glass-forming substances, *J. Non-Crystalline Solids*, **275**, 7–51 (2000).

Ngai K. L., An extended coupling model description of the evolution of dynamics with time in supercooled liquids and ionic conductors, *J. Phys. Condens. Matter.*, 15, S1107–S1125 (2003).

Norrish, K., The swelling of montmorillonite, *Trans. Faraday Soc.*, **18**, 120–134 (1954).

Oberdisse, J., and Boué , F., Rheology-structure relationship of a model nanocomposite material, *Prog. Colloid Polym. Sci.*, **126**, 124–129 (2004).

Okada, A., Fukushima, Y., Kawasumi, M., Inagaki, S., Usuki, A., Sugiyama, S., Kurauchi, T., and Kamigaito, O.,Composite material and process for manufacturing same *U.S. Patent* 4,739,007, Apr. 19, 1988, Toyota Chuo Kenkyusho.

Okamoto, M., Morita, S., Taguchi, H., Kim, Y. H., Kotaka, T., and Tateyama, H., Synthesis and structure of smectic clay/poly(methyl methacrylate) and clay/polystyrene nanocomposites via in situ intercalative polymerization, *Polymer*, **41**, 3887–3890 (2000).

Okamoto, M., Morita, S., Kim, Y. H., Kotaka, T., and Tateyama, H., Dispersed structure change of smectic clay/poly(methyl methacrylate) nanocomposites by copolymerization with polar comonomers, *Polymer*, **42**, 1201–1206 (2001a).

Okamoto, M., Nam, P. H., Maiti, P., Kotaka, T., Hasegawa, N., and Usuki, A., A house of cards structure in polypropylene/clay nanocomposites under elongational flow, *Nano Lett.*, **1**, 295–298 (2001b).

Okamoto, M., Nam, P. H., Maiti, P., Kotaka, T., Nakayama, T., Takada, M., Ohshima, M., Usuki, A., Hasegawa, N., and Okamoto, H., Biaxial flow-induced alignment of silicate layers in polypropylene/clay nanocomposites foam, *Nano Lett.*, **1**, 503–505 (2001c).

Onogi, S., and Asada, T., Rheology and rheo-optics of polymer liquid crystals, in Rheology, Vol. 1, Astarita, G., Marrucci, G., and Nicolais, L.,Eds., Plenum Press, New York, 1980.

Perrin, F.,personal communication, 2002.

Porter, R. S., and Johnson, J. F., The rheology of liquid crystals, in Rheology, Vol. 4, Eirich, F. R.,Ed., Academic Press, New York, 1967.

Pramoda, K. P., and Liu, T., Effect of moisture on the dynamic mechanical relaxation of polyamide-6/clay Nanocomposites, *J. Polym. Sci. B*, **42**, 1823–1830 (2004).

Pryamitsyn, V., and Ganesan, V., Mechanisms of steady-shear rheology in polymer–nanoparticle composites, *J. Rheol.*, **50**, 655–683 (2006).

Pukánszky, B., Influence of interface interaction on the ultimate tensile properties of polymer composites, *Composites*, **21**, 255–262 (1990).

Quemada, D., and Berli, C., Energy of interaction in colloids and its implications in rheological modeling, *Adv. Colloid Interface Sci.*, **98**, 51–85 (2002).

Ren, J., Silva, A. S., and Krishnamoorti, R., Linear viscoelasticity of disordered polystyrene–polyisoprene block copolymer based layered-silicate nanocomposites, *Macromolecules*, **33**, 3739–3746 (2000).

Ren, J., Casanueva, B. F., Mitchell, C. A., and Krishnamoorti, R., Disorientation kinetics of aligned polymer layered silicate nanocomposites, *Macromolecules*, **36**, 4188–4194 (2003).

Ren, J., and Krishnamoorti, R., Nonlinear viscoelastic properties of layered-silicate-based intercalated nanocomposites, *Macromolecules*, **36**, 4443–4451 (2003).

Reynaud, E., Jouen, T., Gauthier, C., Vigier, G., and Varlet, J., Nanofillers in polymeric matrix: a study on silica reinforced PA6, *Polymer*, **42**, 8759–8768 (2001).

Russel, W. B., Saville, D. A., and Schowalter, W. R., Colloidal Dispersions, Cambridge University Press, New York, 1989.

Sakai, Y., Ikehara, T., Nishi, T., Nakajima, K., and Hara, M., Nanorheology measurement on a single polymer chain, *Appl. Phys. Lett.*, **81**, 724–726 (2002).

Sammut, P., Elongational flow of polymeric nanocomposites 4th International Symposium on Polymer Nanocomposites Science and Technology (PNC-2007), National Research Council Canada—Industrial Materials Institute, Boucherville, Quebec, Canada, Oct. 18–19, 2007.

Sammut, P., and Utracki, L. A.,unpublished work, 2004.

Sammut, P., Sepehr, M., and Utracki, L. A.,unpublished work, 2007.

Sarvestani, A. S., Modeling the solid-like behavior of entangled polymer nanocomposites at low frequency regimes, *Eur. Polym. J.*, **44**, 263–269 (2008).

Sarvestani, A. S., and Jabbari, E., Modeling the viscoelastic response of suspension of particles in polymer solution: the effect of polymer-particle interactions, *Macromol. Theory Simul.*, **16**, 378–385 (2007).

Sarvestani, A. S., and Picu, C. R., Network model for the viscoelastic behavior of polymer nanocomposites, *Polymer*, **45**, 7779–7790 (2004).

Sarvestani, A. S., and Picu, C. R., A frictional molecular model for the viscoelasticity of entangled polymer nanocomposites, *Rheol. Acta*, **45**, 132–141 (2005).

Schmidt, D., Shah, D., and Giannelis, E. P., New advances in polymer/layered silicate nanocomposites, *Curr. Opin. Solid State Mater. Sci.*, **6**, 205–212 (2002).

Sedlacek, T., Zatloukal, M., Filip, P., Boldizar, A., and Saha, P., On the effect of pressure on the shear and elongational viscosities of polymer melts, *Polym. Eng. Sci.*, **44**, 1328–1337 (2004).

Sedlacek, T., Cermak, R., Hausnerova, B., Zatloukal, M., Boldizar, A., and Saha, P., On *PVT* and rheological measurements of polymer melts, *Int. Polym. Process.*, **20**, 286–295 (2005).

Sepehr, M., and Utracki, L. A.,unpublished work, 2006.

Sepehr, M., Ausias, G., and Carreau, P. J., Rheological properties of short fiber filled polypropylene in transient shear flow, *J. Non-Newtonian Fluid Mech.*, **123**, 19–32 (2004).

Sepehr, M., Utracki, L. A., Zheng, X., and Wilkie, C. A., Polystyrenes with macro-intercalated organoclay: Part II. Rheology and mechanical performance, *Polymer*, **46**, 11569–11581 (2005).

Sepehr, M., Kabanemi, K. K., and Hétu, J. F., Rheological behavior of polyamide-6 based nanocomposites: experimental study and modeling, in *XVth International Congress on Rheology, The Society of Rheology 80th Annual Meeting, Monterey, CA, Aug. 3–8*, 2008.

Simha, R., The influence of Brownian movement on the viscosity of solutions, *J. Phys. Chem.*, **44**, 25–34 (1940).

Simha, R., and Somcynsky, T., On the statistical thermodynamics of spherical and chain molecule fluids, *Macromolecules*, **2**, 342–350 (1969).

Simha, R., Utracki, L. A., and Garcia-Rejon, A., Pressure–volume–temperature relations of a poly-ε-caprolactam and its nanocomposite, *Compos. Interfaces*, **8**, 345–353 (2001).

Smith, J. G. Jr., Connell, J. W., Delozier, D. M., Lillehei, P. T., Watson, K. A., Lin, Y., Zhou, B., and Sun, Y. -P., Space durable polymer/carbon nanotube films for electrostatic charge mitigation, *Polymer*, **45**, 825–836 (2004).

Solomon, M. J., Almusallam, A. S., Seefeldt, K. F., Somwangthanaroj, A., and Varadan, P., Rheology of polypropylene/clay hybrid materials, *Macromolecules*, **34**, 1864–1872 (2001).

Somcynsky, T., and Simha, R., Hole theory of liquids and glass transition, *J. Appl. Phys.*, **42**, 4545–4548 (1971).

Starr, F. W., Douglas, J. F., and Glotzer, S. C., Origin of particle clustering in a simulated polymer nanocomposite and its impact on rheology, *J. Chem. Phys.*, **119**, 1777–1788 (2003).

Stratton, R. A., and Butcher, A. F., Stress relaxation upon cessation of steady flow and the overshoot effect of polymer solutions, *J. Polym. Sci. Polym. Phys. Ed.*, **11**, 1747–1758 (1973).

Takahashi, T.,Studies on the effect of macromolecular chain structure on elongational rheology, *Ph.D.* dissertation, Yamagata University, Yonezawa, Japan, 1996.

Tanner, R. I., The changing face of rheology, *J. Non-Newtonion Fluid Mech.*, **157**, 141–144 (2009).

Tanoue, S., Utracki, L. A., Garcia-Rejon, A., Tatibouët, J., Cole, K. C., and Kamal, M. R., Melt compounding of different grades of polystyrene with organoclay: Part 1. Compounding and characterization, *Polym. Eng. Sci.*, **44**, 1046–1060 (2004a).

Tanoue, S., Utracki, L. A., Garcia-Rejon, A., and Kamal, M. R., Melt compounding of different grades polystyrene with organoclay: Part 2. Rheological properties, *Polym. Eng. Sci.*, **44**, 1061–1076 (2004b).

Uthirakumar, P., Hahn, Y. B., Nahm, K. S., and Lee, Y.-S., Preparation of polystyrene/montmorillonite nanocomposites using a new radical initiator–montmorillonite hybrid via in situ intercalative polymerization, *Eur. Polym. J.*, **40**, 2437–2444 (2004).

Utracki, L. A., Temperature dependence of liquid viscosity, *J. Macromol. Sci. Phys.* **B10**, 477–505 (1974).

Utracki, L. A., Pressure dependence of Newtonian viscosity, *Polym. Eng. Sci.*, **23**, 446–452 (1983a).

Utracki, L. A., Temperature and pressure dependence of liquid viscosity, *Can. J. Chem. Eng.*, **61**, 753–758 (1983b).

Utracki, L. A., The shear and elongational flow of polymer melts containing anisometric filler particles, Part I: Review, *Rubber Chem. Technol.*, **57**, 507–522 (1984).

Utracki, L. A., A Method of computation of the pressure effects on melt viscosity, *Polym. Eng. Sci.*, **25**, 655–668 (1985).

Utracki, L. A., Correlation between P–V–T behavior and the zero – shear viscosity of liquid mixtures, in *Thermodynamics and Rheology,* (Hartmann, B., Ed.), *J. Rheol.*, **30**, 829–841 (1986).

Utracki, L. A., Rheology of two–phase flows, in Rheological Measurements, Collyer, A. A., and Clegg D. W., Eds., Elsevier, London, 1988 Chap. 15.

Utracki, L. A., Polymer Alloys and Blends, Hanser-Verlag, Munich, 1989.

Utracki, L. A., The rheology of multiphase systems, in Rheological Fundamentals of Polymer Processing, Covas, J. A., Agassant, J. F., Diogo, A. C., Vlachopoulos, J., and Walters, K., Eds., Kluwer Academic, Dordrecht, The Netherlands, 1995, pp. 113–137.

Utracki, L. A., Clay-Containing Polymeric Nanocomposites, 2-vol. monograph, RAPRA, Shawbury, UK, 2004.

Utracki, L. A., Interphase between nanoparticles and molten polymeric matrix: pressure–volume–temperature measurements, *Compos. Interfaces*, **14**, 229–242 (2007).

Utracki, L. A., Nanocomposites with elastomeric matrix, *Int. J. Plast. Technol.*, **12** (2), 969–1002 (2008).

Utracki, L. A., Mechanical properties of clay-containing polymeric nanocomposites, in Handbook of Polymer Nanocomposites, Gupta, R., Kennel, E., and Kim, K.-J.,Eds., CRC Press, Boca Raton, FL, 2009.

Utracki, L. A., Rheology of polymer blends, in *Encyclopedia of Polymer Blends*, Vol. 2: Processing, Isayev, A., Ed., Wiley-VCH Verlag, Weinheim, Germany (2010).

Utracki, L. A., and Fisa, B., Rheology of fiber- or flake-filled plastics, *Polym. Compos.*, **3**, 193–211 (1982).

Utracki, L. A., and Ghijsels, A., Temperature dependence of the melt viscosity of epoxy resins, *Adv. Polym. Technol.*, **7**, 35–37 (1987).

Utracki, L. A., and Kamal, M. R., The rheology of polymer alloys and blends, in Polymer Blends Handbook, Kluwer Academic, Dordrecht, The Netherlands, 2002, Chap. 7.

Utracki, L. A., and Lyngaae-Jørgensen, J., Dynamic melt flow of nanocomposites based on ε-caprolactam, *Rheol. Acta*, **41**, 394–407 (2002).

Utracki, L. A., and Sedlacek, T., Free volume dependence of polymer viscosity, *Rheol. Acta*, **46**, 479–494 (2007).

Utracki, L. A., Sepehr, M., and Boccaleri, E., Synthetic, layered nano-particles for polymeric nanocomposites (PNC's), *Polym. Adv. Technol.*, **18**, 1–37 (2007).

Utracki, L. A., and Simha, R., Viscosity of polymer solutions: scaling relationships, *J. Rheol.*, **25**, 329–350 (1981).

Utracki, L. A., and Simha, R., Relationships between viscosity and equilibrium properties of liquids, *ACS Polym. Prepr.*, **23**, 67–68 (1982).

Utracki, L. A., and Simha, R., Analytical representation of solutions to lattice–hole theory, *Macromol. Chem. Phys., Mol. Theory Simul.*, **10**, 17–24 (2001a).

Utracki, L. A., and Simha, R., Free volume and viscosity of polymer–compressed gas mixtures during extrusion foaming, *J. Polym. Sci. B*, **39**, 342–362 (2001b).

Utracki, L. A., and Simha, R., Pressure–volume–temperature dependence of polypropylene/organoclay nanocomposites, *Macromolecules*, **37**, 10123–10133 (2004).

Utracki, L. A., Simha, R., and Garcia-Rejon, A., Pressure–volume–temperature relations in nanocomposites, *Macromolecules*, **36**, 2114–2121 (2003).

Vaia, R. A., and Giannelis, E. P., Lattice model of polymer melt intercalation in organically-modified layered silicates, *Macromolecules*, **30**, 7990–7999 (1997a).

Vaia, R. A., and Giannelis, E. P., Polymer melt intercalation in organically-modified layered silicates: model predictions and experiments, *Macromolecules*, **30**, 8000–8009 (1997b).

Van de Ven, T. G. M., Colloidal Hydrodynamics, Academic Press, New York, 1989.

Van der Waals, J. D., Over de continuïteit van de gas-en vloeistoftoestand, Ph.D. dissertation, University of Leiden, 1873.

Varghese, S., and Karger-Kocsis, J., Layered silicate/rubber nanocomposites via latex and solution intercalation, in Polymer Composites from Nano- to Macro-scale Friedrich, K., Fakirov, S., and Zhang Z.,Eds., Springer-Verlags, Berlin, 2005, pp. 77–90.

Varlot, K., Reynaud, E., Kloppfer, M. H., Vigier, G., and Varlet, J., Clay-reinforced polyamide: preferential orientation of the montmorillonite sheets and the polyamide crystalline lamellae, *J. Polym. Sci. B*, **39**, 1360–1370 (2001).

Verleye, V., and Dupret, F., Numerical prediction of fiber orientation in complex injection molded parts, *ASME Winter Annual Meeting,* MD, **49**, *HTD*, **283**, 264–279 (1994).

Vermant, J., Ceccia, S., Dolgovskij, M. K., Maffettone, P. L., and Macosko, C. W., Quantifying dispersion of layered nanocomposites via melt rheology, *J. Rheol.*, **51**, 429–450 (2007).

Viola, G. G., and Baird, D. G., Studies on the transient shear flow behavior of liquid crystalline polymers, *J. Rheol.*, **30**, 601–628 (1986).

Vlasveld, D. P. N., de Jong, M., Bersee, H. E. N., Gotsis, A. D., and Picken, S. J., The relation between rheological and mechanical properties of PA6 nano- and micro-composites, *Polymer*, **46**, 10279–10289 (2005).

Wagener, R., and Reisinger, T. J. G., A rheological method to compare the degree of exfoliation of nanocomposites, *Polymer*, **44**, 7513–7518 (2003).

Walker, L. M., Wagner, N. J., Larson, R. G., Mirau, P. A., and Moldenaers, P., The rheology of highly concentrated PBLG solutions, *J. Rheol.*, **39**, 925–952 (1995).

Wang, K. H., Choi, M. H., Koo, C. M., Xu, M., Chung, I. J., Jang, M. C., Choi, S. W., and Song, H. H., Morphology and physical properties of polyethylene/silicate nanocomposite prepared by melt intercalation, *J. Polym. Sci.*, **40**, 1454–1463 (2002).

Wang, L., and Sheng, J., Preparation and properties of polypropylene/org-attapulgite nanocomposites, *Polymer*, **46** 6243–6249, (2005).

Wang, T., Sakai, Y., Nakajima, K., Miyawaki, A., Ito, K., and Hara, M., Nanorheology measurements on single circularly permuted green fluorescent protein molecule, *Colloid Surf. B*, **40**, 183–187 (2005).

Wang, X., Wu, Q., and Qi, Z., Unusual rheological behavior of ultrahigh molecular weight polyethylene/kaolin composites prepared via polymerization-filling, *Polym. Int.*, **52**, 1078–1082 (2003).

Wang, Y., Chen, F. -B., Wu, K. -C., and Wang, J. -C., Shear rheology and melt compounding of compatibilized-polypropylene nanocomposites: effect of compatibilizer molecular weight, *Polym. Eng. Sci.*, **46**, 289–302 (2006a).

Wang, Y., Xu, J., Bechtel, S. E., and Koelling, K. W., Melt shear rheology of carbon nanotube/polystyrene composites, *Rheol. Acta*, **45**, 919–941 (2006b).

Wapner, P. G., and Forsman, W. C., Fourier transform method in linear viscoelastic analysis: the vibrating reed, *Trans. Soc. Rheol.*, **15**, 603–626 (1971).

Watabe, H., Nakajima, K., Sakai, Y., and Nishi, T., Dynamic force spectroscopy on a single polymer chain, *Macromolecules*, **39**, 5921–5925 (2006).

Weissenberg, K., The Testing of Materials by Means of the Rheogoniometer Farol Research Engineering Bognor Regis Sussex, UK, 1964.

Whitmore, R. L., Principles governing the viscous flow of suspensoids, *Br. J. Appl. Phys.*, **13**, 182 (Letter to the Editor) (1962).

Wilhelm, M., Fourier-transform rheology, *Macromol. Mater. Eng.*, **287**, 83–105 (2002).

Williams, M. L., Landel, R., and Ferry, J. D., The temperature dependence of relaxation mechanisms in amorphous polymers and other glass-forming liquids, *J. Am. Chem. Soc.*, **77**, 3701–3707 (1955).

Winberg, P., Eldrup, M., Jørgen Pedersen, N., van Es, M. A., and Maurer, F. H. J., Free volume sizes in intercalated polyamide 6/clay nanocomposites, *Polymer*, **46**, 8239–8249 (2005).

Wissbrun, K., Rheology of rod-like polymers in the liquid crystalline state, *J. Rheol.*, **25**, 619–662 (1981).

Wu, D., Zhou, C., Hong, Z., Mao, D., and Bian, Z., Study on rheological behaviour of poly(butylene terephthalate)/montmorillonite nanocomposites, *Eur. Polym. J.*, **41**, 2199–2207 (2005a).

Wu, J.-Y., Wu, T.-M., Chen, W.-Y., Tsai, S.-J., Kuo, W.-F., and Chang, G.-Y., Preparation and characterization of PP/clay nanocomposites based on modified polypropylene and clay, *J. Polym. Sci. B*, **43**, 3242–3254 (2005b).

Wu, Q., Olafsen Sjåstad, A., Vistad, Ø. B., Knudsen, K. D., Roots, J., Pedersen, J. S., and Norby, P., Characterization of exfoliated layered double hydroxide (LDH, Mg/Al = 3) nanosheets at high concentrations in formamide, *J. Mater. Chem.*, **17**, 965–971 (2007).

Yasuda, K.,Ph.D. dissertation, Massachusetts Institute of Technology, 1979.

Yziquel, F., Carreau, P. J., Moan, M., and Tanguy, P. A., Rheological modeling of concentrated colloidal suspension, *J. Non-Newtonian Fluid Mech.*, **86**, 133–155 (1999).

Zax, D. B., Yang, D. K., Santos, R. A., Hegemann, H., Giannelis, E. P., and Manias, E., Dynamical heterogeneity in nanoconfined polystyrene chains, *J. Chem. Phys.*, **112**, 2945–2951 (2000).

Zeng, Q. H., Yu, A. B., and Lu, G. Q., Multiscale modeling and simulation of polymer nanocomposites, *Prog. Polym. Sci.*, **33**, 191–269 (2008).

Zhang, Q., and Archer, L. A., Poly(ethylene oxide)/silica nanocomposites: structure and rheology, *Langmuir*, **18**, 10435–10442 (2002).

Zhang, Q., and Archer, L. A., Monte Carlo simulation of structure and nanoscale interactions in polymer nanocomposites, *J. Chem. Phys.*, **121**, 10814–10824 (2004).

Zhang, Z., Zhang, L., Li, Y., and Xu, H., Styrene–butadiene–styrene/montmorillonite nanocomposites synthesized by anionic polymerization, *J. Appl. Polym. Sci.*, **99**, 2273–2278 (2006).

Zhong, W., Qiao, X., Sun, K., Zhang, G., and Chen, X., Polypropylene–clay blends compatibilized with MAH-*g*-POE, *J. Appl. Polym. Sci.*, **99**, 2558–2564 (2006).

Zhu, Z., Thompson, T., Wang, S. -Q., von Meerwall, E. D., and Halasa, A., Investigating linear and nonlinear viscoelastic behavior using model silica–particle-filled polybutadiene, *Macromolecules*, **38**, 8816–8824 (2005).

Zirnsak, M. A., Hur, D. U., and Boger, D. V., Normal stress in fibre suspensions, *J. Non-Newtonian Fluid Mech.*, **54**, 153–193 (1994).